UNIVERSITA' DEGLI STUDI DI PADOVA

Laurea Magistrale in Ingegneria Aerospaziale

Tesi:

Design, construction and performance characterization of a system for detecting the absolute position of a pointing mechanism with two degrees of freedom

Autore:

Marco Scarambone

Dipartimento di Ingegneria Industriale

Dipartimento di Ingegneria dell' Informazione

Relatore: Prof. Maria Elena Valcher, Università degli Studi di Padova

Co-relatore: Dr. Alexander Hoehn, Institute of Astronautics, TUM

ANNO ACCADEMICO 2015/2016

A mio padre e alla mia famiglia

Ringraziamenti

Questo lavoro è il risultato del mio periodo di scambio con l' Università di Monaco di Baviera (TUM), ma soprattutto il risultato di sei anni di impegno e dedizione qui all' Università di Padova. In questa breve parte introduttiva mi preme ringraziare le persone che mi sono state vicino nelle tappe di questa mia avventura accademica per poter rendere reale il risultato che sto per conseguire. Rivolgo questo discorso in primis alla mia famiglia: a mio padre che ha saputo instillarmi quella curiosità nel mio spirito, indispensabile a mio avviso per affrontare l' università, partendo dalla lettura dei Poemi Omerici e da Le Storie di Erodoto sin da quando ero un bambino, fino agli anni più recenti nei quali si è dimostrato un saggio consigliere nelle mie scelte meno immediate; a mia madre che con la sua grinta e perseveranza sa tenere unita e salda la mia famiglia; a mio fratello con il quale negli ultimi anni ho potuto apprezzare il ancor più il tempo trascorso con lui; a mia Zia Tatiana e a mio nonno Dino. Rivolgo il ringraziamento a Elisa e la sua famiglia che mi sono sempre rimasti vicino anche nei momenti di titubanza e insicurezza. Vorrei ringraziare tutta la mia vecchia squdra di basket con la quale ho trascorso buona parte dei miei anni (Stefano, Daniele, Luca, Enrico, Thomas, Alessandro, Alberto) e i miei compagni di corso che hanno questi ultimi anni dell' università indimenticabili (Francesco, Alberto, Mattteo, Filippo e Marco) insieme ai miei ex-conquilini di via Belzoni (Matteo, Chiara, Claudia e Marianna). Rivolgo i miei ringraziamenti infine alla professoressa Valcher, mia relatrice qui a Padova, e al porfessor Hoehn, mio supervisor di Monaco, nonchè ad entrambi i dipartimenti di Ingegneria, di Padova e di Monaco di Baviera che hanno permesso che questo traguardo prendesse forma.

Summary

LIST OF FIGURES

LIST OF TABLES

List of Symbols

V Voltage

V_t Threshold Voltage

V_{to} Optimal Threshold Voltage

V_d Default Threshold Voltage

N number of samples

sr sampling rate

f electrical frequency

Std dev standard deviation

Δ_{max} Max deviation

V_{max} Max Voltage

d magnet diameter

v tangential velocity

w cogwheel rotational velocity

r distance of the magnet from rotational axis

s linear distance travelled by the magnet

theta swept angle by the magnet

w_{fr} width flat region

w_s width of the signal

l size of the laser target

x_{max} position of the maximum

x_t position of the start of the sampling

t loop period

C circumference

Abbreviations

LISA Light-weight Inter-Satellite Antenna

LISA$_{ms}$ Lightweight Inter-Satellite Antenna – Mechanical Steerable

APM Antenna Pointing Mechanism

ISL Inter Satellite Link

AM Azimuth Mechanism

LEO Low Earth Orbit

GEO Geostationary Orbit

GR gear ratio

SR sampling rate

PSD Position Sensing Device

Ni Nichel

Cu Copper

CPU Central Processing Unit

BB Bread-Board

ADC Analog to Digital Converter

MPF Mid-Point Finder

PD Peak Detection

LRT Lehrstuhl für Raumfahrttechnik

TUM Technische Universität München

MOVE Munich Orbital Verification Experiment

HS Hall sensor

SC Spacecraft

RF Radiofrequency

Abstract

This Master Thesis describes the design of an absolute encoder for the LISA (Lightweight Intersatellite Antenna). The work was conducted at the Lehrstuhl für Raumfahrttechnik (LRT) of the Technische Universität München (TUM) during the 8 months exchange period through the Erasmus project, a European program which allows students to do an internship period in another European University. In this particular case, the exchange period was possible due to the agreement between the University of Padova and TUM.

LISA is a project handled by the Department of Astronautics (LRT) of the Thechnical University of Munich that aims to develop an inter-satellite communication subsystem that will allow a LEO satellite to have and an? extended period of downlink to a ground station of almost 41 minutes: the satellite's antenna requires a performing pointing mechanism (APM, Antenna Pointing Mechanism) able to point the radio source toward the desired target. To move this mechanism a couple consisting of a stepper motor (Azimuth and Elevation angles) and gear box has been chosen, to provide the movements with the required precision. One drawback of this choice is that a loss of power of the main system due to an unpredictable event could lead the mechanism to forget the position at the moment of shutdown. The purpose of this paper is to design a device able to detect the zero/starting position of the mechanism (absolute encoder), by processing the signal acquired by the hovering of a magnet over a pre-selected Hall sensor (magnetic sensing technology). The thesis' work required: a research on the state of the art on the magnetic absolute encoder and a test on the most effective methods to find the zero position, several sets of tests to verify the reliability of the chosen method (mid-point finder) and a description of the further steps to perform to complete the development of the device.

1 INTRODUCTION

1.1 Lisa Overview

LISA (Lightweight Inter Satellite-link Antenna) is a project handled by the institute of Astronautics Engineering in Munich (LRT) with the support of DLR (German Aerospace Center). The purpose of the system is to provide a longer satellite communication between a satellite in LEO and a ground station, extending the available direct downlink time for LEO satellites to earth from 7 minutes (the average amount of time that a LEO satellite takes to cross the area over a generic ground station) to approximately 45 minutes. The Inter Satellite Communication Link (ISL) is between a satellite in LEO and a satellite in GEO orbit, both equipped with an express antenna, that provide the communication channel between them. The LISA antenna main array is a 400x400x200 mm antenna that weights 5000g, it transmits at a frequency of 23.205/27.350 GHz with 15 years of estimated operative life.

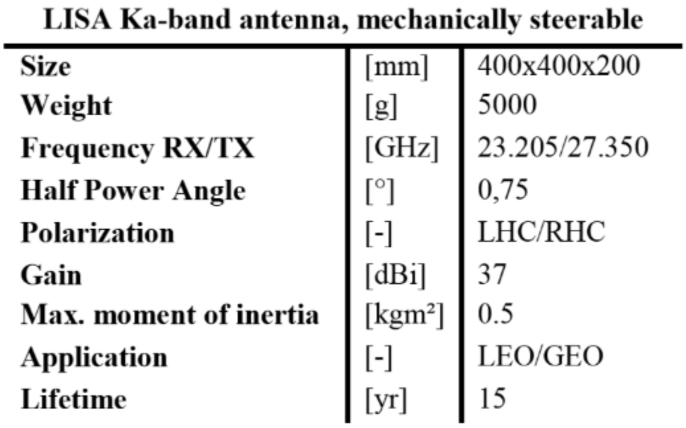

LISA Ka-band antenna, mechanically steerable

Size	[mm]	400x400x200
Weight	[g]	5000
Frequency RX/TX	[GHz]	23.205/27.350
Half Power Angle	[°]	0,75
Polarization	[-]	LHC/RHC
Gain	[dBi]	37
Max. moment of inertia	[kgm²]	0.5
Application	[-]	LEO/GEO
Lifetime	[yr]	15

Figure 1: The LISA antenna main properties [2].

In the last years the amount of data that Low Earth orbiting satellites need to transmit to the ground is increasing. The most common used frequency is the Ka-band due the potentially higher data rate allowed with respect to the X and S bands. More frequently, the time of the transmission is becoming insufficient for more applications, due the elevate orbiting speed of this kind of satellite (7/9 km/s) that allow a link period to a generic ground station of a period of 7 minutes. For this reason, geostationary relay satellites are becoming an interesting option for this application. With a Ka-band antenna, it is possible to transmit data at high rates (typically it can support a range 10-100 Mbps for download) and, thanks to the increasing population of GEO satellites, transmit a wider data volume in comparison with a classic direct download link to earth.

To maintain a continuous link (relay link) between a LEO satellite and a GEO satellite, two antennas, that are able to point to the partner satellite and to be steered enough to assure the tracking of its position, are required. It is useful to remark that the period of a GEO orbit is of 24 hours, the one of a LEO orbit is of 90 minutes, a GEO orbit has an average altitude from the surface of the Earth of 36000, a LEO between 160 and 2000 km. This means that steering rates required for a pointing mechanism are [1]:

- LEO satellite: typ. 180 degrees in 45 minutes (4°/min);
- GEO satellite: typ. 22 degrees in 45 minutes (0.5°/min).

Figure 2: The LISA$_{ms}$ system [1].

There are different applications that require a larger amount of data to download: for example, real-time on orbit servicing missions with higher images resolution, larger frame rates and larger number of camera, or haptic feedback for a ground station operator.

During the last years, the DLR and the LRT have developed several models of the antenna. The development of this first models led to the LISA$_{ms}$ (Lightweight Inter – Satellite link Antenna – Mechanical Steerable), a copper-galvanically manufactured antenna with a wave guide distribution network. The system is equipped with a 2-axes waveguide rotary joint included in the 2- axes steering/pointing system of the antenna array. The spherical coordinates of the position of the latter in a half hemisphere were provided by:

- Elevation mechanism, angle 0-90°
- Azimuth mechanism, angle 0-360°

As previously told, the angular tracking velocity are high, if compared to the GEO application (20°/ min in direct downlink) and due the narrow width of the Ka-band antenna (36db = 1.6°) a precision of up to 0.16° is required for the steering mechanism.

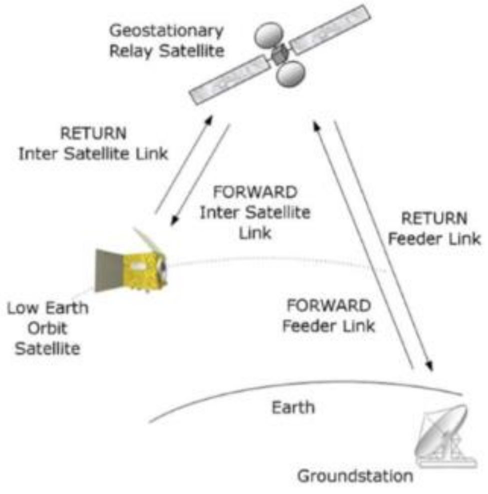

Figure 3: The Inter- satellite link [2].

1.2 Lisa APM Overview

In this paragraph the main functions of the antenna pointing mechanism are introduced. The requirements of this two degree of freedom Antenna Pointing Mechanism (APM) is to maintain the ISL, between LEO and GEO satellites, constant, and to guarantee the continuity of the communication link. The rates of the slip rings of this support are between 0.05deg/s to 5deg/s in both degrees of freedom, considering the much higher altitude of a GEO satellite looking at a LEO satellite. To ensure a continuous link between satellites, the antenna must be accurately pointed. The pointing itself is accomplished by two independent degrees of freedom (2Dof). Due to the small antenna aperture and the high frequencies, the main lobe is limited to approximately 1.5°. The tracking of a relay satellite involves a slow motion within a limited angular range. The required angular ranges, velocities and pointing accuracies are summarized in the table below.

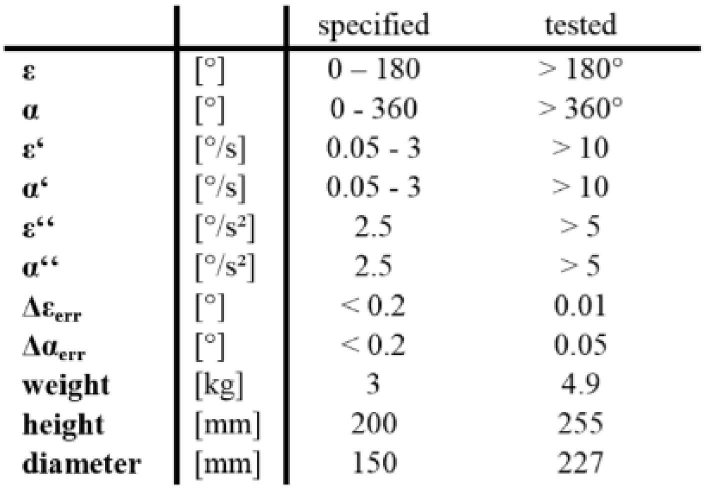

		specified	tested
ε	[°]	0 – 180	> 180°
α	[°]	0 - 360	> 360°
ε'	[°/s]	0.05 - 3	> 10
α'	[°/s]	0.05 - 3	> 10
ε''	[°/s^2]	2.5	> 5
α''	[°/s^2]	2.5	> 5
$\Delta\varepsilon_{err}$	[°]	< 0.2	0.01
$\Delta\alpha_{err}$	[°]	< 0.2	0.05
weight	[kg]	3	4.9
height	[mm]	200	255
diameter	[mm]	150	227

Figure 4: Comparison between specified and tested EM (electrical model) performances [1]

For a constant communication link, the APM must be capable of transmitting the continuous wave (CW) Ka-band signal with a minimum loss through the mechanism at any operational time.

The usage of the APM on geostationary platforms is expected to have a lifetime of 15 years. For these reasons all ball bearings and moving parts within the APM must be lubricated in order to guarantee performance over lifetime.

The thermal environment for the APM phases has been distinguished between operational and non-operational phases. During the non-operational phase the temperature of the APM shall remain within the limits of -40°C to +80°C, while for the operational phases within -20°C to +40°C [2].

1.2.1 Azimuth mechanism

The azimuth axis is driven by a stepper motor identical to the elevation drive. Thus the overall gear ratio of the azimuth is identical to the elevation drive. The rotation around the azimuth axis is achieved by a 5:1 ratio spur gear and a 50:1 ratio harmonic drive. The spur wheel of the first stage is directly attached to the elevation housing. The bevel is driven by another stepper motor (identical to the elevation motor) with an integrated planetary gear. The adjustment of the spur gear is critical to the azimuth pointing accuracy and must be carefully established due to the open exposure of the spur gear.

The mounting of the azimuth RF-rotary joint is analogue to the elevation rotary joint. In this case the 90° bent knee rotates together with the complete elevation assembly around the azimuth axis. The final rotary joint part, which leads out of the APM into the satellite, is fastened to the azimuth housing. The Azimuth housing comprises the complete elevation assembly, the RF exit to the satellite and the mounting interface to the satellite structure. Analogously to the elevation housing, this essential part of the APM is made of Aluminum 7075. The complete elevation assembly is fastened to a hollow spindle, which is mounted in the azimuth housing. An unlimited rotation around the azimuth axis is provided by the integration of a slip ring assembly. This slip ring provides electrical power and control signals to the elevation assembly.

1.3 Existing Hardware

At the beginning of this work, the hardware available, provided by the department of Astronautics, included (the list and the whole setup will be better described in the next chapters):

1. a package containing the electronic hardware for the preliminary tests: An Arduino Mega2560 board, wires, set of magnet of different size, and a small homemade rotating arm to simulate the circular motion of the magnet, Hall sensors chosen from previous work [4]).
2. The stepper motor inserted in the case of the pointing mechanism, including cogwheel and elevation case fastened at the top of the rotating shaft of the Azimuth mechanism.

3. A set of Microprocessors to make the motor move and to collect data from the Hall sensor through the ADC; a board to connect each IC (Integrated Circuit) a communicate ??? to the Laptop/PC connected for the tests.
4. Labiew2015 has been used to interface each component/board, display data, and to perform the motor rotation.

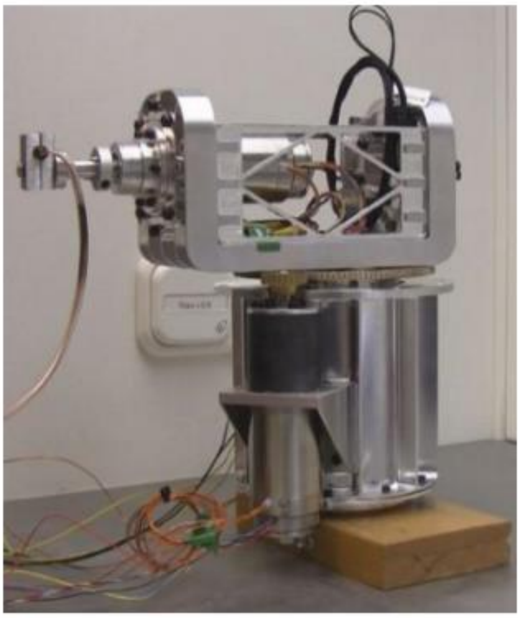

Figure 5: Model of the APM (Antenna Pointing Mechanism), [2]

1.4 Problem statement

The pointing direction is provided in a hemisphere by the two Azimuth and Elevation angles, controllable trough the two stepper motors. Both of them require a system to find a starting position from which to start the rotation and to use as a reference point, in case of power loss / shut down of the main system and consequent loss of information on the position of the rotors of the pointing mechanism. This information will allow us to know, in terms of degree, the relationship between the absolute reference system and the relative reference system, both described below.

1. Azimuth joint: the satellite/support is the absolute system of reference; the case of the elevation mechanism is the relative/moving/rotating system of reference
2. Elevation joint: the case is the absolute system of reference; the antenna support is the relative system of reference

The required level of resolution will be an important aspect to consider: knowing less precisely the absolute position of one shaft can inevitably lead to a wrong knowledge of its orientation, in terms of current pulses in the coils of the motor: the device to design will be useful in case of shut-down of the main-system and loss of all the information concerning the relative position between the stator (support) and the rotor (the shaft), due to an unpredicted event. In previous works several sensing systems (magnetic sensors, proximity sensors, optical sensors) have been evaluated, that can efficiently provide the signal and the information used to detect the zero position, and that could withstand reliably in the space environment. [2]

1.5 Outlines of the thesis

The aim of this thesis is to create a reliable sub-system able to detect the absolute position of the rotation. In the first part (chapters 2 and 3) the requirements needed for the device, in term of resolution, temperature and electrical constraints, have been analyzed. The state of the art on the absolute encoders has been analyzed, focusing on the type most commonly used in the aerospace sector with a resolution over 16-bit, both in the industrial and the scientific field, then has been evaluated the most affordable and reliable configurations and methods for the system have been evaluated, considering the available time, hardware and funds.

In chapter four the analytical model used, the physics behind the problem and the approximation used in this context are explained. The sets of preliminary test are described. They have been made to understand the possible shapes of the signal and the independent variable involved, their possible ranges for the simulations and the most convenient solutions to optimize the system of detection of the zero position. Next, in chapter five, the setup used for the main tests is described. The test was made to investigate the best possible solutions among the fit methods proposed in chapter 4. Subsequently each hardware and software component (datasheet available at the bottom of the paper) and the main aspects of the used setup, from a mechanical, electrical and computational point of view, are listed. The discussion continues with the description and discussion of the test performed and the search of the most reliable method to find the absolute position, changing the independent variables listed in the previous chapter and evaluating some ways to improve the processing of the signal acquired. Chapter 7 is focused on the set of validation tests performed to verify if the system developed is able to accomplish the required tasks: this was done using a laser pointer stuck at the top of the rotating shaft used for the Azimuth mechanism that pointed on a light-sensitive surface provided in the available PSD (Position Sensitive Device). The Hardware used is described and the results obtained are discussed. In the last part of the thesis (chapter 8 and 9) a general discussion on the results is reported and the conclusions made, describing the final mechanical and operational configuration chosen. The thesis ends with possible further developments and extensions of the studied method, and its integration in the LISA system, such as the possible test to perform and the discussion on the elevation mechanism.

2 ENGINEERING REQUIREMENTS

2.1 Chapter overview

In this chapter the technical requirements that the device must satisfy are listed. A precision up to 16-bit of resolution in the detection of the zero position is needed. The temperature range that the instrumentation (sensor, circuit, gears, micro-controller) has to face, being exposed to the space environment, both in LEO and in GEO, will be analyzed. In the last paragraph the problem of the restart of the main system after a shut-down will be described: the device will have to gather the information after the restart of the motor without any memory of the previous activity, considering the computational constraints that the main computer of the satellite has, like the limited CPU frequency.

2.2 Resolution requirements

In space applications, most of the pointing mechanisms require a very strict precision and reliability features: talking about the APM and its stepper motors, (motor has a resolution of 200 steps per revolution, and the gear ratio is of 250 with respect to the main cogwheel/motor shaft a resolution of 16-bit is needed, that means, in terms of degrees:

$$\text{16-bit} = 2^{16} = 65536 \text{ positions} \qquad 360/65536 = 0.005431°. \tag{2.1}$$

To give an idea of the precision of the device: the zero position requires an angle information of at least three digits of precision after the comma. The signal that will be displayed through the sensor will be a function of different variables, such as the position of the magnet on the cogwheel and the rate of the main cogwheel: for instance, having a slower rotation speed of this mechanical element will lead the user to a flatter/wider signal that will need to be processed with an express software to yield the exact angular position; on the other hand, having a too high rotational speed will provide a signal that results too “slim“ (enhancing the shape of the signal in figure 6a) to be sampled without a higher resolution and a high sampling frequency. The right trade-off between the two listed conditions is needed.

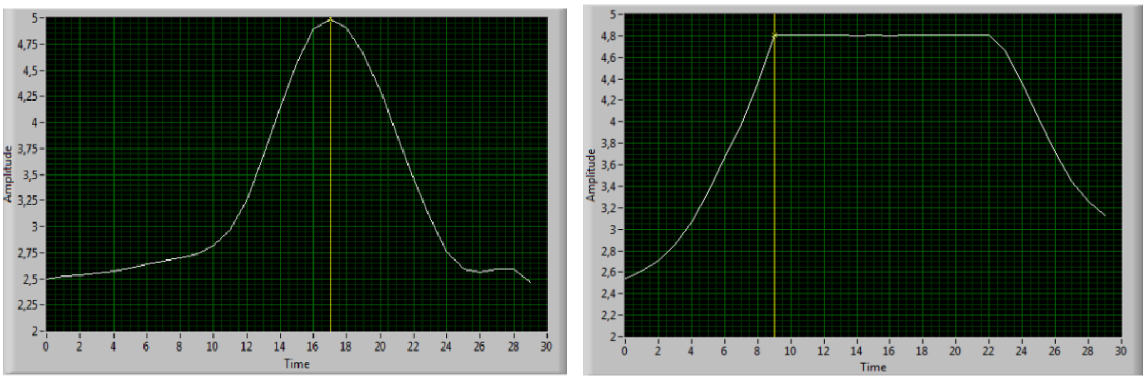

Figure 6: Different shapes of the signal: (a) thinner shaped and unclipped signal (b) flattened shaped and clipped signal

Similar considerations can be done when considering the position in which the sensor/magnet, will be placed: by increasing the distance from the rotational axis of the cogwheel, assuming that the rotational speed is constant, the tangential velocity grows. This can be easily evaluated by using the well-known formula:

$$V= w*r\ [m/s]\ \text{whit}\ w = 2pi/T\ [rad/s] \tag{2.2}$$

For this reason, having a sensor near the axis will provide a flat signal, while having it far from the axis will result in a thin one.

Furthermore, the shape of the signal could be assumed for most of the cases symmetric, but it is necessary to consider some factors depending on the used sensor used. For instance, a magnetic sensor could be influenced by events like the proximity to some magnetized part or to the earth magnetic field, and an optical sensor by some unpredicted path of light detected by the sensor. Indeed, some attention has to be paid to the environment in which the sensor has to operate.

Another constraint to consider is the capability of the satellite processor: it is not possible to use an algorithm which is too "heavy" in terms of calculations. It is fundamental to adopt a light method with a reduced amount of operations. Most of the time, the CPU of a satellite is not comparable to the one of an average computer available on the market today, for this reason, the test that will be performed from the simplest algorithm, the threshold method, will start by assuming the plot of the signal as symmetric.

2.3 Temperature requirements

The space environment is characterized by extremely harsh conditions and, most of the time, forces an engineer to design systems able to resist to really adverse situations: one of these aspects is the thermal environment. For a specific device, being exposed to the space means to face a wide range of temperatures, that could go, in the most critical environments, from nearly the absolute zero (-273° C) to the temperature of the sun surface. As far as the temperature range for our application is concerned, it is important to consider a satellite orbiting in LEO (Low Earth Orbit) and GEO (Geostationary Earth Orbit). In this paragraph the main aspects of these two kinds of orbits in terms of power absorbed by the spacecraft will be briefly described.

2.3.1 LEO thermal environment

The following table summarizes the range of Direct Solar, Reflected Solar (Albedo), and Planetary Infrared light from the planet Earth.

Table 1: Thermal power received by a LEO satellite

	Perihelion	**Aphelion**	**Mean**
Direct solar	1414 W/sqM	1323 W/sqM	1367.5 W/sqM

Albedo (global annual average)	0.30+/-0.01	0.30+/-0.01	0.30+/-.01 W/sqM
Planetary IR (global annual average)	234 +/-7 W/sqM	234+/-7 W/sqM	234 +/7 W/sqM

The variation in the solar constant of approximately +3.5% about the mean value of 1367.5 w/m2 is due to the eccentricity of the Earth orbit. Perihelion (closest position to the Sun) occurs on or near December 21 each year and aphelion (furthest position from the Sun) occurs on or near June 21. For spacecraft thermal balance problems, this variation is frequently ignored, and either the perihelion value of 141 w/m2 or the annual mean value of 1367.5 w/m2 is used.

Another aspect that has a much more profound effect on Direct Solar energy for LEO missions is the orbital Beta angle which, in combination with altitude, determines the percentage of time spent in sunlight. Beta angle is defined as the angle between the orbit plane and the vector from the Sun as shown below.

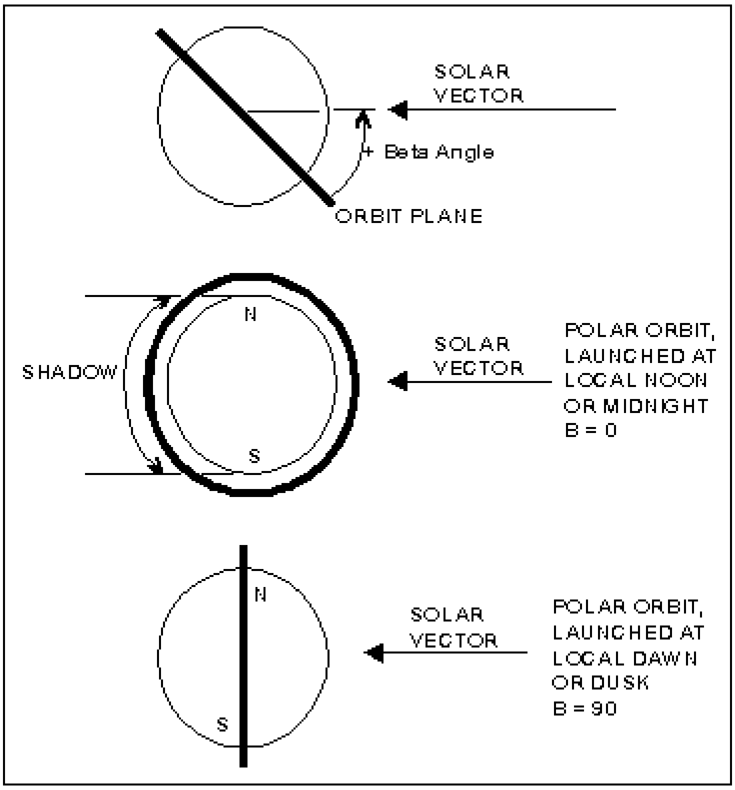

Figure 7: Beta Angle [7].

The extreme effects on orbital shadowing are shown above. For a polar orbit launched at local noon or midnight, the resulting initial Beta angle is 0 degrees which gives maximum Earth shadowing. For an orbit altitude of 280 km, which is the lowest generally practical considering orbital decay physics for a LEO orbit, the resulting sunlight is 59% of the orbit time (i.e., about 53 minutes of sunlight, 37 minutes of shadow, a LEO orbit lasts one hour a half). Similarly, a polar orbit mission launched at local dawn or dusk results in a 90° Beta angle, with 100% sunlight.

Beta angle depends on all the following variables and it is therefore somewhat complex: inclination of the orbit, altitude, time of the mission, time of the year of the launch, and time of the day of the launch. It varies as the mission progresses due to changes in the Earth-Sun inertial relationship (rotation of the Earth around the Sun), and orbit precession effects (non-uniformity of the Earth's gravitational field, etc.). The extreme values of the Beta angle over a year's time for a mission launched at a given orbit inclination, denoted by I, are +/-(I+23.45) degrees. In other words, for a launch from KSC, with I=28.5 degrees, the Beta angle will vary from about +52 degrees to -52 degrees over the course of a year.

The fundamental effect of the Beta angle is its influence on the percentage of sunlight during any given orbit. Note that the percentage of sunlight does not fall below 59% for normal LEO missions.

The variation in the Earth's albedo is a function of latitude, cloud cover, ice fields and the time of year.

The albedo of the Earth is normally treated as fully diffuse, but there has been some theoretical work implying the reflection (forward scattering) of the polar ice caps.

The Earth's planetary infrared emission is a function of latitude, cloud cover, large area weather phenomena, land masses, forestation, and the time of year. Note that the peak values are in the tropical zones, about 20 degrees either side of the equator, and the minimums are at the poles where the albedo is maximum. As in the case of albedo, most spacecraft thermal balance problematics ignore the variations and assume a uniform emission of 241 W/sq. M (81 BTU/sq.). Again, long duration polar missions should consider the reduction of emissions at the poles [15].

2.3.2 GEO thermal environment

The following table summarizes the range of direct Solar, Reflected Solar (Albedo), and Planetary Infrared radiation for a Geosynchronous orbit about Earth.

Table 2: Thermal power received by a GEO satellite

	Perihelion	Aphelion	Mean
Direct Solar	1414 W/sq M	1323 W/sq M	1367.5 W/sq M
Reflected Solar (Albedo)*	7.19 W/sq M	6.72 W/sq M	6.95 W/sq M
Subsolar Peak	2.72 W/sq M	2.54 W/sq M	2.63 W/sq M
Orbit Average Planetary Infrared	5.52 W/sq M	5.52 W/sq M	5.52 W/sq M

The thermal environment in Geosynchronous Earth Orbit is much simpler to define than in LEO. The direct solar thermal power varies only with the time of year except for two occultation periods when the spacecraft enters the Earth shadow each year. This occultation occurs every day over a 45- to 50-day period, twice a year, and lasts up to 71 minutes.

Both the reflected solar terms and planetary infrared terms are small in GEO. In the table above, the view factor from a spacecraft at 35,743 km (22,204 St. mi.) has been included since altitude is constant. In addition, for the reflected solar term, an orbit average value is shown. The values of these terms are so small at this altitude that they are encompassed by any reasonable uncertainty in the direct solar term.

2.4 Electrical requirements

One of the features that the device needs to satisfy is the capability to start from an unknown position and detect the zero position with one or more maneuvers. It is common for a satellite and its components to be shut down during their lifetimes for some reason; for instance, we can consider the Rosetta Mission, that during its ten year trip around the solar system reaching the comet 67/P, entered in the so called hibernation phase, during which it was shut down for 11 months because it was considered useless to keep it operative during such a long phase of inactivity as the final trip outside the Asteroid belt. A shut down of the system can be predicted or unpredicted and the device that will be developed will have to be reliable even in this case.

The motor that moves the joints is a stepper motor: this kind of electrical motor works using the well know Faraday Law that relates the amount of current with a certain variation of magnetic flux (magnetic field in a certain area). The basic principle of the motor is that the position of a rotating shaft is associated with a combination of the current inputs: specifically, each angle that the shaft can take is a unique function of the actual combination and the positions of these inputs. This means that, without laborious calculations, there is no relationship between a given position and the previous one and a user is not able to estimate the actual position of the rotor in case of loss of information caused by an unpredicted event that lead to the shutting down of the whole system.

This thesis will provide a simple and quick way to find the position that is reliable for a user ???, thus avoiding complex procedures to estimate it and the need to keep record of each position previously assumed by the rotor.

Another requirement to consider is the limited capability of a spacecraft CPU: at the state of the art, a space qualified CPU like the RAD470, used for example on the Curiosity rover, landed on Mars in 2012, or in the Juno probe, programmed flyby to Jupiter 2016, has a maximum clock rate between 110 MHz to 200 MHz, almost, for example, one tenth of the capability of an average PC at the department of Astronautics in Garching (Munich). The method that will be implemented has been chosen also for its simplicity and fast use.

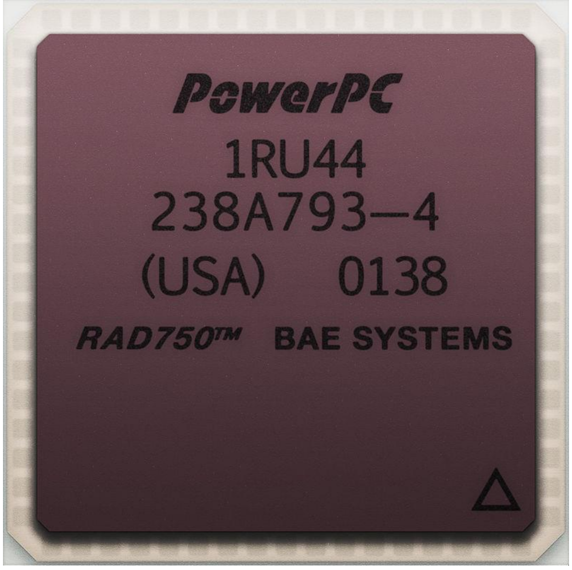

Figure 8: RAD750, CPU for space applications

3 ENCODER BACKGROUND

3.1 Chapter overview

In this chapter several types of encoders, available in the industrial field today, will be presented, considering the previously listed requirements. Based on previous works, the magnetic sensing technology has been selected, since it is able to resist to a wider range of temperatures. Then, the technical differences between the on and off axis encoder and the absolute and incremental encoders will be described. The chapter continues describing some of the different configurations that are used in the space sector to detect the absolute position of a generic shaft, and which of their features have been used for the development of the proposed device.

3.2 Types of sensing system

3.2.1 Valuable alternatives

An encoder is a device that provides the information on the angle of a rotating system. There are several ways to detect this information and in the recent decades the technology, thanks to the huge development of the electronic sector, has made it possible to have more compact and precise sensors, suitable for application in the space industry. Based on the way the angular position is detected, it is possible to distinguish: magnetic encoder, optical encoder and potentiometers. Based on previous works [3], these three technologies have been selected as the best options in the space, which is characterized by a harsh thermal and pressure environment. Hereafter the main principles underlying their functioning are described:

1. Magnetic encoder: a semiconductor is able to change the amount of current that is flowing in the circuit by the proximity a polarized magnet, as it will be explained in the next paragraphs (Hall sensor technology), properly placed in the geometry of a rotating shaft.
2. Optical encoder: it is able, by means of a photodiode or a photo-resistance, to detect the amount of light coming from a light source. Most of the time, the device is coupled with a hole, allowing the sensor to detect its position by changing the amount of incident light. The most famous configuration of this encoder is the Gray code encoder.
3. Potentiometer: by changing the angular position of a needle placed at the center of a circular resistance (most of the time a coil) the amount of current through the cable will change, by the 2nd Ohm's Law, providing a signal which is a function of the position of the rotating shaft.

Based on the geometrical aspect of the encoder, we are able to distinguish other two kinds of encoders:

1. On-axis encoders: an encoder that is located on the rotation axis of a generic rotor.
2. Off-axis encoder: an encoder that is located outside of the rotation axis of the rotor.

Next paragraph will be focused on the working principles of the magnetic encoder and will describe some of the possible configurations suitable for this work.

3.2.2 Magnetic Encoders

The magnetic encoder here considered uses the Hall-effect sensing technology. A Hall-effect sensor is a type of transducer that is able to detect the presence of a magnet in its proximity, by the variation of the module of the magnetic field of the environment. There are a high variety of applications in the modern technology, especially in the space sector. This sensor is able to give information on the position, velocity and acceleration, of a motion.

The simplest configuration in which it can be used is as an analog sensor that provides a voltage as an output: knowing the magnetic field provided by a magnet it is possible to determine its distance from the detecting surface. By combining different magnet/sensor systems, a user can know the position of an object in the space. This kind of sensor is widely used in the industrial sector: from the determination of the position of a piston in an internal combustion engine to an anti-lock braking systems (ABS).

As in the majority of the industrial fields, the development of the semiconductor technology provided several advantages in the construction and the way we use these sensors: for example, the most common component used is the indium Antimonite, which is mounted on an Aluminum plate, all encapsulated in the main head. The positions of the crystal of Indium are perpendicular to the probe handle: when feeding the probe, the positions of these crystal change. When the sensor is in close proximity to a magnetic field, it will sense the Hall-effect through the Lorentz force expressed on electrons. The effect will be similar to a charge separation and it will lead to the creation of positive and negative areas.

The current is a flow of charges; when they pass through the sensor held in the proximity of the magnetic field they change their path providing a change of voltage (known as Hall-effect Voltage).

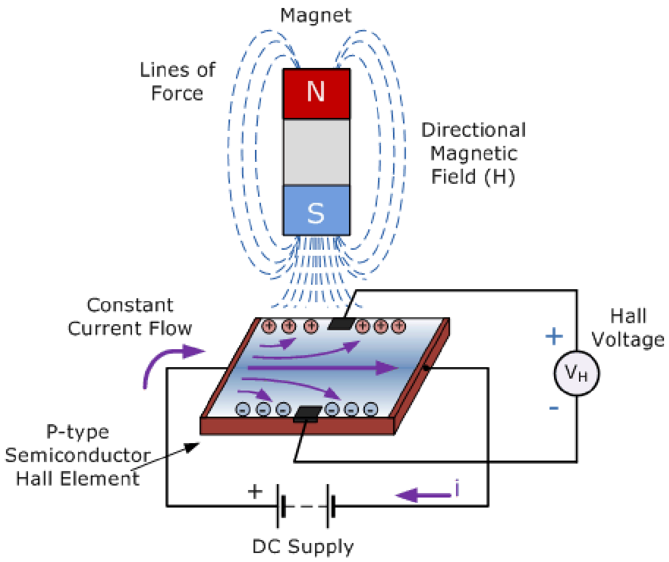

Figure 9: Schematic view of the working principle of a Hall effect sensor

Indium is not the only material used for the construction of this kind of sensors: Gallium Arsenide, Indium Arsenide, Indium Phosphide and Graphene are also commonly used for these applications.

These are some advantages in this technology: lower cost with respect to a mechanical switch but higher reliability, operative range up to 100 kHz, possibility of using it in different environments (it cannot be affected by contaminants) and, most of all, they can operate in a wide range of temperatures. In the last year the research has extended the range of admissible temperatures (from -270° to 300°) [5], thus perfectly matching with the previously mentioned requirements in chapter 2. A Hall sensor can, besides, measure both a positive and negative magnetic field.

As far as the disadvantages are concerned, we have a low accuracy: the shape of the signal is a function of the distance of the magnet [4] and for slow rotation it can become more flat, decreasing the possibility of a sufficiently precise position as required by this application.

Commonly, a magnetic encoder uses a series of magnetic dipoles to survey the position of a magnet on a shaft: The Hall sensor, combined with an express software (a specific algorithm), will be placed on the stator thus making the encoder capable to detect the magnet. Therefore, a microprocessor/microcontroller will be required, to take the information from the sensor, used as an input for the calculator, and, after having processed it, to evaluate the angle of the shaft.

3.2.3 Absolute Encoders, On/off axis Encoder

An absolute encoder is able to keep the information on the position of a rotation shaft in case of removal of the power. It is possible to obtain it once the system power is restored. Differently from a generic incremental encoder, it does not require a recording of the previous position. Increasing the resolution means to increase the precision of the position to be detected, as previously introduced.

An on-axis magnetic encoder typically uses a Neodymium diametrically polarized magnet coupled with a Hall-effect sensor array: placing the magnet over the surface of the sensor (contact is not required), the latter will be able to capture the orientation of the magnetic field provided by the magnet poles as shown in figure 10. The magnet is usually stick or sold to the rotating shaft, perfectly aligned with the rotation axis: in this way the reference system of the magnet will be the same of the shaft one, providing its angular position.

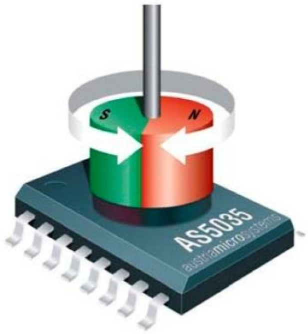

Figure 10: A common on-axis magnetic encoder

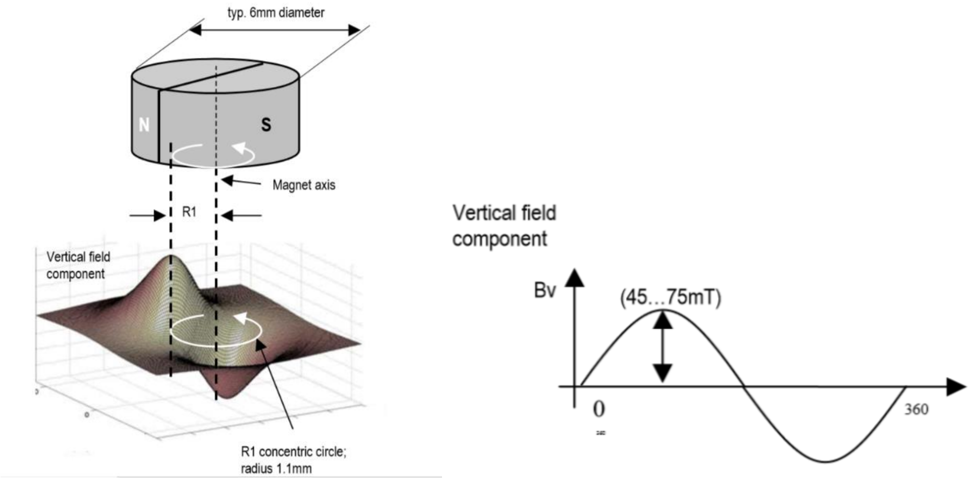

Figure 11: a) A common magnetic field distribution over an AS5145 sensor with a magnet (6x3 mm) diametrically magnetized b) vertical field component

The other type of magnetic encoder is the off-axis encoder, with the sensing system placed out of the rotation axis. Commonly, a magnetic off-axis encoder can use an array of magnetic stripes placed in the rotating component. The working principle is similar to a Gray code optical encoder, replacing the optical pattern with a magnetic dipoles pattern: the sensor, passing over the source of the signal, will be able to recognize the position of the shaft by combining the signal sources. The resolution of these sensors increases with the complexity of the patterns. Another way to provide the signal for this kind of sensors is to use a magnetic polarized ring, as shown in the picture below.

Figure 12: A common off-axis encoder (AS5304, 12-bit of resolution)

3.3 State of the art/patents consulted

Based on previous articles [4], the magnetic technology has been selected for the construction of the device: a few configurations for the magnetic encoder have been considered before starting the work, focusing on those that have specific application in the aerospace field. A research in the industrial field has also been performed, trying to evaluate the cost-benefit relationship of a generic absolute encoder. For a higher resolution than the required 16-bit resolution, the cost ranges from 800 € to 1000 €. Just to give an example, an absolute encoder with a housing of 38 mm of diameter, 17- bit of resolution, and an operative temperature ranging from -15° to 100° costs 833 €, with 22-bit of resolution 1,433 € [9].

Figure 13: Absolute encoder Dynipar AC36, 17-bit of resolution

3.3.1 High resolution absolute orientation rotary magnetic encoder

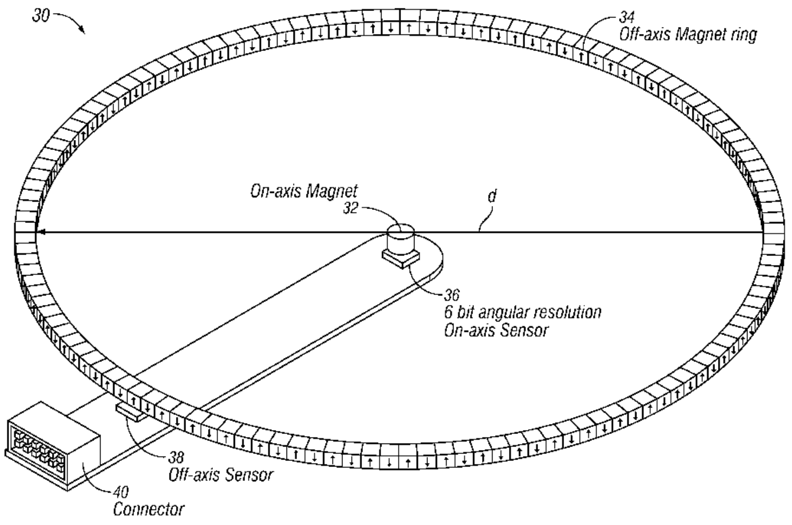

Figure 14: Magnetic encoder configuration with on/off-axis magnetic sensor

The patent combines the information from an off-axis encoder and an on-axis encoder; to this end a polarized ring needs to be placed coaxially to the shaft and to rotate with it, plus a central magnet must be placed over the on-axis sensor that has to move with the magnetic ring. The first sensor is placed over the magnetized ring, and is able to detect, by the changing of the voltage, the polarization of the portion of the ring in which it is placed at each time. Is required that the number of the pole pair dipoles matches the angular resolution of the on-axis sensor, achievable with a preliminary work of precise calibration. Then, the off-axis sensor will hover the portion of rotation covered by each single magnetic dipole, by discretizing it with a resolution of 12-bits.

It is important to consider some numbers for a better understanding of the device. For instance, an angular resolution of 18-bit can be obtained by combining a sensor of 6-bit of resolution on the on-axis sensor, and the 12- bit resolution sensing system. Matching the resolution of the on axis sensor and the pole pair solution is of fundamental importance (as explained in the patent [9]), this allows the user to:

1. Divide an entire turn, with the 6-bit resolution on-axis encoder in 64 steps (2^6=64, 360/64=5,5625°);
2. Divide further the obtained angle of 5,5625° in 4096 steps (2^{12}= 4096, 5,5625/4096 = 0,00137°);

This is equal to 360/2^{18} that corresponds to a resolution of 18-bits [8].

However, this configuration cannot fit the needs of our pointing mechanism for several reasons: first of all, the center of the axis is “filled” by the wave guide in this mechanism (the rotation axis is coincident with the rigid system that allows the signal to “flow” to the main system), so the on-axis sensor has to be rejected; furthermore, a preliminary precise calibration procedure is required in order to adapt it to the system and, in this work, this was not possible. Finally, considering the required money and resources, the multipole magnetized ring is not a cheap component (during the research some magnets manufacturer, like Dexter Magnetic Technology or Supermagnete, have been consulted). For the example showed here, an AS5311 for the off-axis sensor (working principle showed in figure below) and AS5145 for the on-axis sensor have been used.

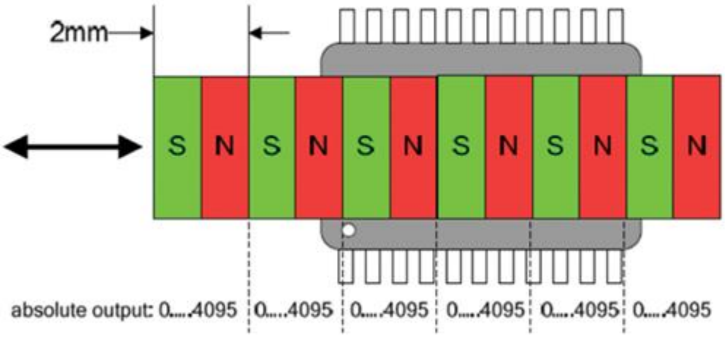

Figure 15: The AS5311 in a linear sensing mode (off axis sensor).

However, this patent results useful to understand the meaning of resolution and for the future considerations that will be made in this thesis.

3.3.2 Disk type of an absolute-position magnetic encoder for rotary devices

The working principle is similar to that of a Gray code optical encoder. In this case the source of information is not a light-source but an arrangement of permanent magnets; these are magnetic rings shaped and mounted as shown in the picture to reduce the radius of the rotating component They are placed coaxially one above the other and fastened with the rotating shaft. With the rotation, the system will provide as output an array of binary identification signals as shown in the picture (b). Using this array of outputs, it is possible, through an express calculator, to evaluate the position of the shaft in each moment. The sensing technology can be placed outside (on the support) or inside (in a fixed shaft) the drum made of permanent magnets, as showed in the picture below. By increasing the number of polarized coaxial magnetic rings, it is possible to improve the resolution of the encoder but this can also be achieved by increasing the diameter of the rings, allowing to host more dipoles and further improving the resolution [10]. This configuration requires several hardware components to reach the position with the required resolution: for example, to have a resolution of 16-bit would mean to have an array of 16 sensors and 16 magnetic rings of the same diameter that would lead to a too large device.

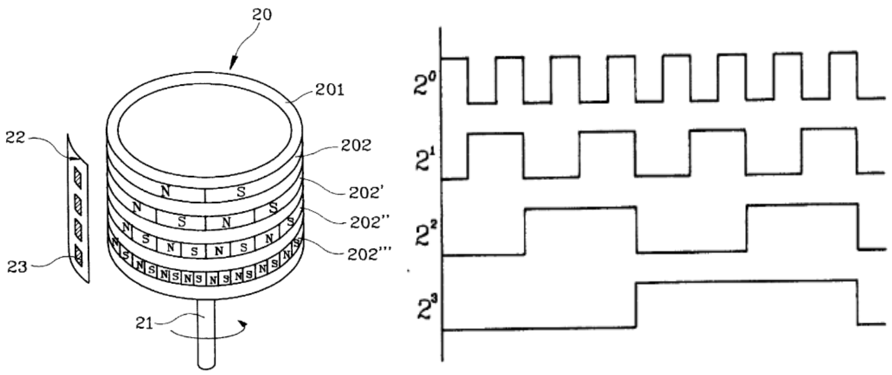

Figure 16. Manufacturing of the drum and sampling of the signals

3.3.3 Rotation detecting device and bearing assembly.

Another practical configuration can be obtained by placing the magnet rings coaxially but in the same rotating plane, as shown in figure 15, with the corresponding number of Hall-effect sensors placed over them. By rotating, the sensor will detect the magnetic field of the ring providing a signal that can be easily approximated with a sinewave function, with a constant period coinciding with the width of the pole magnet. As in the previous example, the polarity of the magnet of the rings is alternated as shown in figure 15. The key feature is to have a different number of poles for each whole ring (i.e. see figure 17 below), this can provide two different sinewave plots with different frequencies. Considering these amount of dipoles in the magnetic rings, the amplitudes of the two plotted sinewaves will be equal only for some rotation angle, as shown in the figure 18. The information on each position of the rotating component is obtained by evaluating the phase of each plot and by comparing them to each other (by subtracting one to the other). In this way we can obtain the delay of one of the two plots compared to the other: this delay can be converted into an angular position with an express calculator.

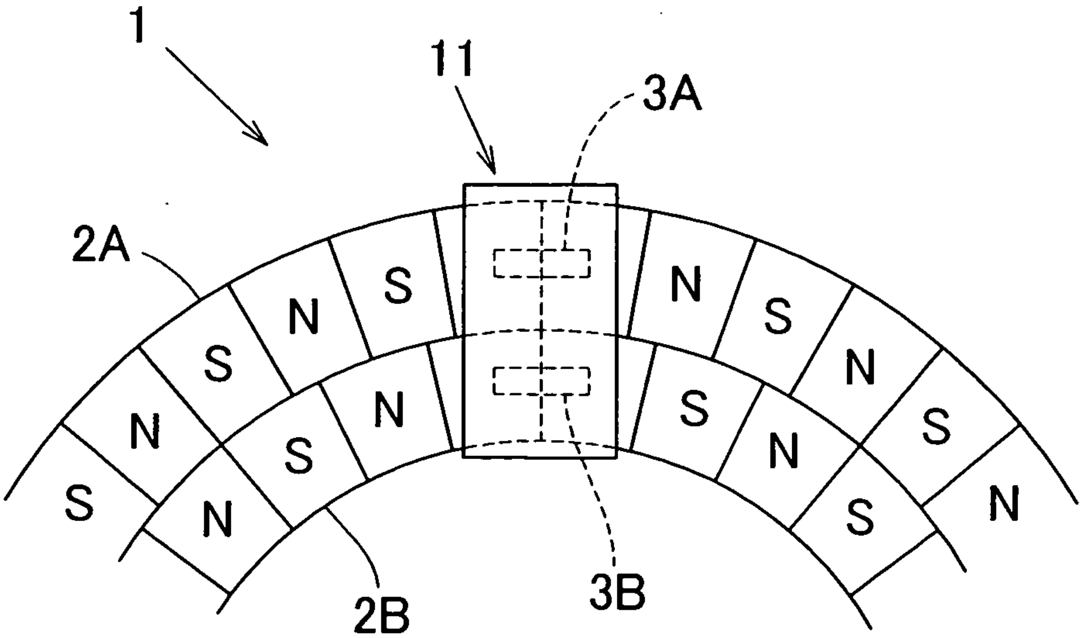

Figure 17: Set up of the magnetic rings

Fig. 6

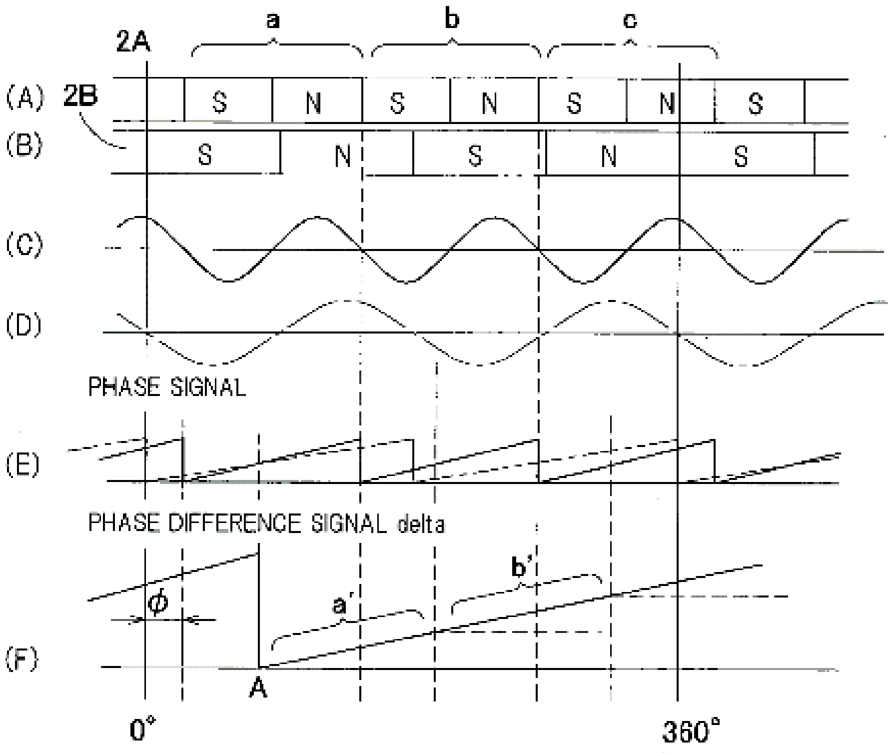

Figure 18: Outputs from the magnetic sensors placed in the considered patent

The advantage of this set up is to allow a sensor to sample the trend of the magnetic field and fit the data with an approximate sin function with a constant frequency, that function can be used as mathematical parameter to find the zero-position.

3.3.4 Enhanced revolution

Another solution to easily detect the zero position that has been evaluated during the study can be obtained by using a gear-box to enhance the revolution of the main cogwheel. Considering the well-known relation of the gear train:

$$N1/N2 = W1/W2 \tag{3.1}$$

In the equation N1 and N2 are respectively the numbers of teeth of the first and the second cog-wheel, W1 and W2 the rotating velocity, it is possible to see that increasing the gear ratio we can increase the velocity of the second wheel. Placing a magnet on a wheel sold in the same shaft of the second wheel is equal to having a magnet positioned at a higher distance from the main rotation axis; this allows to have a thinner signal displayed through a Hall sensor, using the consideration made in paragraph 2.2 (figure 6). The set up can be better understood by observing the CATIA file shown below. In the figure 19 20 two Hall sensors placed in an express support row can be seen: the one that is placed on the top surface of the row is able to detect the presence of the magnet placed in the main cogwheel; this can give to the user an idea of which portion of the rotation the zero position is in. The second Hall sensor, placed beneath the support row, will detect a magnet placed on the rotating flywheel; this one will display a signal much “thinner” than the one for the magnet detected on the main cogwheel. Therefore, this signal, during the rotation of the main cogwheel, will be repeated for a number of times equal to the gear ratio of the joint: the function of the first Hall sensor is to distinguish which of these signals is the one that provides the zero position. This solution will be taken into consideration in the case in which the first tests, mechanically more simple, will fail to give a precise detection of the zero position.

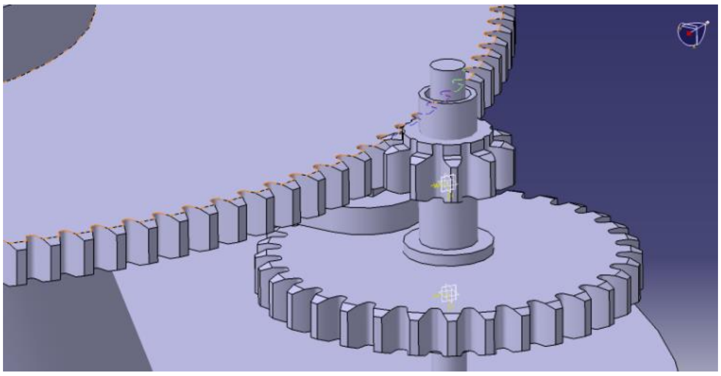

Figure 19: Isometric view of the mechanical improvement

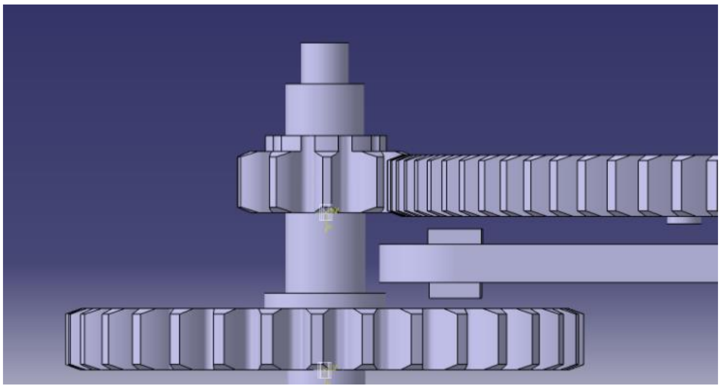

Figure 20: Set up for enhancing the revolution of the main cogwheel

4 ANALYTICAL MODEL

4.1 Chapter overview

The purpose of this chapter is to describe the main aspects of the selected configuration. In the first paragraph the series of preliminary tests performed with the Arduino instrumentation will be listed, describing the Hardware and the Software used. Thus, the way in which the setup will operate to record the signal and the way it will be processed to find the position will be described, analyzing its shape, what is the best mathematical approach among the ones considered in the preliminary tests (peak detection, threshold, cubic spline, b-spline, coupled sensors).

4.2 Preliminary tests

4.2.1 Hardware setup

In the first part of the work some fit interpolation methods have been studied and tested using a coarse simulation of what would be the shape of a signal displayed from a sensor in an analog output. The LRT department provided a box containing of the following items:

1. An Arduino Mega2560 Board.
2. A Hall effect sensor SS495A1 [12].
3. A set of Ni-Cu-Ni magnets of different dimensions (S-05-08-N).
4. Wires.
5. Breadboard.

After a simple setting of each pin, a VI has been created with LabVIEW, to display the Voltage variation on the laptop screen, through the Lynx interface, an express software patch optimized for the exchange of data between LabVIEW (Software) and Arduino (Hardware). Making the magnet hover the sensor (with a raw rotating mechanism), it was possible to see voltage variation in a circuit on a Waveform Graph display on the VI. By an express homemade joint, it was possible to simulate the motion of the magnet stick on a shaft rotating over the sensor, and, by changing the speed of the joint, to observe the signal shapes change.

4.2.2 Shapes of the signal

As previously discussed, the shape of the signal changes as a function of the rotational speed: a high rotational speed provides a thin/slim (figure 6a) signal and a low rotational speed provides a flattened shaped signal. The signal is displayed in a Voltage range between 0 and 5 Volts, where:

- ~ 5 Volts corresponds to proximity to the magnet’s positive pole.
- ~ 0 Volts corresponds to proximity to the magnet’s negative pole.
- ~ 2,5 Volts corresponds to no magnet detected.

The signal was recorded only when the Voltage exceeded the value of 2.7 Volts, as shown in figure 22. In these preliminary tests the signal in an array of 30 points through a shift register has been plotted, with a sampling rate of 25ms. In the next paragraph it will be described how this array of points has been used to find the point of interest of the signal. The most promising methods are listed below, according to their increasing complexity: during the test phase the interpolation fit-methods have been tested simultaneously for a most efficient comparison.

4.3 Starting data, variable evaluation

4.3.1 Independent Variables/Dependent variables

As previously mentioned, the independent variables involved in the problem are the following:

1. r: distance from the rotation axis
2. w: rotational velocity of the cogwheel (→ v: linear tangential velocity)

3. d: diameter of the magnet
4. sr: sampling rate
5. V: threshold voltage
6. Methods used to process the signal
7. z: distance between the magnet and the sensors

By changing these elements, will be possible to have a different output in this problem. This output is described by the following parameters, that represent the dependent variables.

1. Shape of the analog signal (dependent on the chosen rotational speed and threshold voltage)
2. Shape relative to time axis (dependent on the rotational speed)
3. Discretization (dependent on sampling rate, speed of the rotor, it will provide a higher or lower resolution on the x axis of the signal plotted)
4. Analog/Digital resolution (dependent on the rotational speed and the sampling rate)
5. Shape relative to the z-axis (Voltage) (dependent on the distance of the magnet from the sensor)
6. Zero position of the rotation (dependent on each of the dependent variables)

The table shows the possible variable ranges for the application:

Table 3: Independent variable ranges

	Independent Variable / Parameter	Ranges / Step Size	Comment
1	ROTATION RADIUS (r):	40 mm, 50 mm, 60 mm, 70 mm	Range of distances allowed by the geometry of the cogwheel
2	VELOCITY (w): (main cogwheel):	1°/sec, 5°/ sec, 2°/sec, 10°/sec	Range of velocity similar to the ones during the operative phase

3	DYMENSION OF THE MAGNET (d):	2mm, 3mm, 5mm	Diameter of the magnet
4	SAMPLING RATE (sr):	10ms, 5ms, 1ms, 0.5ms	Just to have preliminary idea (in the future won't be allowed by the spacecraft CPU)
5	ANALOG RESOLUTION:	24-bit (Voltage range between 0 and 3,3 V)	Best resolution allowed from the Arduino board and the ADC

4.4 Signal processing methods

4.4.1 Peak detection

The simplest way to find a signal could be finding the peak of the curve displayed. This hypothesis is true only in the case of a symmetric and thin signal. The advantages of this method is to be cheap from a computational point of view: the CPU of a spacecraft usually is not sufficiently powerful to accomplish several operations in a small amount of time and a simple method like this has to be tested to ensure its reliability, due the sensitivity of the sensor to the environment in which it is located (temperature dependent, radiation).

4.4.2 Mid-point finder

Another easy way to determine the point of interest of the signal is to use the its mid-point. Assuming, from the previous hypothesis, a symmetric shape is possible to find the position of the shaft when it is in the middle of the signal. This method could be less affected by the noise present in the environment with a proper selection of the starting and ending points when the voltage exceeds a threshold value previously imposed. For the efficiency of the method, a good choice of the optimal threshold voltage (V_t) value is required.

4.4.3 Cubic spline fit

Considering a more complex mathematical method, the Cubic spline method is a good alternative. With an array of observations (X, Y) with X as the angular position and the Y the output voltage, the cubic spline fit works by minimizing the following function:

$$p\sum_{i=0}^{n-1} w_i (y_i - f(x_i))^2 + (1-p)\int_{x_0}^{x_{n-1}} \lambda(x)(f''(x))^2 dx \tag{4.1}$$

Where:

1. p is the balance parameter.
2. Wi is the weight of the ith element.
3. yi is the ith element of Y.
4. xi is the ith element of X.
5. f"(x) is the second-order derivative of the cubic spline function,
6. f(x). (x) is the piecewise constant

(x) = i, xi x < xi+1, for i = 0, 1, n–2

where i is the ith element of smoothness.

By changing with the balance parameter (range 0-1) it is possible to obtain a function that best fits the need of the user. After that, it is simple to find the peak of the curve. In the following figure it is shown how the fits shape changing the balance parameter on a random array of sampled points. The setting of this parameter is useful when we need to process a highly flattened signal: finding the right value would mean to shape the output fit in a more parabolic way, enabling the user to easily find his maximum.

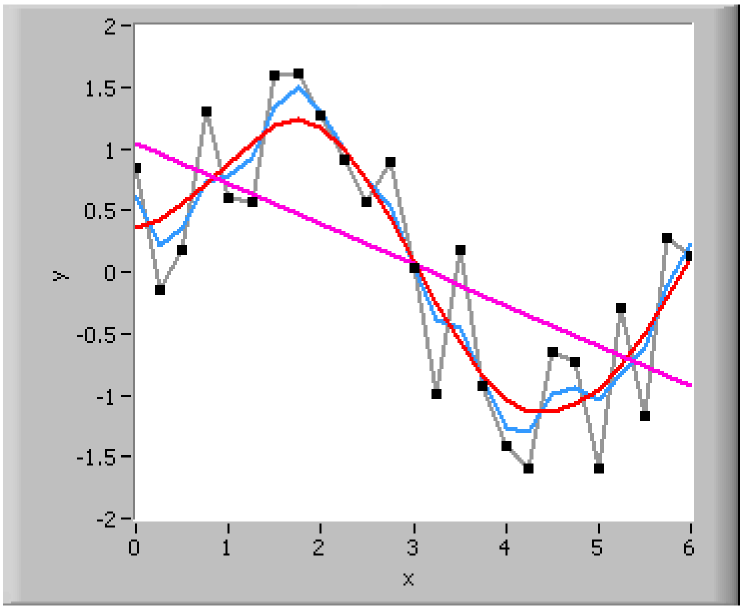

Figure 21: linear interpolation (grey), cubic spline with balance parameter equal to: 0 (purple), 0,9 (red), 0,9555 (blue), 1 (grey)

4.4.4 B-spline fit

The B-spine fit is a particular kind of spline that calculates the best B-spline-fit by minimizing the residue according to the following equation:

$$\frac{1}{N}\sum_{i=0}^{N-1} w_i \bullet \left\|(x_i,y_i)-(x'_i,y'_i)\right\|^2 = \frac{1}{N}\sum_{i=0}^{N-1} w_i \bullet \left[(x_i-x'_i)^2+(y_i-y'_i)^2\right] \tag{4.2}$$

where:

- N is the length of the vector Y.
- wi is the ith element of Weight
- (xi, yi) is the ith pair of the input sequences (X, Y)
- (x’i, y’i) is the ith pair of (Best B-Spline Fit X, Best BSpline Fit Y)

By looking at the obtained results we can observe that the plot of the fitted model tends to be continuous, by avoiding discontinuities (a behavior similar to the FFT). This allows to have a lower region in the center of the flat region of the signal: the minimum of this region can be used to detect the central point of the signal (figure 22). As the previous one, this method is reliable in the majority of the sampling cases but, considering the limited capability of a generic spacecraft processor (200Mhz), it is not an affordable solution. In the next picture a comparison between the different fit methods is given.

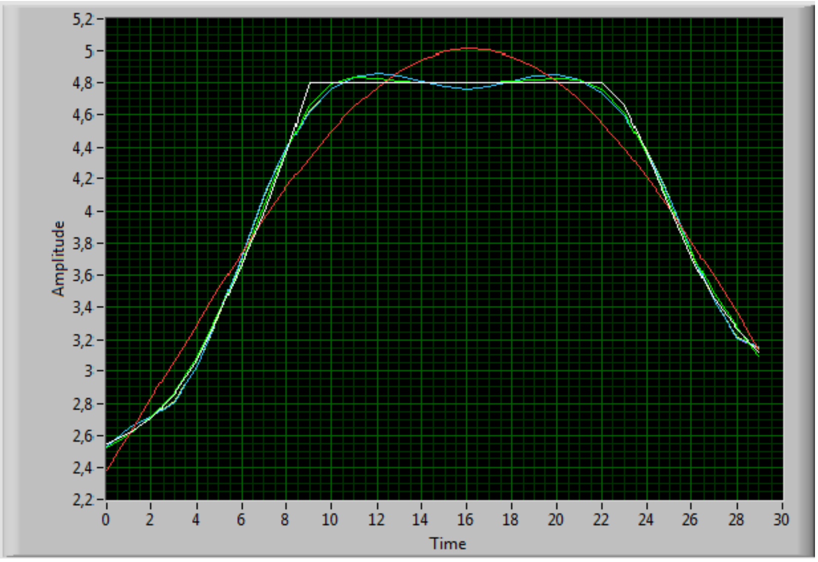

Figure 22: Comparison between different fit methods: original signal (white), Gaussian fit (red), B-spline (light blue, green)

4.4.5 Gaussian fit

This method uses the iterative general Linear Square method and the Levenberg-Marquardt method to fit data to a Gaussian curve in a form described by the following equation:

$$f = a \bullet \exp\left(-\frac{(x-\mu)^2}{2\sigma^2}\right) + c \tag{4.3}$$

Where:

1. x is the amplitude
2. μ is center,

3. σ is standard deviation
4. c is the offset.

This VI finds the values of *a*, *μ*, and *c* that best fit the observations taken (**X**, **Y**). The following equation specifically describes the Gaussian curve resulting from the Gaussian fit algorithm:

$$y[i] = a \bullet \exp\left(-\frac{(x[i]-\mu)^2}{2\sigma^2}\right)+c \qquad (4.4)$$

If the noise of **Y** = **Y** is Gaussianly distributed, use the Least Square method. The following figure shows the Gaussian fit obtained using this method. The magnet noise affecting the displayed signal can be easily processed by this method at this level of accuracy but, as the previous two methods, it requires a superior amount of calculation to display the results.

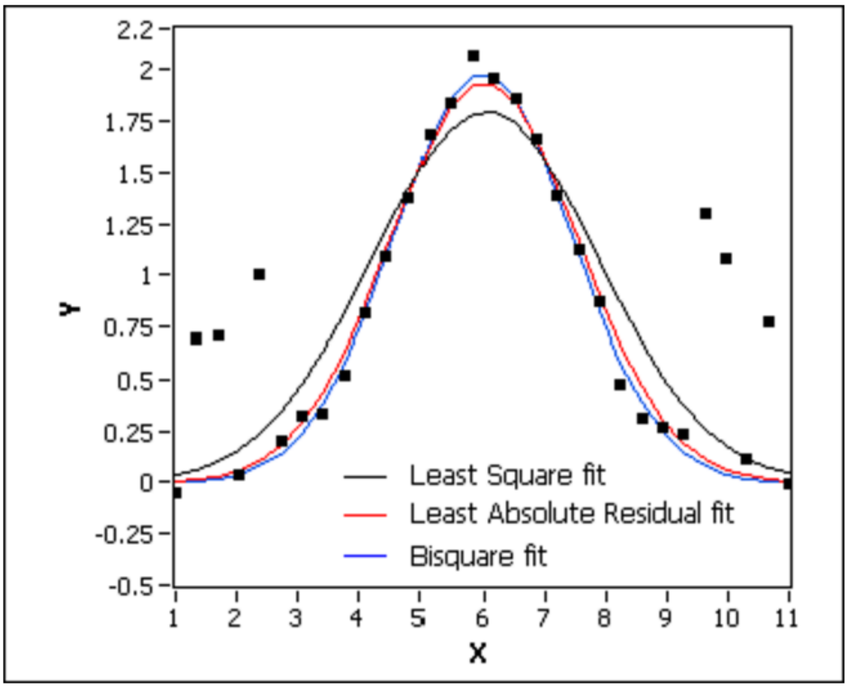

Figure 23: Different Gaussian methods

4.5 Linear approximation

The Zero position accuracy required is 16-bit, so, with easy calculations:

$$2^{16} = 65536,\ 360°/65536 = 0{,}005493° \qquad (4.5)$$

That is the required accuracy in angular terms. The table below shows an example of the angular resolutions achievable, in terms of degree, with different sampling rates (rows) and different main cogwheel rotational velocities.

Table 4: Angular resolution achievable by changing the main cogwheel speed and the sample rate

main gear speed[°/s] **sampling rate[ms]**	**1**	**2**	**5**	**10**
0.5	0.0005	0.001	0.002	0.005
1	0.001	0.002	0.005	0.01
5	0.005	0.01	0.025	0.05
10	0.01	0.02	0.05	0.1

It is easy to see that by increasing the sampling rate of the device it is possible to achieve a higher angular resolution, assuming a fixed angular velocity.

Some considerations to simplify the problem have been made: to obtain an easy analytical model it is possible to switch from the angular configuration to the linear one, by adopting the small angle approximation (<15° per step).

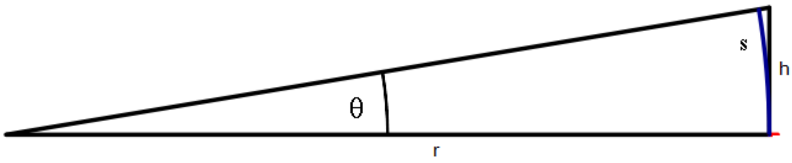

Figure 24: Geometrical elements to linearize the problem

$$h = r * \sin(\theta)\ [mm] \qquad (4.6)$$

In this set-up, for angles under 15° it is possible to adopt the small angle approximation, to switch from a non-linear function to a linear one and hence to consider the motion of the magnet as linear. Starting from the well-known relationship:

$$V = w*r \text{ [mm/s]} \tag{4.7}$$

V is the tangential velocity, w the rotational velocity and r the radius. Now, as the angular resolution required, also the linear has restriction in term of resolution. The next table shows the resolution required achievable in terms of linear distances [mm] as the the distance of the magnet from the rotation axis, r [mm] changes; in the table it is easy to see how by increasing the distance (between the position of the magnet and the center of rotation) the linear resolution decreases (the maximum linear/angular distance required between one sample and the next one is larger). In the table below it is possible to notice that the most convenient configuration, in terms of allowed sampling frequency, is the one corresponding to 70 mm of distance from the rotational axis.

Table 5: Linear resolution required for each selected radius

Radius [mm]	Linear resolution required [mm]
40	0.00376
50	0.00471
60	0.00565
70	0.00659

For different configurations, it is possible to achieve different linear velocities, expressed in millimeter per second: this table list the tangential velocity of a generic point placed on a given rotational radius and with a given rotational speed.

Table 6: Tangential velocity [mm/s] achievable changing the radius and the angular velocity

Rotational speed [°/s] Radius [mm]	1	2	5	10
40	0.698	1.396	3.490	6.980
50	0.872	1.745	4.363	8.726
60	1.047	2.094	5.235	10.471
70	1.221	2.443	6.108	12.216

Table 7 below shows, using the results of the previous table 6, the linear accuracy achievable [mm] with several sampling rates (sr) and different main cogwheel velocities, with a radius of 70mm (in grey the configuration allowed by the level of resolution required). In the table the highest angular accuracy achieved is 0.0005° and the lowest 0.1°, the highest linear accuracy is 0.0006 mm and the lowest 0.122 mm. The most important fact that is shown in this table is that to achieve a high angular or linear resolution it is necessary to have a low rotational speed of the cogwheel and a high sampling rate.

Table 7: Angular resolution [°/s] achievable by changing the sampling rate and the rotational speed (in grey the resolution allowed for this application)

Main gear speed[°/s] sampling rate[ms]	**1**	**2**	**5**	**10**
0.5	0.00061	0.0012	0.0024	0.0061
1	0.0012	0.0024	0.0061	0.012
5	0.0061	0.012	0.03	0.061
10	0.03	0.024	0.061	0.122

4.6 Features of the clipped signal

Depending on the position of the sensor over the magnet, it is possible to obtain two different configurations: the clipped or the unclipped signal. In the next two sections are exposed the main features of and presented some of the most convenient methods to process it. After the test phase, the unclipped signal has been selected as the most convenient solution to find the zero position; here it is shown an alternative way to process a clipped signal too, in case the geometric constraints of the support would not allow to freely choose the magnet/sensor distance.

Considering the clipped signal:

1. Main width (in the picture, Voltage exceeded: ~2.5Volts) length of the signal that has exceeded the threshold voltage of 2,5 V

2. Width of the flat region (in the picture, Voltage exceeded: ~4.8Volts) length of the signal when the voltage exceed the maximum voltage allowed by the hardware

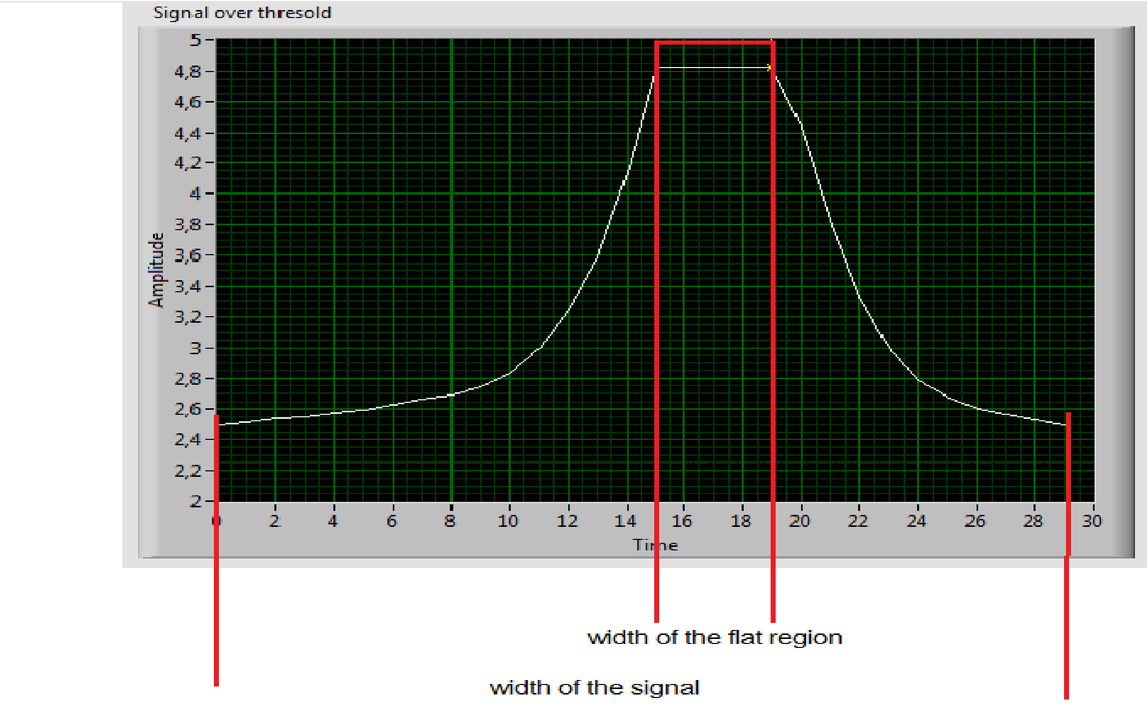

Figure 25: Characteristic parameters of the clipped signal

From preliminary tests: flat region, function of the dimension of the magnet (when the magnet stands over the sensor, the voltage output, using a resolution of 10bit, appears constant on a value around 4.8 Volts). It is important to keep in mind that this voltage amount is theoretically reached when the face of the magnet starts to cover the sensitive surface of the Hall sensor.

Considering for instance the set-up used in the preliminary tests, represented in the figure below, with a Hall sensor with a square sensing surface of 3x3 mm and a magnet of 3mm of diameter, it has been observed that, using an analog resolution of 10bit, the Voltage reaches 4.8Volts (ideally) from the time at which the front side (considering the direction of the motion) of the magnet starts to cover the sensing surface of the sensor, till the time the back side of the magnet stops covering it.

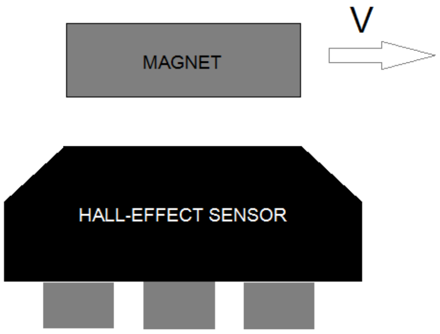

Figure 26: Magnet crossing the sensitive surface of the Hall sensor

On a first approximation, the signal can be assumed to be symmetric for the following reasons:

1. The tests are performed in an environment without any magnetic perturbation, nor proximity to ferromagnetic materials.
2. The velocity of the cogwheel does not change.
3. The vertical distance of the magnet from the sensor is constant.

4.6.1 Check on the resolution:

This kind of motion (geometrical features chosen: magnet with a diameter 3mm, sensing surface 3x3mm) can be compared to the motion of a discrete point over the sensor whose length is the triple of the real surface length and hence takes the triple of the time to cross the sensing surface.

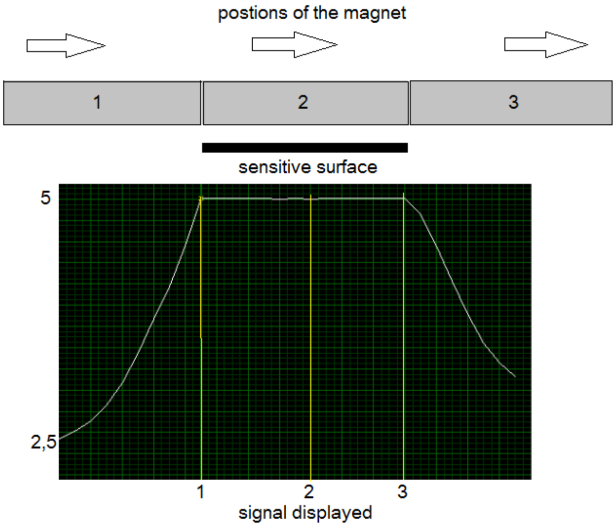

Figure 27: Motion of the magnet over the sensitive surface of the Hall sensor

Table 7: Linear resolution required [mm] per each radius selected

Radius [mm]	**Linear resolution required [mm]**
40	0.00376
50	0.00471
60	0.00565
70	0.00659

Now, for a better understanding of the working principle, some examples are given: let us consider a magnet of 3mm placed at a distance of 70mm from the rotation axis of the shaft, that rotates at:

1. 1°/sec, sr = 10ms
2. 1°/sec, sr = 5ms
3. 10°/sec, sr = 0.5ms

1. <u>Angular velocity 1°/sec</u>: linear velocity of the magnet (whose radius is r=70mm): v = 1.221 mm/s

V = s/t (s = 9mm) → t = 7.371s

N = t /sr (sr=10ms) = 737.1 = number of samples in the flat region of the signal

Check procedure on the resolution: 9mm/737=0.0122 mm → not good enough (>0.00659 mm, see table of the linear resolution required).

The sr needs to be increased.

2. <u>Angular velocity 1°/sec</u>: linear velocity of the magnet (r=70mm): v = 1.221 mm/s

t = 7.371s

sr = 5ms

N = t/sr =1474.2

9mm/1474 = 0.0061mm → ok! (< 0.00659mm)

3. <u>Angular velocity 10°/sec</u>: linear velocity of the magnet: v = 12.216 mm/s

t = 0.7371s

sr = 0.5ms

N = t/sr =1474.2

9mm/1474 = 0.0061mm → ok! (<0.00659mm)

The same calculations have been done for each pair speed/radius. The table shows the lowest resolution/sample rate in [s], among the ones chosen for these tests, allowed for each configuration, diameter of the magnet 3mm, with the corresponding linear resolution achieved [mm] (strictly less than the values appearing in table 7):

Table 8: Lowest sampling rate allowed to reach the required resolution

Rotational speed [°/s] Radius [mm]	**1**	**2**	**5**	**10**
40	5 (0.00349mm)	1 (0.00139mm)	1(0.00349mm)	0.5 (0.00349mm)
50	5 (0.00436mm)	1 (0.00174mm)	1(0.00436mm)	0.5 (0.00436mm)
60	5 (0.00523mm)	1 (0.00209mm)	1(0.00523mm)	0.5 (0.00523mm)
70	5 (0.00615mm)	1 (0.00244mm)	1(0.00618mm)	0.5 (0.00618mm)

In the previosu table we can see how the distance from the rotation axis does not affect significantly the required sampling rate. Considering the range admitted in the future tests, having a magnet close to the rotational axis or far will not have an influence on the hardware required for this accuracy.

4.6.2 Signal width as function of the number of samples

In the next table 9, differently from the previous one, the number of samples used for the flat region (N) is shown, with the same geometry considered (3x3 mm of sensing surface and 3 mm of diameter of the magnet)

Table 9: Estimated number of samples on the flat region, for a magnet of 3mm of diameter over a sensitive surface of 3x3 mm

Rotational speed [°/s] Radius [mm]	**1 (5ms)**	**2 (1ms)**	**5 (1ms)**	**10 (0.5ms)**
40	2578	6474	2578	2578
50	2064	5172	2064	2064
60	1720	4306	1720	1720
70	1463	3688	1463	1463

It is easy to see how the solution with the highest distance from the rotation axis (70 mm) uses the smallest number of samples. The width of the flat region (number of samples) as a function of the time, the rotational speed and the dimension of the magnet (fixed 70mm radius), obtained with the sampling rate previously selected for each case:

Table 10: Number of samples required for each magnet diameter and rotational speed

Rotational speed [°/s] Dimension of the magnet [mm	**1 (5ms)**	**2 (1ms)**	**5 (1ms)**	**10 (0.5ms)**
2 (s=7mm)	1146	2865	1146	1146
3 (s=9mm)	1474	3683	1473	1473
5 (s=13mm)	2129	5321	2128	2128

NOTE: We can easily see that the most convenient solution is to choose the smallest magnet (less number of samples).

The goal of the tests will be to find the right threshold voltage that allows the user to have the same number of samples calculated in the analytical model.

4.6.3 Proposed algorithm

Here is proposed an algorithm for the processing of the signal obtained in case of unclipped signal. The loop is able to adjust the threshold voltage comparing the number of samples obtained in the first sweep of the magnet over the sensor with the expected ideal number. For each loop a new sweep is required.

Inputs (starting threshold voltage (V_t), rotational speed (w), radius (r), dimension of the magnet (d))

1. V, linear/tangential velocity of the magnet
2. Dimension of the magnet → s (ideal width of the flat region) → t → N_i (ideal number of samples)
3. Record signal when exceeds the stated threshold voltage → N_r (real number of samples)
4. If $N_i > N_r$ → increase V_t
5. If else $N_i < N_r$ → decrease V_t
6. Else $N_i = N_r$ → $N_r/2 = N_{mid}$ → associate the angular position of the shaft to N_{mid}

4.7 Features of the unclipped signal

The choice of the best method is limited to a mid-point or a peak detection, with the use of the other fit method to help the analysis: the way to process the signal shape it is simpler and hence preferable with respect to the clipped signal. Whenever it is possible, it is advisable to place the magnet at a distance that would avoid the clipping of the signal, if not, the solution has been proposed in the previous paragraph. The tests presented in this thesis (chapters 5, 6 and 7) have been made only with an unclipped signal.

4.8 Discussion on the size of the magnet

The LRT department provided a set of magnets of different dimensions. It has been noticed that each magnet provides a different magnetic field magnitude. For this reasons, it is necessary to adjust the distance between the magnet and the sensitive surface: for instance, having a bigger magnet (kept the distance fixed), would provide a higher value of the maximum voltage reached at the moment of maximum proximity with the magnet. Nevertheless, having a wider voltage range to detect, provided by a wider “magnetic jump” from a bigger magnet is useless using an ADC or the Hall sensor chosen previously; the voltage range is limited by the devices. Considering for instance the ADC, the possible voltage range to display in a graph of LabVIEW varies between 1,6 V and 3,3 V. In terms of analog resolution, the size of the magnet is un-influent. As far as the number of samples is concerned, having a bigger magnet would mean having a more flattened shape (in both the clipped and unclipped signal case) of the signal and, in terms of data, a higher number of samples o take to display the whole number of times that the voltage exceeds the threshold value.

5 TEST SETUP

5.1 Chapter overview

In this chapter the description of the selected configuration will be presented and the best way to integrate it with the existing hardware will be proposed. The selected hardware like the sensors and the mechanical component used and the way to control the motor are described and the mechanical constraints for building of the device like the gear ratio required for the running of the device will be exposed. Subsequently, it will be described: the way the data are sampled, how the sensors communicate to Arduino (electrical setup) with LabVIEW and the way in which the circuit has to be placed to fit the physical constraints of the existing hardware. Finally, an overview of the files used and how they interact with each other will be given.

5.2 List of materials and methods

Here are listed the Software and Hardware components used to perform the following tests:

5.2.1 Mechanical:

1. Stepper motor (VSS Python stepper motor for ultra-vacuum application)
2. Rotating cogwheel (gear ratio with the motor: 1:250, considering the harmonic drive of the mechanism (gear ratio 1:50) and the mechanical gear ratio between pinion and main cogwheel 1:5)
3. Breadboard
4. Support with a changing height (in this case made by a piece of wood stick bracket and the sensors/ aluminum support)
5. Magnet stuck to the cogwheel (Ni-Cu-Ni), S-02-02-N

5.2.2 Electrical:

1. Arduino Mega2560 board (+ supplement for LISA$_{ms}$ + ADC converter integrated)
2. Wires
3. Hall-effect sensor (SS495A1)
4. TMC4210+TMC2660 Motor Control Board
5. Connectors
6. VOLTCRAFT HPS-16010 (High-power laboratory power supply)
7. Resolver (EVAL- AD2S1210SDZ)
8. Laser pointer class 2 (Picotronic Laser module DI650-1-3(8x21)-ADJ)
9. PSD (S5990-01)
10. Arduino Mega2560 board (to interface PSD with Laptop used)
11. Laptop (Acer S3)

5.2.3 Software (LabVIEW VIs):

1. VI for the stepper motor control and settings of the its modes: Allow the user to set the motor velocity, the mode and a target position)
2. Zero position finder VI: uses the signal processing methods included and find the zero position of each fit method
3. VI for the laser pointer/target: used in the final test phase, to validate the developed model

5.3 Mechanical setup

In this paragraph it is described how the mechanical components have been set up to perform the tests; several pictures are provided, for a better understanding of the arrangement of each component.

Below a schematic view of the setup used to perform the tests is reported: the magnet is stick without using any kind of glue in the beginning (it was thought that the magnetic attraction was sufficiently strong to keep the magnet fixed on the Aluminum AA7075) in the rotating cogwheel at a distance of 65 mm (most convenient configuration, based on the considerations that will be made in the next chapter) from the rotational axis. In this way the magnet will cross the Hall Effect sensor maintaining the same distance (along the z axis) from it, moving on the same plane (also the most convenient distance between magnet and sensor will be discussed in the next chapter). The sensor is fed by a Voltage of 3.3Volts and sends its analog output (V_{out}) to the ADC (not displayed in the picture below.)

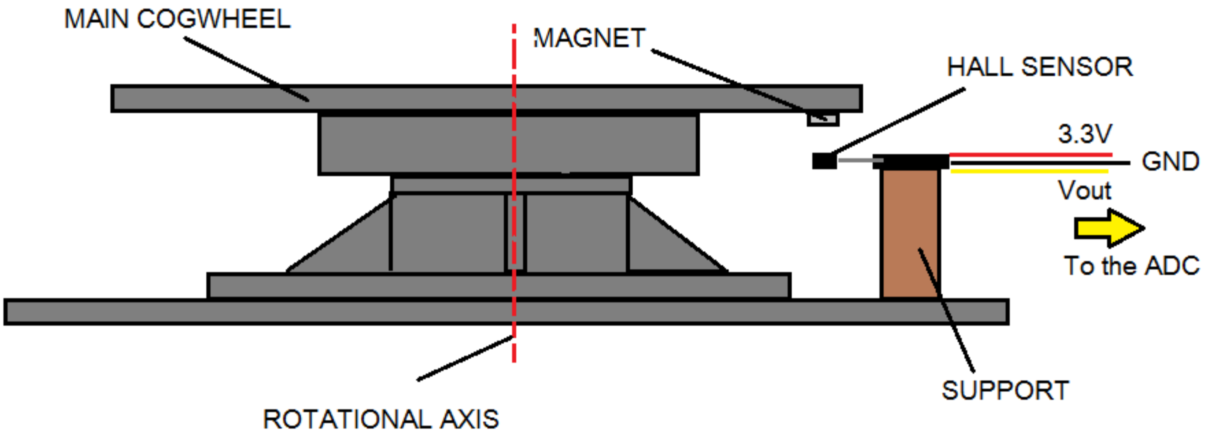

Figure 28: Mechanical setup of the tests

In figure 29 below a detail of the previous picture is shown, zoomed on the dimension that will be useful for the display of the results in the next chapter. It has been possible to change the height of the support to have several distances between the sensor and the magnet, a different maximum voltage recorded and a clipped or non-clipped signal depending on the conditions. Here the variables of figure 29, used in the following test phase, are listed:

1. H: height of the support
2. D: distance between the sensor and the support

3. h: height of the used magnet

DA QUI *****The sensing surface of the Hall sensor is considered at the same height of the support. Included in the hardware are also a set of cylindrical magnets provided by the institute with different diameters (2, 3, 5 mm), made of an alloy of Ni-Cu-Ni. The cogwheel was moved by a stepper motor PhytronVSS, an express device for high-vacuum applications (not displayed in the pictures).

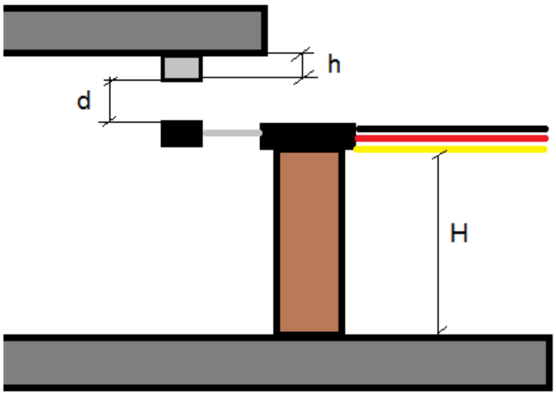

Figure 29: Characteristic mechanical parameters

The gear ratio between motor shaft and cogwheel is 1:50 and the internal harmonic drive of the motor has a gear ratio of 250:1. The angular velocity of the cogwheel has been calculated with a sub.vi included in the software, taking in consideration the values just presented. Bi-adhesive strips have been used to attach each component to the proper position.

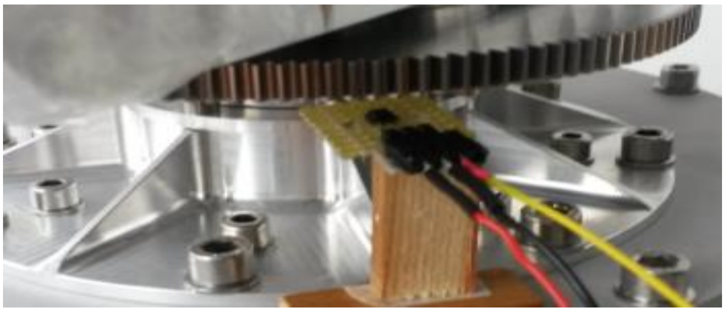

Figure 30: Setup made in laboratory

5.4 Electrical setup

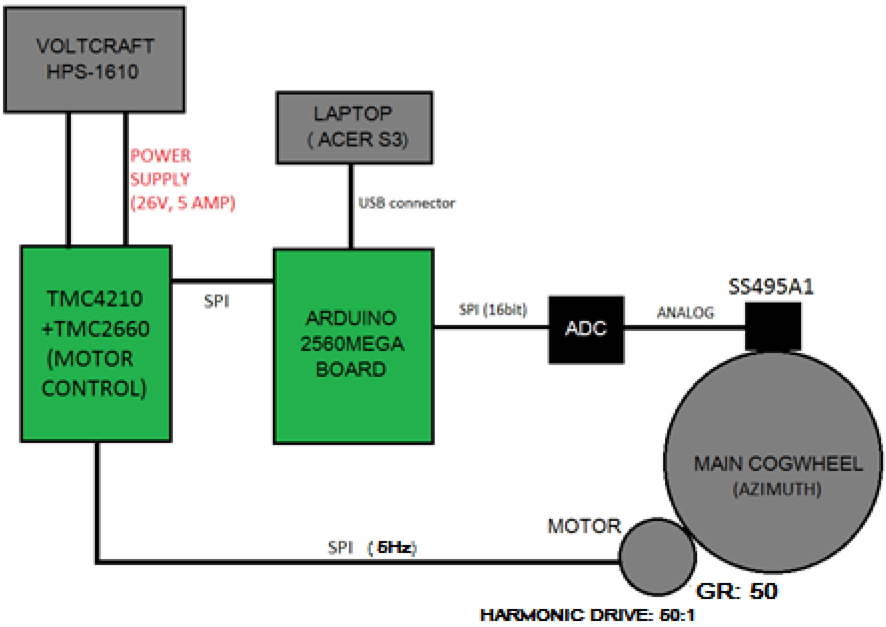

Figure 31: Electrical setup

Figure 31 shows the main electrical components of the setup used for the test, and it gives a representation of the mechanical parts involved: the power is provided by a Voltcraft HPS-16010 to the TMC4210, an express board for the current impulses for the motion of the stepper motor, controlled by the inputs sent by the laptop trough the Arduino board using an USB interface (mode, velocity), that transmit the motion to the main Azimuth cogwheel, in which the magnet is stuck. The latter will cross the SS495A1 Hall sensor that will send the signal to the Arduino Board trough the ADC converter. The signal will be displayed on the monitor of the Laptop in an express window created in the Front panel of the main VI**.**

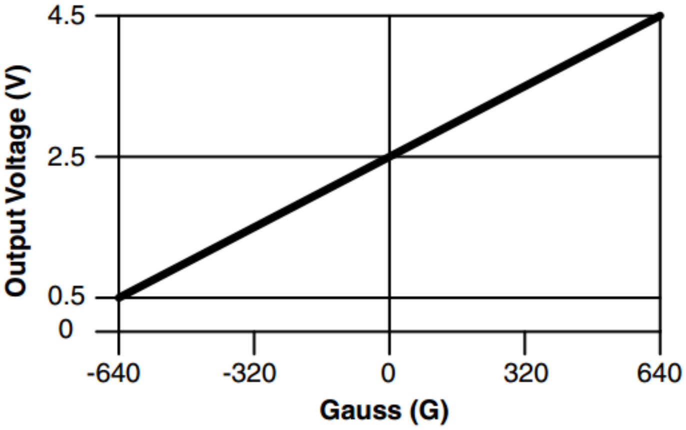

Figure 32: Typical output vs Magnetic field module (SS495A1)

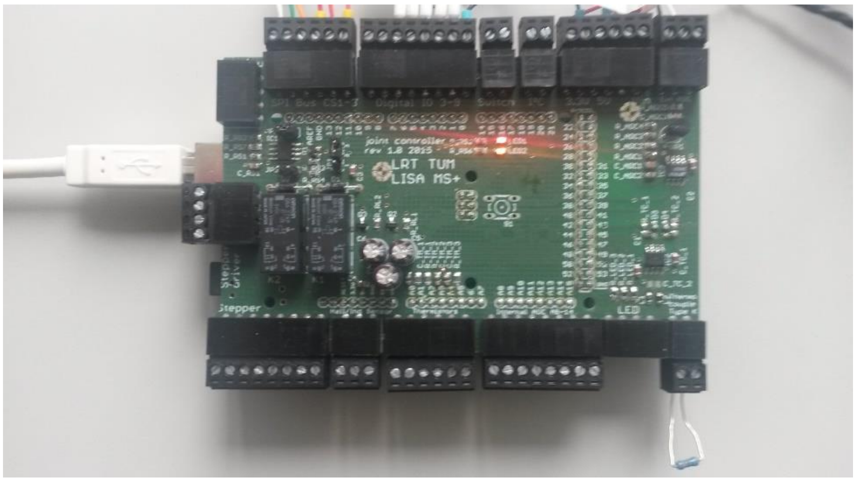

Figure 33: Mother board sold with the Arduino Mega 2560

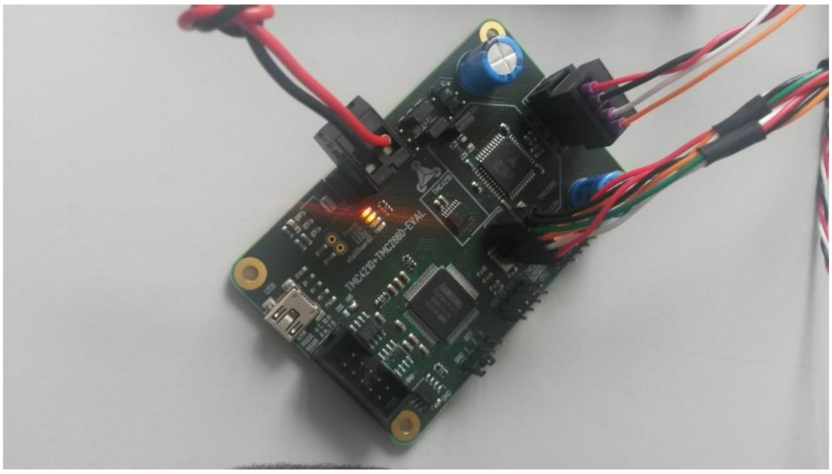

Figure 34: Control Board for the stepper motor Phytron VSS

5.5 Software setup

LabVIEW 2015 has been used as data acquisition and control software for all tests (including the supplements/patches for the DAQ, VISA, FPGA and Lynx). A schematic view of the Main VI used to control the motor and to record the signal is reported in figure 35. To communicate through the VI to the Arduino Board, the Lynx software interface (available on the list of packages provided by NI instrument) has been used through the SPI serial interface. The loop rate was 200 ms (maximum compatible with the Hardware available in the lab). In the Front Panel of the main VI, the user is able to set the serial port (COM), the mode of the motion (in this case velocity mode) and the velocity of rotation (for most of the test has been used 3 a velocity, in the front panel of the main vi). Through the SPI interface it is possible to select the chip of the board that makes the Hall sensor communicate to the PC and sends the data to an express VI included in the control panel of the main vi (Zero position finder) to display and process it (to find the peak of the “hump” in this case).

In the zero position finder sub.vi an express tool to evaluate when the maximum differential difference? between voltages occurs has been added. The tool used for this purpose is called derivative.vi in the LabVIEW 2015 library. After a coarse first detection of the signal it is possible to establish a proper value of the threshold to be used after a second swipe of the magnet over the sensor.

In the picture below the main software components of the main vi are shown. They include:

- the motor configuration sub.vi, useful to set the step frequency of the stepper motor and the angle of rotation for each step,
- the command sub.vi, to set the working modes of the motor,
- the set motor sub.vi, to apply the commands set to the configuration used at the moment,
- the ADC reader, to take the output of the converter and use it inside the zero position finder as input for the detection of the zero position.

All the data are exchanged trough an SPI serial interface.

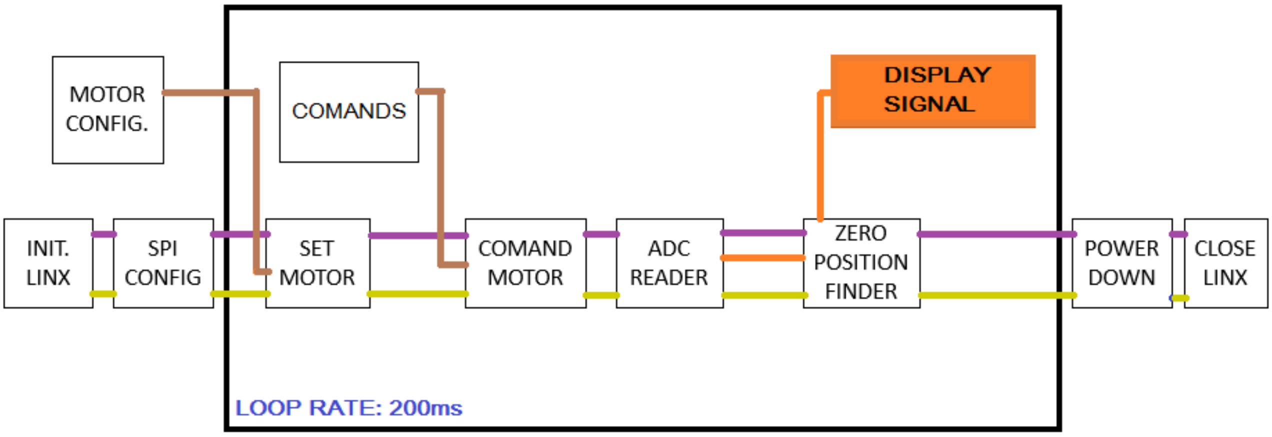

Figure 35:Schematic view of the main VI (described in detail in Appendix A)

6 TEST RESULTS

6.1 Chapter overview

The chapter will list the series of tests performed with the mechanism, to verify the reliability of the chosen method. First, some considerations will be made on the starting values chosen to better simulate the operative conditions of the motor and to reach the requested angular accuracy. Then the proper distance between sensor and magnet will be discussed, to optimize the future results, working on the position of the sensor trough the z axis and the related height of the support to be used in future. Next the peak detection method (maximum of the signal) and the mid-point finder (half position on the hump of the signal) are discussed and compared, in term of repeatability, the finding of the same point. The chapter continues by proposing a method to optimize the threshold value for the detection of the magnet, in order to minimize the effect of the noise on the processing of the information. In the test the fit methods previously presented have been used; to filter the signal and having a cleaner plot. Nevertheless, the use of these methods is limited as a support of the test phase and to have more data to compare and evaluate, due the amount of calculations required for the operation that is not compatible with the capabilities of the spacecraft CPU.

6.2 Sensor/magnet distance test

6.2.1 Preliminary considerations

The most practical signal shape to process to find the zero position has been evaluated. The alternatives are: a clipped signal or a non-clipped signal, both shown in the pictures below. Clipping is caused by the limitation of the Voltage range detectable by the ADC.

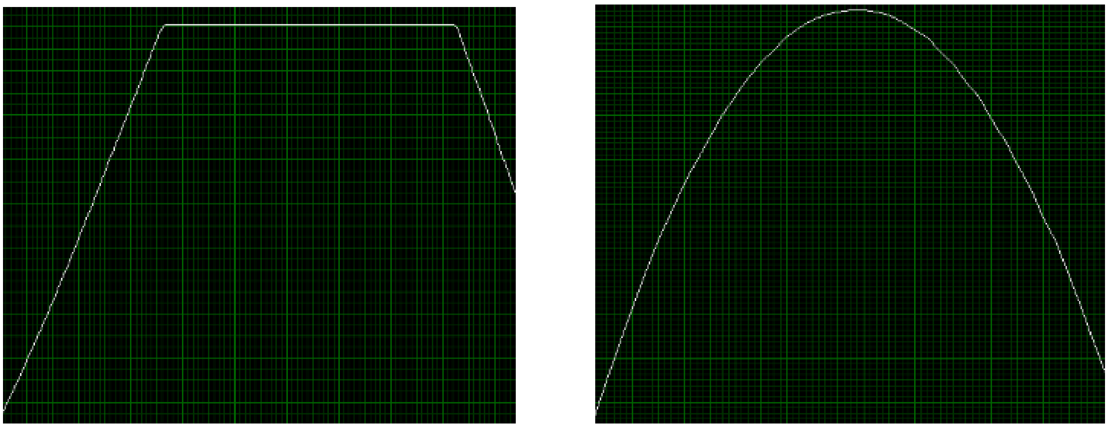

Figure 36: Clipped signal and a not-clipped signal

1. Clipped signal: caused by the max voltage detectable from the ADC: 3,3V. This generates the presence of a flat region in the signal: not just one maximum but several samples at the same Voltage (this is an approximation: it has been observed with the 16bit resolution of the ADC that the voltage varies in a range of +-0,0005 Volts). Further processing methods, presented in the previous paragraph, are required.
2. Non-clipped signal: output voltage remains inside the detectable range of the sensor. A signal with a complete curvilineal shape is provided, the maximum of the curve is easily detectable and so a quick zero position determination is possible.

In term of variables, the objective is to find a proper distance range (z-axis) between the sensing surface of the sensor and the magnet to distinguish the occurrence of the two cases. The ranges of measurements selected to better simulate the real mechanical motion of the cogwheel and the sensor/hardware available during the real operative phases of the APM are:

Voltage range of the sensor: Analog sensor output “filtered” through the ADC and the Arduino 2560Mega board → ADC only digitizes voltages from 0 to 3.3 V.

Analog Resolution / Quantization: Hall-effect sensor signal converted from analog to digital by the 16-bit ADC, i.e., 2^{16} values available (65536) between 0 and 3.3 V, resulting in a resolution of 0,05 mV.

<u>Discretization:</u> maximum sampling rate smaller than 5 Hz (period of 200 ms). It is not possible to sample faster with the A/D converter and the microprocessor.

<u>Maximum number of sampling used:</u> 1000 is only a reference number. The real number depends on speed of rotation and sensor geometry. It was estimated that for the desired resolution, 1000 points should be measured, i.e., with the maximum sampling rate, a test would require 1000 * 0.2 s =~3,33 min.

6.2.2 Results

The sensitive surface of the Hall sensor is considered to be at the same height as the top of the support.

The first sampling is at the highest height at which the sensor starts detecting the presence of the magnet. In figure 37 below some main features of the slot in which the support of the sensor has been placed are represented.

In the next table 11 also the situation in which there is no magnet in the close proximity, that correspond to a quasi-constant voltage of 1,5Volts, has been included.

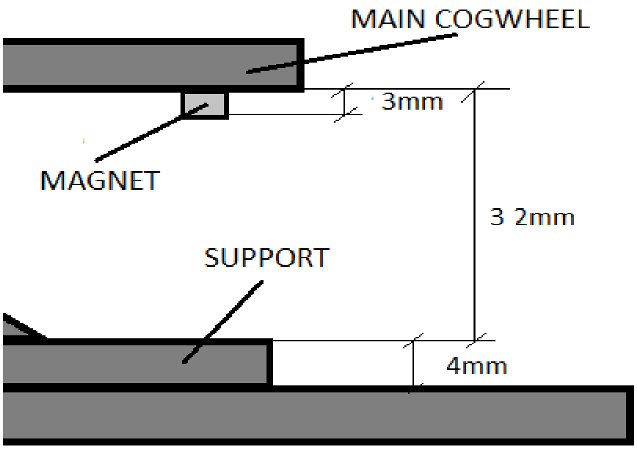

Figure 37:Dimensions of interest for the mechanical setup

Table 11: Max Voltage changing the distance sensor/magnet ???

H[cm]	d[cm]	Vmax[V]	Clipped signal
/	∞	1,5	No
1,8	1,8	1,652	No
2,5	1,1	1,714	No
2,8	0,9	1,845	No
2,95	0,65	2,022	No
3	0,6	2,769	No
3,2	0,4	3,205	Yes
3,3	0,3	3,215	Yes

6.2.3 Conclusions

A possible range of distances between the sensing surface of the sensor and the face of the magnet to use has been evaluated, in order to have a curvilineal signal and to avoid the presence of a flattened region at the center of the signal. The range, using a magnet of 2 mm of diameter and 3mm of height, polarized at Ni-Cu-Ni, is between 1,8 cm (when it starts detecting the presence of the magnet) and 0,6 cm (when the signal starts to be clipped).

The convenience of an unclipped signal is that it makes easier to detect the absolute position (peak detection), instead of using an express algorithm to find the “mid-point” of the signal on the flattened region, as previously discussed: dealing with a clipped signal imposes more calculations on the user and the processor.

It is advisable to place the magnet at the lowest distance from the sensor that avoids the clipping (distance of 3mm) to have a wider range of amplitudes to quantize. Another aspect to take into consideration is the dependence of the signal on the temperature [4]. It has been observed that the signal is influenced by the thermal environment of the room: are required more tests for the determination of a safe distance to avoid the clipping (vacuum chamber).

6.3 Comparison between Peak detection and mid-point finder methods stability

6.3.1 Preliminary considerations

It is possible to evaluate the maximum allowed angular velocity using simple calculations, based on the precision required, for the given maximum sample rate of 200ms. For the following calculation, it has been assumed that each step-pulse of the motor corresponds to a pulse of the sensor. For a higher resolution, the user could use a higher sensor pulse count per motor pulse count.

Circular path of magnet at radius r 65 mm x 2 π → 408.2 mm

Distance traveled per bit (@16 bit) 408.2 mm / 65536 bins → 0,006228 mm

Tangential velocity at magnet V = s/t → 0,0311 mm/s

(t: Loop rate = 0.2 s)

Angular velocity ω = v/r → 0,0274°/s

This is the maximum velocity allowed to achieve the required precision; proceeding slower it is possible to achieve a better resolution, considering the previous fixed values (starting data). For a better understanding of the theory, the magnet has been considered fixed and the sensor as moving linearly over it pulsing at the frequency of 5Hz (approximation of a linear motion above the direction of the tangential velocity, as previously described in paragraph 4.5).

6.3.2 Results

In this set of test between the mid-point method and the peak detection method provides more stable results. The same magnet, fixed at a certain position of the cogwheel (always 65 mm of radius, the best trade off distance from the rotational axis), has been swept several times. Furthermore, the repeatability (here also defined as the stability) of this calculation has been verified: to this purpose, the step count of the motor was associated to each sampling to verify whether it was possible to achieve with different sweeps the same position of the shaft at the time the magnet was moving over the sensor.

In the table 12, to demonstrate the repeatability of each method, the Δ_{max} parameter (difference between the highest and the lowest linear positions detected) and the Standard deviation, have been provided, to have an idea of the variation intervals of the results.

These are two cases considered with different threshold values:

Angular velocity: 0,0173°/s, target velocity in the main.vi = 2, diameter of the magnet = 2 mm, magnet/sensor distance 3mm, sample rate 200 ms

Threshold 1,8: (less samples, shorter sampling time (around 4,3 min), sampling in the less sensitive part of the signal: the almost flat/top region)

Table 12: Comparison between the stability (the standard deviation is highlighted in yellow) of the mid-point finder method and the peak-detector method, assuming 1,8 V as threshold voltage

Test n°	*Peak*	*Mid-point*	*Samples over the threshold*	*V_{max}[V]*
1	*651*	*644*	*1288*	*2,053*
2	*638*	*644*	*1288*	*2,060*
3	*662*	*654,5*	*1309*	*2,061*
4	*651*	*657,5*	*1315*	*2,083*
5	*668*	*663,5*	*1327*	*2,105*
6	*655*	*666*	*1332*	*2,113*
Δ_{max}	*30*	*22*	*44*	*0,060*
Std.Dev.	*10,34247*	*9,399025*	*18,79805*	*0,025333*

Threshold 1,7V (to use the most sensitive part of the signal to start the detection of the signal, time of sampling around 6 min with sr 200ms)

Table 13: Comparison between the stability (the standard deviation is highlighted in yellow) of the mid-point finder method and the peak-detector method, assuming 1,7 V as threshold voltage

Test	**Peak**	**Mid-point**	**Samples over the threshold**	**V_{max}[V]**
1	918	900,5	1801	2,205
2	879	906,5	1813	2,214
3	900	904	1808	2,218
4	885	903,5	1807	2,223
5	911	903,5	1807	2,227
6	892	910,5	1821	2,230
Δ_{max}	33	10	20	0,025
Std.Dev.	15,0831	3,402205	6,80441	0,009182

Some factors that influence the peak detection are: the magnetic environment of the room, the thermal environment of the room, support not perfectly fixed.

These elements not only may lead to a wrong detection of the peak but also to a not repeatable point at which the sampling phase starts: it is possible to see in the table 12 that the number of samples is much unstable than in the second table, in which the threshold value has been set on a more sensitive part of the signal (rising slope). At this quantization/discretization level, the peak of the signal is too much dependent on the noise, for this reason the mid-point method is more reliable.

When the support will be properly fixed, it will be necessary to set a proper threshold value to allow a constant number of samples to by divided them by two. The number of samples is less influenced by the elements previously listed, for this reason in the second cluster of tests also the max Voltage has been recorded in the table, to have an idea of how much the signal can be affected by the thermal environment.

In the next paragraph the fit method previously described will be used, to have an idea of the behavior of the signal when unaffected by noise. In the figure 38 below a quick view of how the plot of a Cubic-spline can help having a clearer vision of the behavior of the signal is shown.

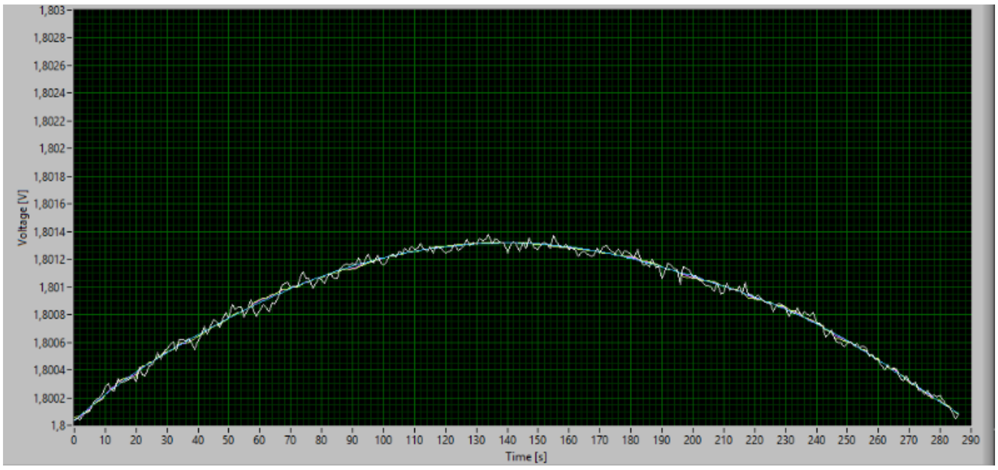

Figure 38: Detail of the top of an unclipped signal, in the presence of noise

6.3.3 Conclusions

A system that allows the user to find a proper threshold value without inserting it manually Is required. The optimal threshold value should be selected so that it corresponds to the steepest side of the signal, thus reducing the influence of the noise. This value cannot be fixed, due the changing thermal environment in which the APM is situated: a satellite orbiting around the planet can switch from high to low temperatures depending on its position in the orbital plane (especially in the LEO orbit). For this reason, an adaptable algorithm capable to choose an “ad hoc” solution is required. In the next paragraph in the main Vi an additional tool to solve this problem and make the results in the test phase more stable has been integrated.

6.4 Threshold optimization

6.4.1 Derivative tool

As we previously said, there is a maximum velocity compatible with the sampling rate of the system, given by the sample rate used. This is the maximum velocity allowed to reach the required precision; by proceeding slower it is possible to achieve a better resolution, considering the fixed values previously described (starting data). For a better understanding, the magnet has been considered fixed and the sensor as moving linearly over it, pulsing at the frequency of 5Hz (approximation of a linear motion above the direction of the tangential velocity, as previously demonstrated). In this set of tests, an additional analytical tool to process the data has been used: it is a sub.vi included in the LabVIEW library that allows the user to see where the maximum increment between a voltage value and the following one occurs: this allows the user to know where the most sensitive (less noise affected) part of the signal is located. To run this sub.vi in parallel to the main vi has been tried, choosing the maximum value of this plot; this yields the voltage value at which the sharpest jump between a value and another has occurred that corresponds to the most sensitive part of the shape of the signal.

Is required to perform a first and fast swept over the sensor with the magnet stuck on the cogwheel on the vi used (in the vi could be 30 as velocity) to yield a proper threshold value for the environment at the time of the sampling (the signal is dependent on the temperature) and to perform a slower and more accurate sweep over the sensor. The pros of this method are shown in the next chapter. Next the plots of the signal at 30 and 3 as target velocity are exposed.

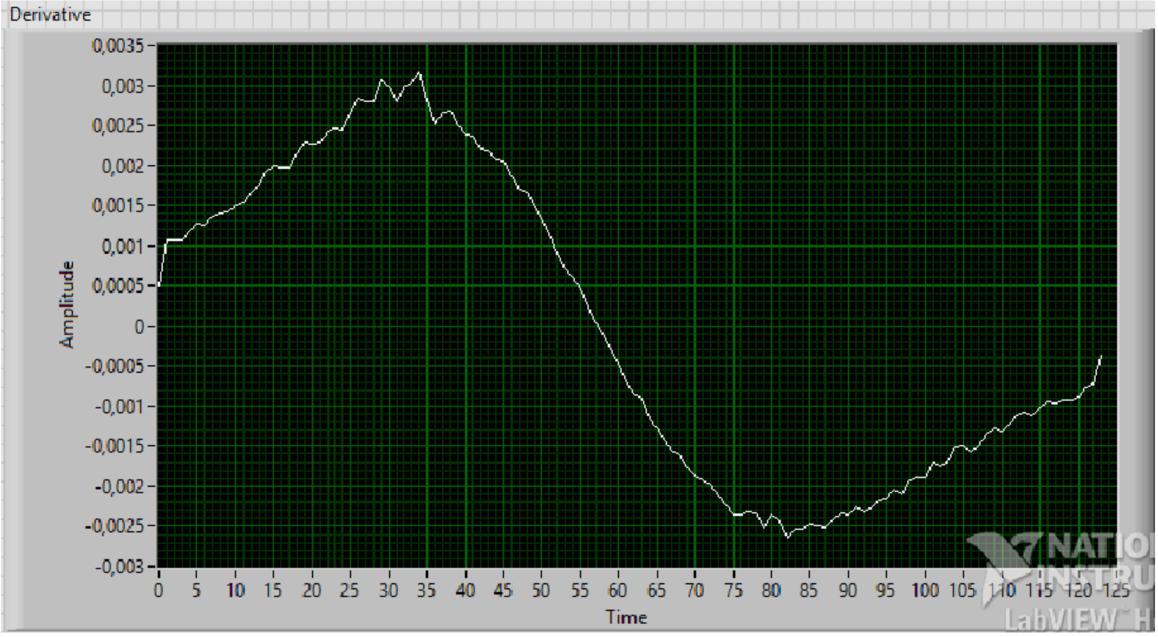

Figure 39: Derivative plot with a fast swipe sweep? (125 samples)

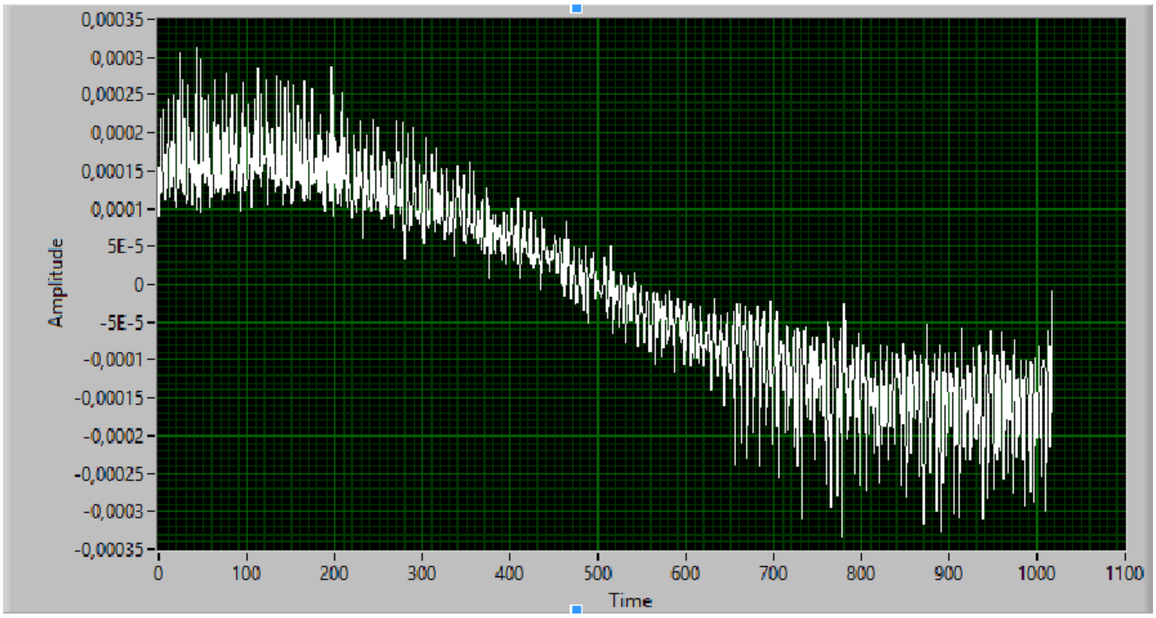

Figure 40: Derivative plot with a slow/accurate sweep (1050 samples)

6.4.2 Results

In these tests the reliability of the method previously chosen and the influence of the optimization method (with the derivative tool) on the results obtained have been verified.

Some test has been made with the help of this supplement tool and it was verified whether it was possible to detect the same position in several iterations. Furthermore, the repeatability of this calculation with the step count of the motor for a more practical application usable in the future (the motor still requires the resolver) has been verified.

The value of the max voltage has been inserted in the VI to determine a possible dependency on the temperature in the test. Having the same max voltage reached in the iterations gives the user an idea of how much the thermal environment changes during the tests; for this reason also this parameter has been included in the tables below (last column of each table).

In the results also the peak position of the curve provided from the Gaussian fit and the B-spline fit have been included to have more parameters to compare. Nevertheless, these methods are presented only as ~~a~~ “help-curves” for this test phase (to have a graphical idea on which is the trend of the signal), because they imposed a computational burden that is not compatible with the CPU of a spacecraft. The work focuses on improving the method of the peak determination and the mid-point finder, less “computationally heavy” methods for this application.

In the next example, a preliminary fast sweep has been performed that yielded a value of 1,72 V (maximum of the plot given by the derivative tool function): some test with different threshold values has been performed to verify the usefulness of this method. The future version of the vi will include an automatic way to set the threshold value:

The methods (peak detection and mid-point finder) allowed for future applications are highlighted in yellow.

1. 4 mm distance, 2 mm magnet diameter, 1,65 V threshold

Table 14: Comparison on the stability of each method (un-optimized threshold) define stability

Test	**Samples**	**Peak**	**Gaussian**	**B-spline 1**	**B-spline 2**	**B-spline 3**	**Mid**	V_{max}
1	1527	761	761	752	751	751	786,0	1,751
2	1545	724	723	729	727	727	772,5	1,749
3	1566	751	751	747	747	747	783,0	1,748
4	1540	716	715	720	718	718	770,0	1,748
5	1573	762	763	753	753	753	786,5	1,750

Delta max	33	49	48	33	35	35	16,5	000,3
Std dev	18,96576	21,44062	22,1991	14,85598	15,7226	15,7226	7,789416	0,001304

2. 4 mm distance, 2 mm magnet diameter, 1,7 V threshold

Table 15: Comparison on the stability of each *method (nearly optimized threshold)*

Test	**Samples**	**Peak**	**Gaussian**	**B-spline 1**	**B-spline 2**	**B-spline 3**	**Mid**	**V_{max}**
1	903	443	443	441	441	441	451,5	1,477
2	899	442	442	439	438	438	449,5	1,477
3	897	443	443	438	438	435	448,5	1,477
4	892	432	432	435	435	433	446,0	1,477
5	893	432	432	433	433	431	446,5	1,478
Delta max	11	9	9	8	8	10	5,5	0,001
Std dev	4,494441	5,8566	5,85662	3,193744	3,082207	3,974921	2,247221	0,000447

3. Threshold voltage: 1, 72V, 4 mm distance, 2 mm magnet diameter (optimal threshold value)

Table 16: Comparison on the stability of each method (optimized threshold)

Test	**Samples**	**Peak**	**Gaussian**	**B-spline 1**	**B spline 2**	**B spline 3**	**Mid**	**V_{max}**
1	661	329	329	326	326	326	330,0	1,479
2	659	316	316	322	322	322	329,0	1,479
3	656	321	321	322	323	323	328,0	1,479
4	657	324	323	322	322	323	328,5	1,479
5	661	331	331	325	326	326	330,0	1,479
Delta max	5	15	15	4	4	4	2	0
Std dev	2,280351	6,058052	6,082763	1,949359	2,04939	1,870829	0,894427	0

Next the table 17, lists the position associated to the step count is shown (with in parenthesis the respective value inside the signal).

4. <u>Distance 3mm, magnet 2 mm diameter, 1,9595 Volt threshold value</u>

NOTE: in this set of tests the sensor has “swept” counterclockwise and clockwise, and it has been noticed that the counter of the motor behaves differently depending on the sense of rotation (the integration of the resolver of the motor to avoid this problem is required). So in the table 17 the results are compared, in terms of delta max (Δ_{max}) and standard deviation, for each sense of rotation. For this reason, the assumptions made in this work apply only to the case when the motor rotates either clockwise or counterclockwise, but not both due to the hardware available at the moment: it is not possible to swipe the sensor in both directions to provide the same results. As usual, the two methods suitable for a practical application are highlighted in yellow.

Table 17: Comparison on the stability of the results of each method (optimized threshold) with step count associated

Test	**Samples**	**Peak**	**Gaussian**	**B-spline 1**	**B-spline 2**	**B-spline 3**	**Mid**	**V_{max}**
1	505	5927(247)	5927(247)	5926(249)	5926(249)	5926(249)	5924(252,5)	2,087
2	509	5939(248)	5939(248)	5940(250)	5940(250)	5940(250)	5942(254,5)	2,087
3	506	5924(251)	5923(250)	5926(248)	5926(248)	5926(248)	5923(253,0)	2,087
4	509	5939(248)	5939(248)	5939(248)	5939(248)	5939(248)	5943(254,5)	2,087
5	507	5923(252)	5923(252)	5925(249)	5925(249)	5925(249)	5922(253,5)	2,087
6	510	5939(249)	5939(249)	5939(249)	5939(249)	5939(249)	5942(255,0)	2,087
7	507	5927(247)	5927(247)	5925(250)	5925(250)	5925(250)	5922(253,0)	2,087
8	511	5937(247)	5937(247)	5939(249)	5939(249)	5939(249)	5943(255,5)	2,088
$\Delta_{max}1$	5	4 (4)	4(4)	1(1)	1(1)	1(1)	2(2)	0,000
$\Delta_{max}2$	2	2(2)	2(2)	1(1)	1(1)	1(1)	1(1)	0,001

Std1	0,957427	2,629956	0,816497	0,816497	0,816497	0,816497	0,408248	0,000
Std2	0,957427	0,816497	0,957427	0,816497	0,500000	0,816497	0,645497	0,0005

In the figures nr? below some details of the plots of the signal provided by the sensor are shown in the first row of the last table. In the first row it is possible to see the influence of the noise on the plot of the signal, in the second row the location of the maximum (sample number 247) and the location of the mid-point (sample number 252,5) compared to the maximum provided by the Gaussian fit (sample number 247), B-spline fit 1 (sample number 249) B-spline fir 2 and 3 (sample number 249). With the B-spline methods is meant: equally spaced, cord length, centripetal method, all available in the LabVIEW library.

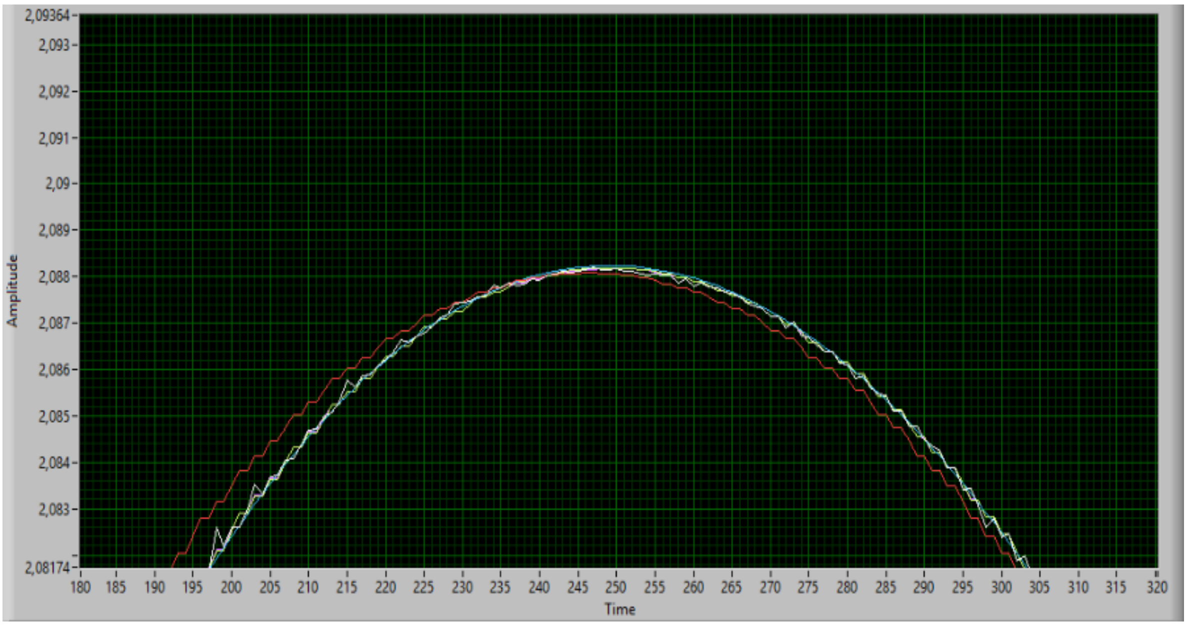

Figure 41: Detail of the signal compared to each fit method

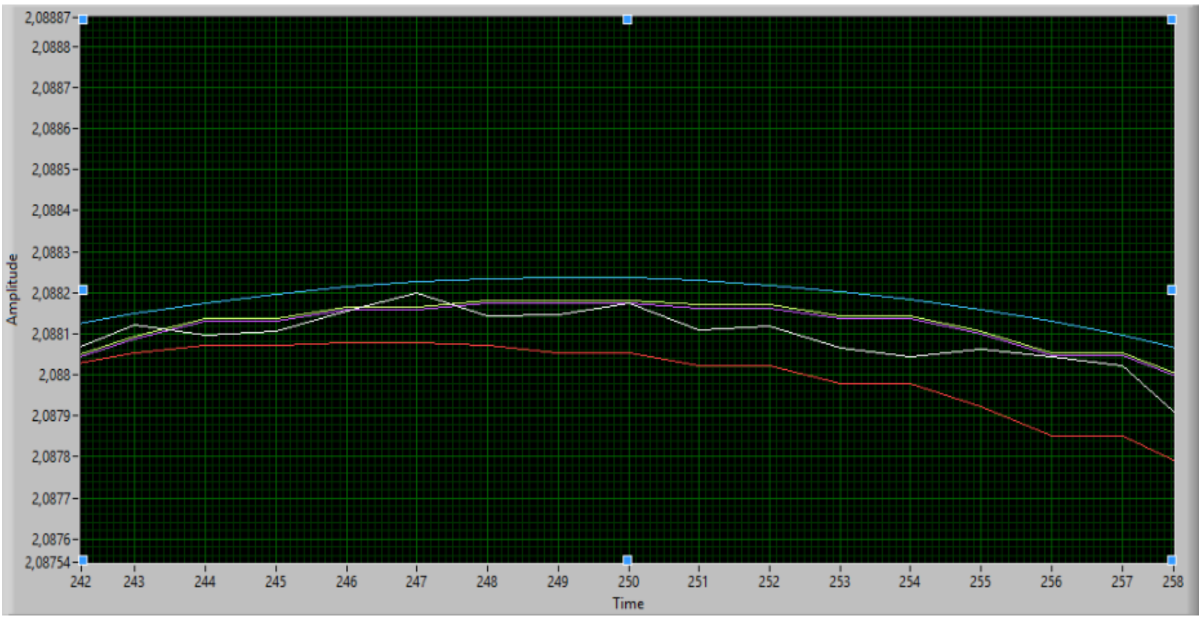

Figure 42: Detail of the top of the signal and comparison with each fitting methods

In figure 42 below the behavior of the differential curve during the crossing of the magnet of the sensor is again represented. It is possible to see which part of the signal is the most sensitive to the magnetic field provided by the magnet. The vi is able to take the voltage corresponding to the maximum of this plot and use it in the following step of the detection.

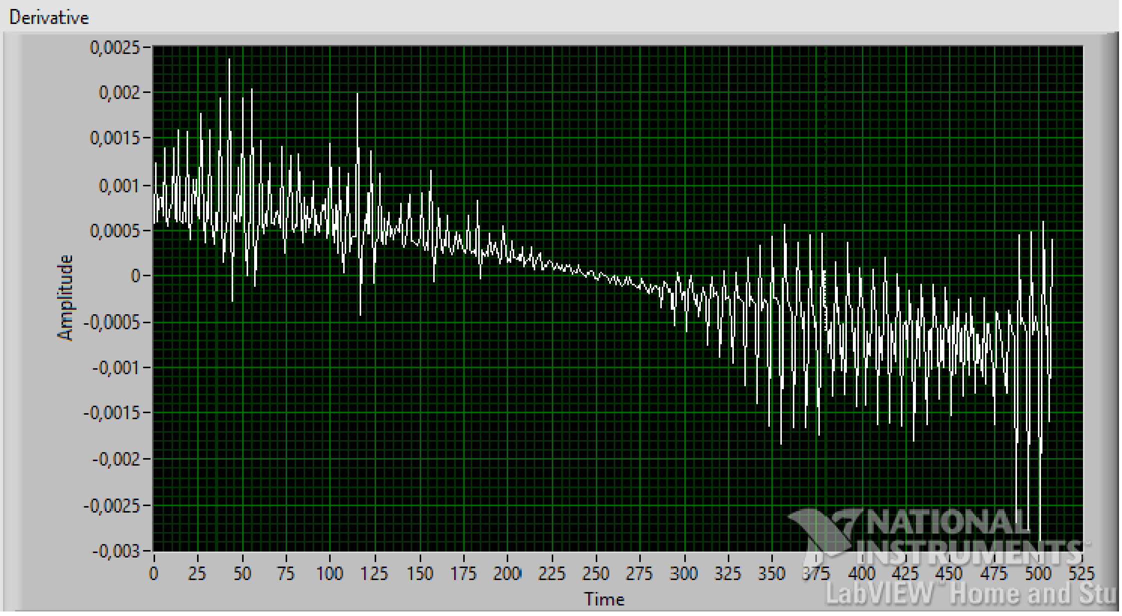

Figure 43: Sensitivity of the signal

By setting the threshold value, with this set up, at 1,72V, we guarantee an almost stable number of samples: the fact is evident by looking at the figures of the pattern of the signal here reported. In the first one, we can see that in the top and flattened region of the signal the peak detection cannot work properly due the presence of noise caused by: the magnetic environment field of the room, the varying thermal conditions of the room.

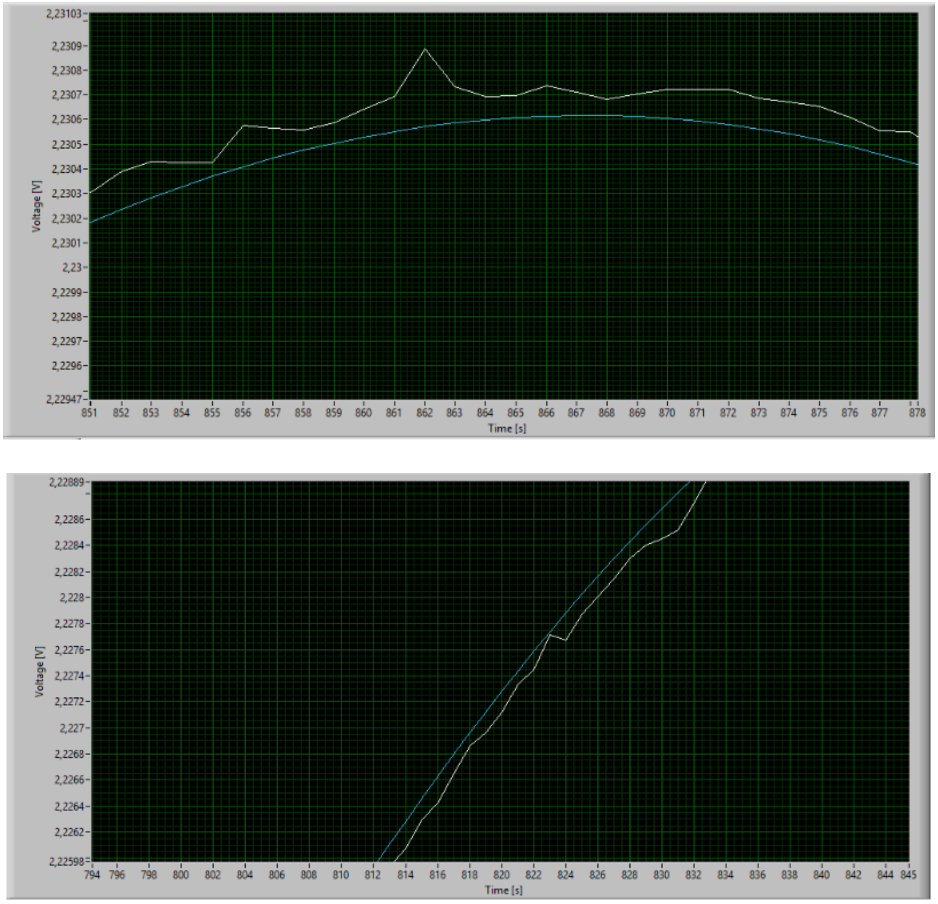

Figure 44: Detail of a generic curve that highlights the influence of the noise in the two parts of the plot. In the steep slope of the signal the main plot of the signal is less influenced by the noise.

6.4.3 Discussion on the results

The results presented in this thesis have been used to test a reliable method to find the optimal threshold value for the detection of the absolute position of the motor. It has been observed how a proper choice of the threshold can provide more stable results.

The results confirmed the higher efficiency of the mid-point finder with respect to the peak detection method. This is easily noticeable looking at figure 44 where it is possible to see the influence of the noise on the output and understand why the peak detection results are more influenced by the noise than the mid-point finder.

The mid-point finder and the peak detection algorithms have been compared to other fit methods like the Gaussian fit and the B-spline fit methods with the aim to "filter" the data obtained and have a "cleaner" vision of the shape of the signal. In the end, the mid-point finder turned out to be the most reliable method providing a smaller standard deviation of the results in each test set-up.

6.4.4 Conclusions

The mid-point finder proved to be the best method to detect the zero position of the Azimuth mechanism for the APM of the LISA project. For the application on the elevation mechanism, the same considerations are valid, decreasing the rotational velocity, calculated. Drawn at the beginning of chapter 4 (the cogwheel is smaller, as discussed in the previous papers, with a constant sampling rate and a smaller rotation radius a lower rotational velocity for the desired precision is required).

The efficiency of this method is less affected by the noise and does not require a significant amount of calculations (it has been possible to prove it by dividing by two the number of samples of voltage that exceeded the chosen threshold value).

In order to find a proper threshold value for practical application, an express tool to calculate the position has been used and the respective voltage value that occur when the maximum voltage difference between a sample and the next one is achieved, to better exploit the most sensitive portion of the shape of the signal (steepest slope).

6.5 Magnet diameter selection

The magnet dimension does not affect the signal steep: having a wider magnet means only having a higher number of samples. The magnetic strength of the field provided is constant in each magnet used in the test phase (residual magnetism, [T] or [G]). It Would be interesting to observe the shape of the signal for a magnet of different magnetic residual: having a higher max voltage would mean having steeper slopes on both sides, for this reason a side of the signal that is further less influenced by the magnetic noise. This will be an interesting future development of the tests here described. During the tests, the magnets available were able, once placed at the same distance from the sensor, to provide the same peak voltage. Below some technical information regarding the magnet used during the tests is shown.

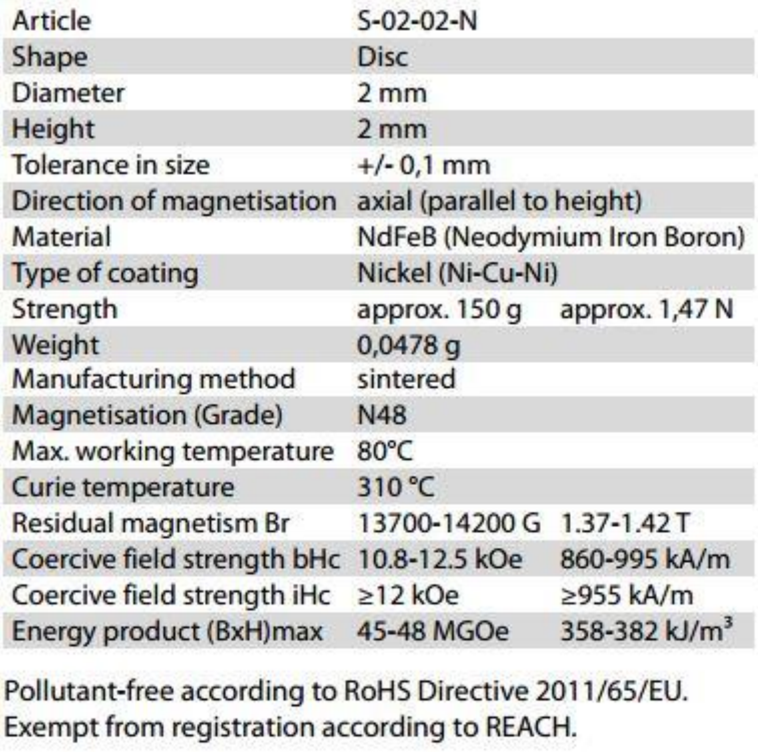

Article	S-02-02-N	
Shape	Disc	
Diameter	2 mm	
Height	2 mm	
Tolerance in size	+/- 0,1 mm	
Direction of magnetisation	axial (parallel to height)	
Material	NdFeB (Neodymium Iron Boron)	
Type of coating	Nickel (Ni-Cu-Ni)	
Strength	approx. 150 g	approx. 1,47 N
Weight	0,0478 g	
Manufacturing method	sintered	
Magnetisation (Grade)	N48	
Max. working temperature	80°C	
Curie temperature	310 °C	
Residual magnetism Br	13700-14200 G	1.37-1.42 T
Coercive field strength bHc	10.8-12.5 kOe	860-995 kA/m
Coercive field strength iHc	≥12 kOe	≥955 kA/m
Energy product (BxH)max	45-48 MGOe	358-382 kJ/m^3

Pollutant-free according to RoHS Directive 2011/65/EU.
Exempt from registration according to REACH.

Figure 45: Technical details of the most frequently used magnet in the tests (S- 02-02-N)

7 VALIDATION TESTS

7.1 Chapter overview

In this chapter the way in which the reliability of the method chosen has been demonstrated to find of the zero position of the mechanism is described. In the first part the analytical model used for the setup is presented: a laser has been used to point a target at a selected distance to verify the precision of the information. By increasing the distance between the laser pointer and the sensitive target It is possible to improve the accuracy, as described below. The chapter continues with a description of the hardware and software. Then the results obtained and the conclusions drawn from them are listed, comparing the information from the resolver, the number of samples and the position of the laser dot in the optical sensor.

7.2 Preliminary considerations

The test on the mechanism has been accomplished by placing a laser pointer on the top of the rotating shaft: by analyzing the position of the light dot at a certain distance, it has been possible to verify if the system implemented can provide an accurate detection of the zero position and the repeatability of its position in the rotation

EXAMPLE: From the requirements in term of accuracy and the already well known formula: 16bit = 65536 positions. To have the laser pointer dot placed in a 1x1mm square area, assuming that the shaft rotates on a plane, it is necessary that:

$$65536 \text{ x } 1\text{mm} = 65536 \text{ cm} = 2\,\pi\, r \qquad (6.1)$$

$$R = 65536/6.2831 = 10453.6687 = 10.453\text{m} \tag{6.2}$$

This means that to verify the precision of the mechanism we need to be able to hit a target of 1 mm at the distance of ten meters. It Is necessary to place an optical sensor at this distance from the mechanism and to verify that the maximum amount of light is occurs in the same point in several different operations. It Is possible to decrease the distance between the two devices by decreasing the size of target, and vice-versa, as it is possible to see in the figure 46.

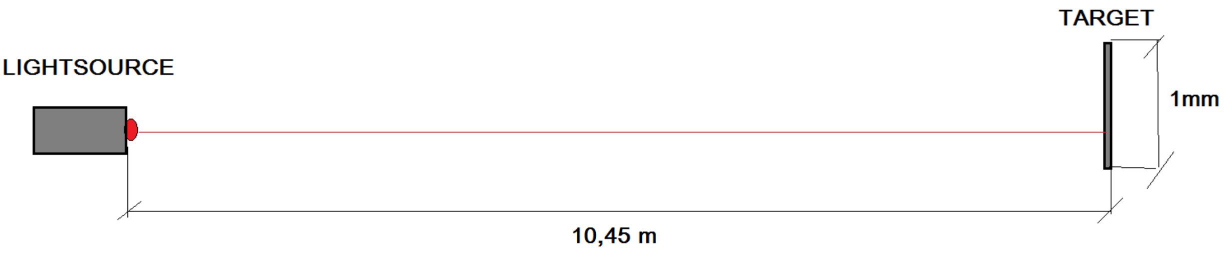

Figure 46: Characteristic parameters of the example exposed (not in scale)

7.3 Test setup

The setup is similar to the previous one, but a laser pointer and an optical sensitive surface has been added to verify the results obtained in the previous chapters. In this phase adding the resolver board will be added, able to let the user know about the exact position of the mechanism. This resolver has a resolution of 16bit, that, multiplied by the gear ratio of the harmonic drive (1:50) and the gear ratio of the main cogwheel (1:5) let the user know ideally each 16384000 ,2^{26}, positions on the rotation, coarsely a resolution of 26bits; the issue is that the rotation of the mechanism is accomplished 250 times for the rotation of interest (cogwheel). The laser pointer has been stuck on the surface of the rotating shaft and pointed to the other side of the room (8 meter of distance), where the PSD was placed, (see picture 48). Another Arduino Mega2560 board to interface the optical sensor with the laptop has been used. Each component of this electrical setup was handled by an Acer S3 Ultrabook. An express wire has been used (length 8 meters) to place the sensor at the required distance and to communicate with it. Furthermore, the sensor has been placed at the proper height with an express support to allow the laser pointer to hit its center while the zero position was crossed.

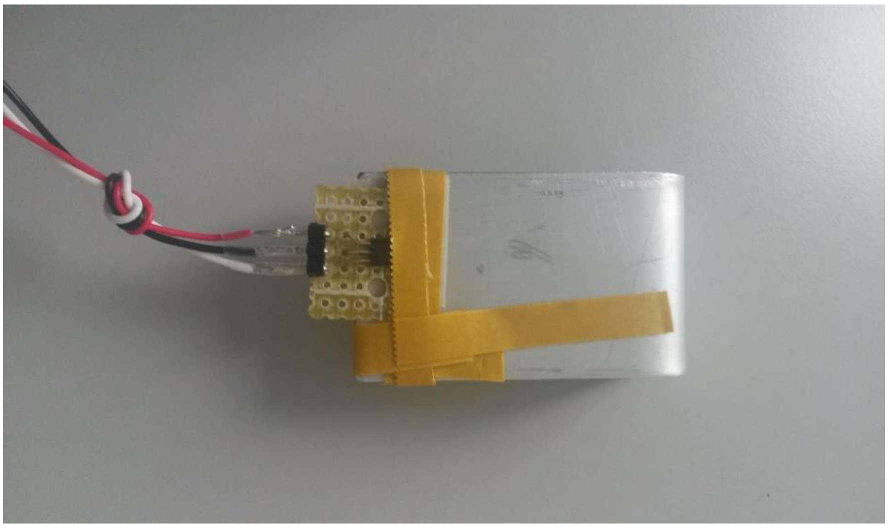

Figure 47: Hall-Sensor glued to the Aluminum support to avoid vibrational effects on the signal

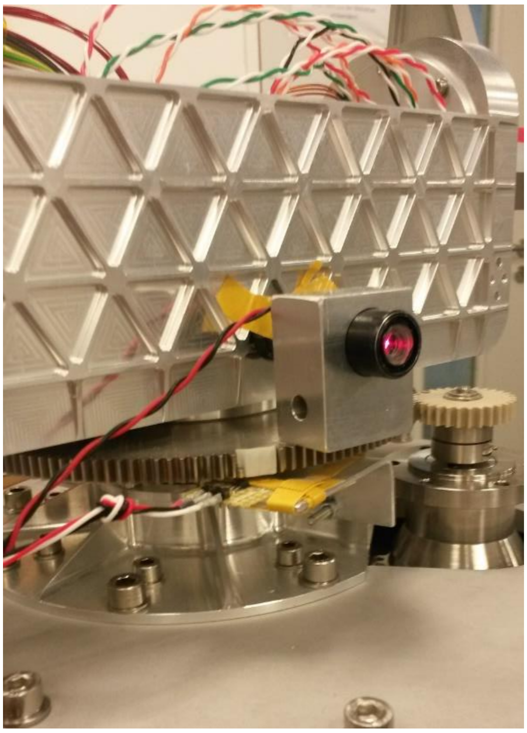

Figure 48: Laser Pointer glued at the top of the Azimuth rotating shaft

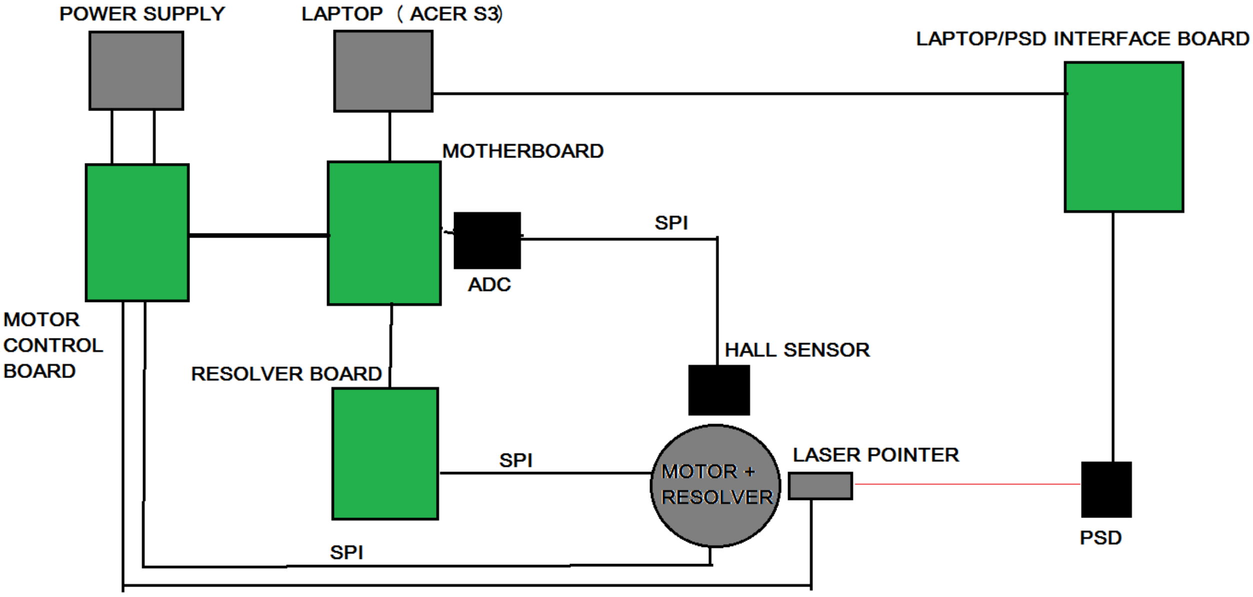

Figure 47: Electrical setup for validation tests

The size of the target was a function of the chosen distance. Using formula (2.1) it is possible to obtain the Table 18 in which is shown each couple distance/size of the magnet:

Table 18: Size of the target for each PSD/laser pointer selected distance

PSD/LASER POINTER DISTANCE (r) [m]	TARGET DIMENSION REQUIRED (l) [mm]
8	0,766
9	0,862
10	0,958
11	1,054

7.4 Additional components

7.4.1 Resolver

In this set it was required to verify the precision and reliability of the device. The installed resolver board (see figure nr.? below) has a precision of 16bit and is included in the motor: for this reason, considering the gear ratio of 1:250, a precision of almost 26bit is achievable ((360/65536)/250=...). Once configured, the resolver yielded that the motor, for each step using a full step configuration, was capable to perform 600 numerical increments for each step. Having a “bugged” step count, (the step count didn’t represent the same angular position in different sweep) the resolver was the best alternative to verify if the zero position occurred in the same angular position performing different sweep of the magnet over the sensor. The board used was an EVAL-AD2S1210SDZ and it communicates through an SPI interface to the motor control board, the main board and the motor. In the main VI a numerical indicator that shows, between a range of 0 to 65536, the position of the motor is displayed.

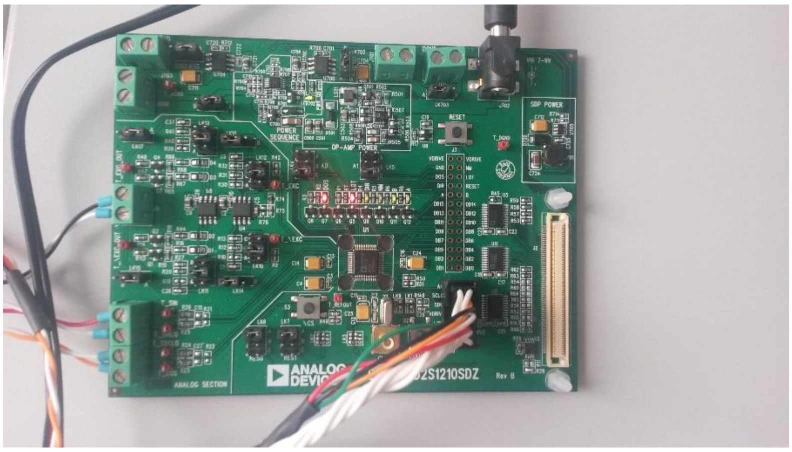

Figure 49: Resolver Board

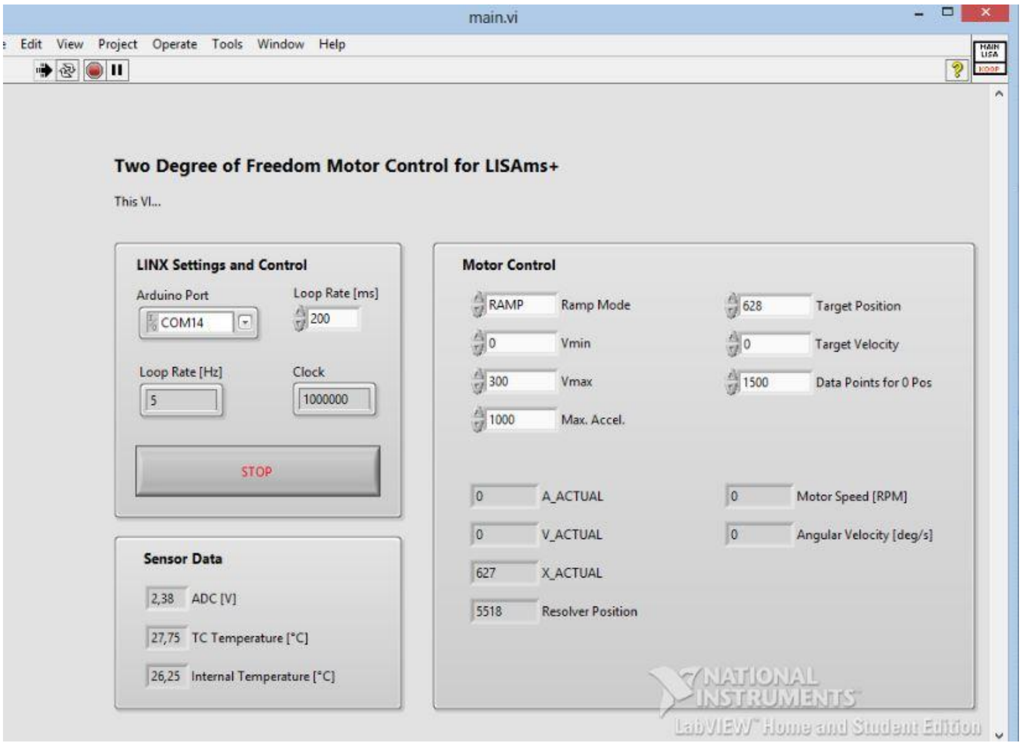

Two Degree of Freedom Motor Control for LISAms+

This VI...

LINX Settings and Control

Arduino Port: COM14
Loop Rate [ms]: 200
Loop Rate [Hz]: 5
Clock: 1000000

Sensor Data

2,38 ADC [V]
27,75 TC Temperature [°C]
26,25 Internal Temperature [°C]

Motor Control

RAMP Ramp Mode
0 Vmin
300 Vmax
1000 Max. Accel.
628 Target Position
0 Target Velocity
1500 Data Points for 0 Pos
0 A_ACTUAL
0 V_ACTUAL
627 X_ACTUAL
5518 Resolver Position
0 Motor Speed [RPM]
0 Angular Velocity [deg/s]

Figure 50: Front Panel of the main VI

7.4.2 PSD

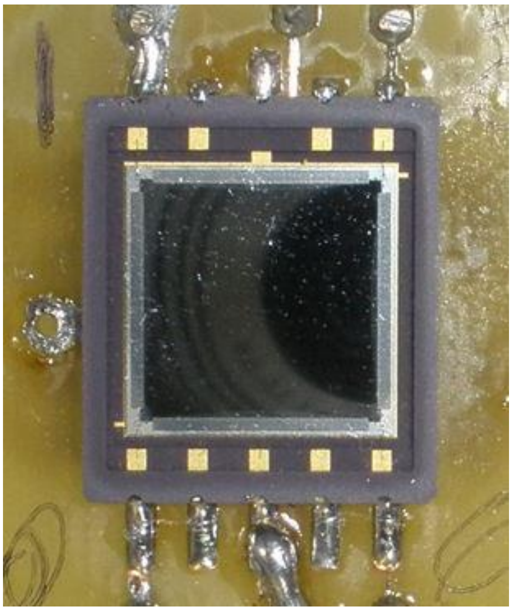

Figure 51: PSD set to the MOVE test board

The PSD (Position Sensing Device) is an analog device sensitive to a specific wavelength, in our case provided by the laser pointer, and capable of finding the position of the peak of the amplitude of the light that hits the sensitive surface and translating it in terms of Cartesian coordinates. The sensor used for our tests was an S5991-01 with an active area of 9X9mm. The sensor was settled in a board used in previous tests (MOVE project). The active surface was 6x6 mm, it communicates through an SPI serial interface and the recommended spot size of the laser dot was 0,2 mm. Further details are included in figure 53. In the PSD board, an analog to digital converted capable of providing a resolution of 10bit to the precision of the position of the laser dot on the display was included in the board.

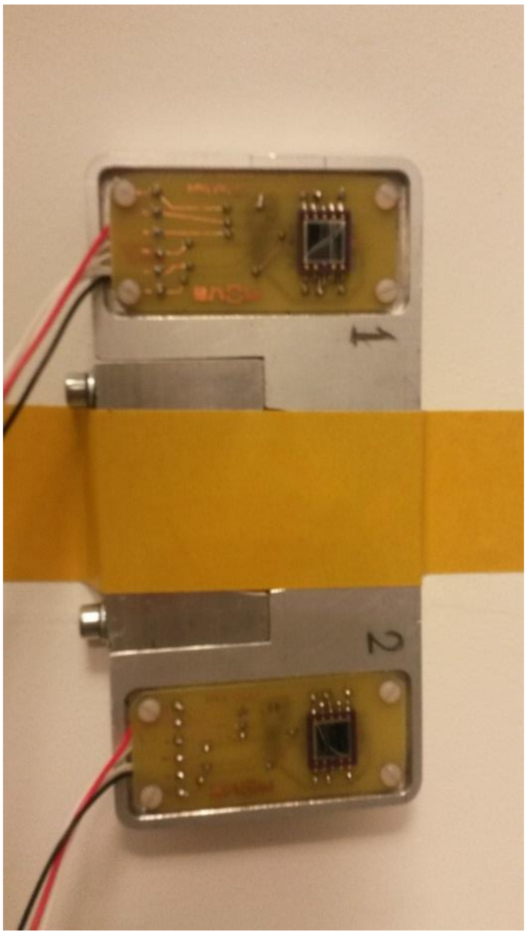

Figure 52: PSD and AD8551 board

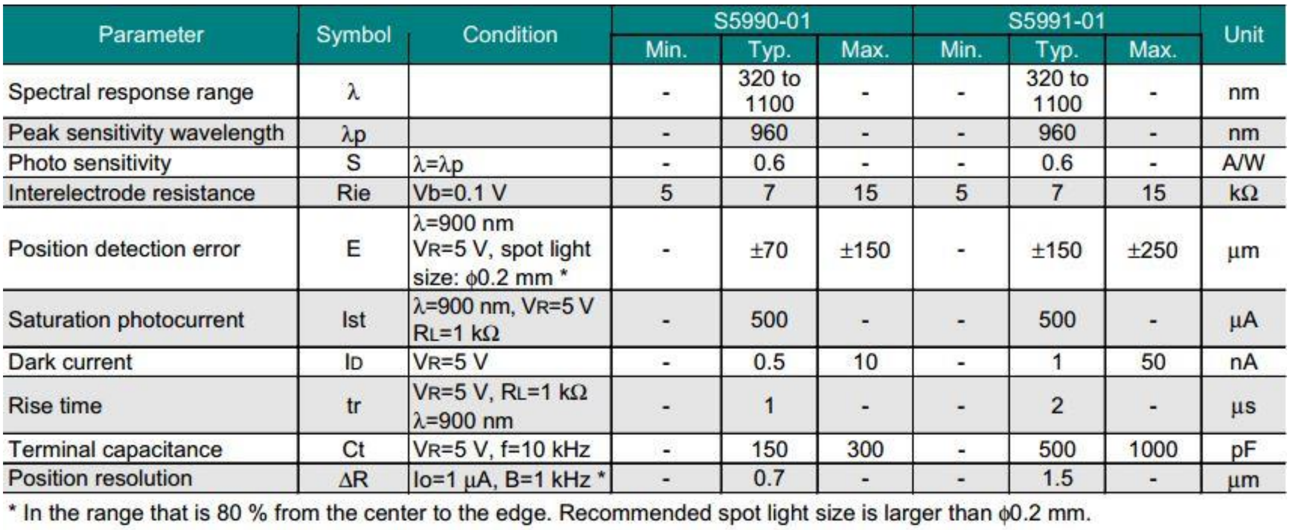

Parameter	Symbol	Condition	S5990-01			S5991-01			Unit
			Min.	Typ.	Max.	Min.	Typ.	Max.	
Spectral response range	λ		-	320 to 1100	-	-	320 to 1100	-	nm
Peak sensitivity wavelength	λp		-	960	-	-	960	-	nm
Photo sensitivity	S	λ=λp	-	0.6	-	-	0.6	-	A/W
Interelectrode resistance	Rie	Vb=0.1 V	5	7	15	5	7	15	kΩ
Position detection error	E	λ=900 nm V_R=5 V, spot light size: ϕ0.2 mm *	-	±70	±150	-	±150	±250	µm
Saturation photocurrent	Ist	λ=900 nm, V_R=5 V R_L=1 kΩ	-	500	-	-	500	-	µA
Dark current	I_D	V_R=5 V	-	0.5	10	-	1	50	nA
Rise time	tr	V_R=5 V, R_L=1 kΩ λ=900 nm	-	1	-	-	2	-	µs
Terminal capacitance	Ct	V_R=5 V, f=10 kHz	-	150	300	-	500	1000	pF
Position resolution	ΔR	Io=1 µA, B=1 kHz *	-	0.7	-	-	1.5	-	µm

* In the range that is 80 % from the center to the edge. Recommended spot light size is larger than ϕ0.2 mm.

Figure 53: Electrical parameters of the S5990-01

7.5 Tests procedure

After calibrating the sensors and using the results of the previous tests (mid-point method selection), a test procedure to verify that the same position (in our case the zero position), is detectable several times was developed. In this test it is assumed that the thermal environment remains stable on a small range of degrees (+- 0,001 °) and that each mechanical component does not change its position, except for the rotation of the main cogwheel. The operative procedure steps were the following.

1. First (fast) sweep (velocity target = 30 in the main VI) with a starting threshold of 1,7 → CHOICE OF THE OPTIMAL THRESHOLD VALUE (DERIVATIVE TOOL)
2. Second (slow) sweep (velocity target = 3 in the main VI) → COUNTING OF THE NUMBER OF SAMPLES
3. NUMBER OF SAMPLES / 2
4. Find the position of the cogwheel in terms of the resolver at the mid-point found
5. Point the laser at the center of the target (0 ± 0,09, 0 ± 0,09) in the display
6. Return to a generic position (under the threshold value, out of the signal)
7. Perform again the sweep, comparing resolver position and PSD position
8. TO DEMONSTRATE THAT THE METHOD WORKS, WE NEED TO VERIFY IF THE SAME RESOLVER POSITION, THE SAME SAMPLE NUMBER AND THE SAME POSITION OF THE LASER POINTER OCCURS SIMULTANEOUSLY

The steps 6, 7, and 8 have been repeated five times to verify the repeatability of the zero position detection, and the results are listed in the next paragraph.

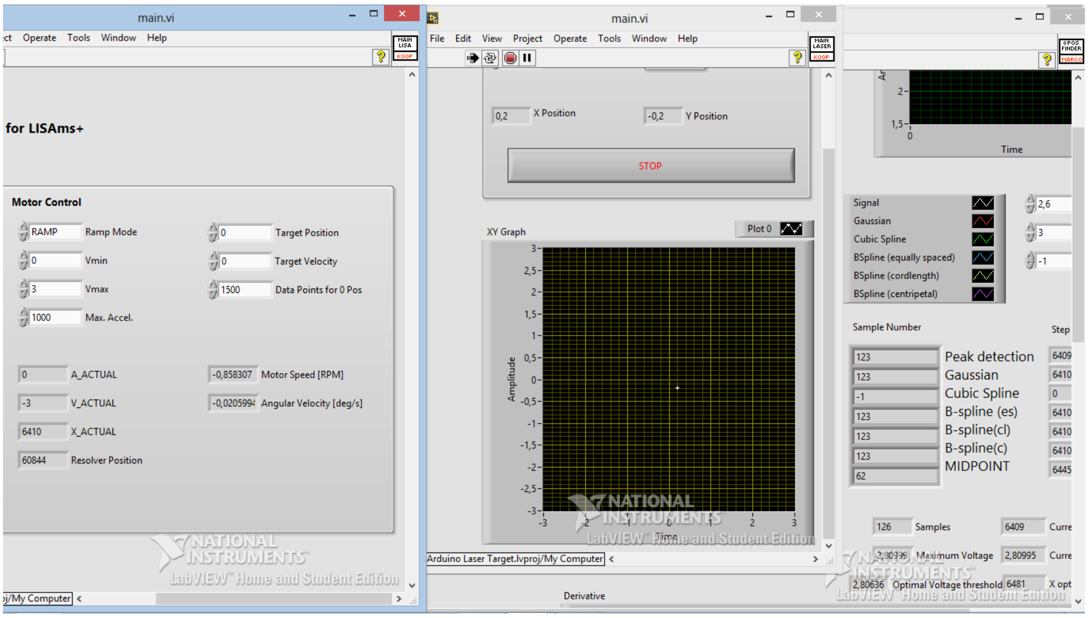

Motor Control

RAMP Ramp Mode
0 Vmin
3 Vmax
1000 Max. Accel.
0 Target Position
0 Target Velocity
1500 Data Points for 0 Pos
0 A_ACTUAL
-3 V_ACTUAL
6410 X_ACTUAL
60844 Resolver Position
-0,858307 Motor Speed [RPM]
-0,0205994 Angular Velocity [deg/s]

0,2 X Position
-0,2 Y Position

2,6
3
-1

Sample Number		Step
123	Peak detection	6409
123	Gaussian	6410
-1	Cubic Spline	0
123	B-spline (es)	6410
123	B-spline(cl)	6410
123	B-spline(c)	6410
62	MIDPOINT	6445

126 Samples
6409 Curre
2,80999 Maximum Voltage
2,80995 Curre
2,80636 Optimal Voltage threshold
6481 X opt

Figure 54: View of the three VI's simultaneously used. Starting from the left: Main VI for the motor control, PSD VI, Zero position finder sub VI.

7.6 Results and Discussion of the results

For the set of tests performed in this phase, the following starting data has been used:

1. Magnet diameter: 2 mm
2. Magnet/Hall sensor sensing surface: 3 mm
3. Starting threshold value: 1,7 V
4. Optimal threshold Value: 2,6 V
5. Main cogwheel used: 0,0205 deg/sec
6. Velocity target: 3
7. Motor mode: Ramp

The starting threshold value has been chosen to allow to display the majority of the signal in the proximity of the magnet. After the fast sweep, the threshold value has been updated to 2,6 V to allow a better stability (optimal threshold) in the amount of samples taken over this threshold (in this case 252).

Table 19: Results of the test validation test: position of the shaft expressed in: position of the resolver, position on the optical sensor, position in the signal

TEST N°	RESOLVER POSITION	PSD POSITION (X,Y)	NUMBER OF SAMPLES	MIDPOINT	MAX VOLTAGE
1	60844	(0,12, -0,12)	252	126	2,948
2	60842	(0,2, -0,2)	252	126	2,949
3	60846	(-0,12 , 0,12)	253	126,5	2,949
4	60842	(0,15, -0,15)	252	126	2,950
5	60844	(0,21 , -0,21)	252	126	2,950

In this case the position of the resolver bounces between + an – 2 unities in the numerical indicator, but considering the gear ratio (1:250) and the resolution achieved, is negligible compared to the accuracy required exposed in chapter 2. The Cartesian position on the PSD display bounces due the presence of noise (see the datasheet [13]) that is between + 0,15 mm and – 0,15 mm. As demonstrated in the previous chapters (4/5), the mid-point finder provides a stable amount of samples over the set threshold and, consequently, mid-point in the same position. Furthermore, the stability of the mid-point has been demonstrated considering its position in the counter of the resolver. The tests were performed in a quiet stable thermal environment, considering that the maximum voltage was quite stable (variations of at most ± 0,002 V).

7.6.1 Step count issue

During the tests the resolver positon as reference to move the motor was used. The step count of the motor resulted compromised when it was necessary to change the sense of rotation of the motor: by changing the sense of rotation it was noticed that there was a loss of steps (the angular position indicated in the numerical indicator of the step count wasn't the same in different sweeps) of the motor that could influence the detection of the position. The problem has a software or electrical origin, considering that the resolver, fully operational, did not recognize the movement of the shaft when the input, through the main VI, was given. A debug of the software (VI) or a check in the mechanism used is required (Phytron VSS).

7.6.2 Erasing of the data sampled

There is the possibility that the signal, after collecting all the samples and exiting from the „over the threshold "area of the signal can erase the signal recorded itself without calculating the zero position. This is caused by the influence of the noise on the main plot of the signal: considering the moment in which the output voltage of the signal goes again under the threshold voltage, the noise, at the operative analog precision in which the user is working through the ADC, can cause to the voltage to go again over the threshold, erasing the signal collected previously (picture 54 below). Using the vi developed in this work, this event leads the user to perform a second slow sweep to collect again the zero position. This phenomenon is avoidable by setting the threshold value at the point of maximum steep, showed in the paragraph threshold optimization (paragraph 6.4). By setting the threshold in the most sensitive part of the signal it is possible to minimize the probability of this event to occur (considering the tests performed, the percentage of times that this event was observed was around the 10% of the times). In the future work section (chapter 9) the main features that the patch will require in order to avoid this occurrence are included. One solution could be to avoid that the vi collects a new signal within two or three steps after the signal sampled, giving a certain range of safety and avoiding to start again to record.

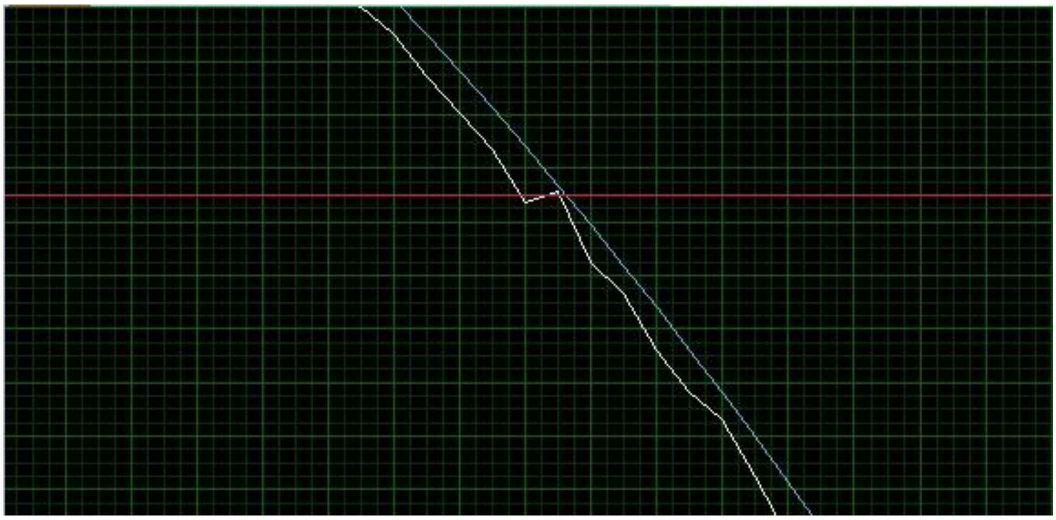

Figure 54: In red, threshold valued setted; in blue main trend of the signal; in white the signal. Is possible to see in this case that the signal goes under and over the threshold value for a second time

7.7 Conclusions

From previous tests, the mid-point finder was considered the most reliable method to find the zero position (accuracy of 16bit). In this final set of tests this reliability has been demonstrated using the optical technology of the PSD. By pointing the laser dot, provided by the laser pointer glued at the top of the rotating shaft, to a target at 8 m of distances, in a sensitive surface of 9x9 mm of the dimension of 0,7x0,7 mm, it was possible to demonstrate that the detection of the position was achievable. Under the previously mentioned conditions, the method turned out to be reliable provided that the thermal environment was stable.

In this chapter the steps to accomplish to find the zero positon (2 sweeps of the magnet over the sensor have been proposed: 1 fast sweep: 0,2 deg/sec, 1 slow sweep 0,002deg/sec), paragraph 7.5 with the test procedure, to optimize the stability of the positon of the motor.

More complex fit methods like cubic spline, Gaussian fit, and B-spline, were used to give to the user an idea on the main trend of the signal shape (see chapter 4), but, as previously discussed, they were not valid candidates for this application, considering the limited processing capability of the CPU of a spacecraft.

8 SUMMARY OF RESULTS

8.1 The project

LISA is a project handled by the Institute of Aeronautics (LRT) of Munich. The aim of this project is to develop an inter-satellite antenna that allows a direct communication link between LEO and GEO satellites, in order to extend the amount of data transmitted by a LEO satellite to a ground station from 7 minutes to 41 minutes. This system requires a high precision pointing mechanism, called APM (Antenna Pointing Mechanism) with two degrees of freedom. The motion is provided by two stepper motors and their respective gear boxes, that are able to perform a rotational motion in the Azimuth and Elevation directions. This kind of motors are moved thanks to a combination of currents inputs and, in case of an unpredicted shut down or loss of power of the system, they can lose the information regarding the last position assumed by the motor before the event. In this case, a system capable to find a reference position (called zero position) in a quick and reliable way is needed. From previous works, the technology chosen to accomplish this task is the magnetic sensing technology through Hall sensor. The purpose of this work was to find a method to process the signal and extract the precise information on the zero/absolute position with the proximity of a cylindrical magnet over the sensing surface of the sensor. One of the main obstacles of the task was the precision: considering the capability of the stepper motor (Phytron VSS for high vacuum application) a 16bit of precision was required (0,005°).

8.2 The method

In the first period the state of the art of the absolute magnetic encoders, analyzing several patents methods and how the magnetic signal was processed in order to obtain the angular position was studied.

Next, a set of preliminary tests was conducted, in order to study and understand how the shape of the signal behaves, the capability of the sensors and to start developing the software to process the signal obtained, choosing among several alternatives (fit methods). The software used was LabVIEW 2015 (National Instruments) and the methods selected were the peak detection, the mid-point finder, the Cubic and B-spline method and the Gaussian fit.

Once the whole mechanism was available, the methods have been compared one with the other with the same starting data needed to perform the detection. The independent variables (as the distance of the magnet from the rotational axis, the sensor/magnet distance, the rotational speed and the sampling rate) were changed in order to find the most convenient configuration for the purpose and to respect the mechanical, electrical and software constraints. After several tests, the mid-point terms resulted to be the best candidate to find the zero position, considering its capability to reproduce the same information for different times and for its simplicity. Also the B-spline method and the Gaussian method provided stable results, but their computational cost is not compatible with the operational capability of the microprocessor of the spacecraft.

After that, a way to optimize the results was developed, introducing the derivative tool in order to exploit the steepest side of the signal to record the information, and later stabilizing the number of samples that exceeded the threshold voltage set. Using this additional tool, the standard deviation on the zero position found was decreased, thus demonstrating the superior efficiency of the selected method.

8.3 The results

The aim of the last set of tests was to verify the performance of this method (mid-point finder). In the test setup the resolver and the PSD (Position Sensing Device, optical sensor) was added: with these two new devices IT was possible to verify whether the method was able to find repeatedly the same angular position, by performing the test different times: the resolver was able to provide a high precision information of the position of the rotating mechanism. The PSD was able to provide further information on the angular position of the shaft and a raw idea of the region in which the zero position was located (the resolver rotates 250 times for each turn of the main cogwheel) . Using this setup IT was possible to verify the reliability of the selected method and the theory behind it.

8.4 Conclusions

The procedure to adopt to find the zero position on the rotating shaft of the APM of the LISA system is the following

1. Using a threshold value of 1,7 (with no magnet in close proximity the Output Voltage of the Hall sensor stands around a 1,6 V value), perform a fast rotation (maximum velocity allowed with a sample rate of 5Hz: 0,2 deg/s, time to perform a complete turn: 30 min) of the cogwheel in order to:

a) detect the presence of the magnet in the complete turn

b) find the optimal threshold value (maximum/minimum of the spline of the derivative of the plot obtained)

2. Return to an outer region of the signal (under the threshold): bring the magnet to the position it was before the voltage of the Hall sensor exceeded the threshold voltage of 1,7 V
3. Perform a slow (maximum velocity allowed 0,02°/s) sweep over the sensor, counting the number of samples taken when the updated threshold voltage is exceeded; the spacecraft CPU will divide this number of samples, find the sample in the middle of them, by dividing this number and the position of the motor at that same time.

In this thesis IT was demonstrated that this procedure is efficient and reliable, in order to find the absolute position with the precision required and the hardware available at the beginning of the work. Is required to automatize the described procedure.

9 FUTURE WORK

An analysis of how the shape of the signal (with the starting data chosen in this work) if affected by the temperature changes is required. The main width and the maximum voltage of the signal can change depending on the thermal environment of the room: decreasing the temperature the signal could have a lower maximum voltage and a thinner flat region (lower number of samples over the threshold). Increasing the temperature, the area under the curve of the signal grows and it is possible to see the clipping of the signal. The method here proposed can work only on an unclipped signal and the development of a software able to distinguish which method to use is required. For this purpose, will be required several thermos-couple, placed on the main board, to monitor of the thermal environment and support the Hall-sensor in processing the signal. In this work an algorithm to solve (paragraph 4.6.3) the clipped signal has been proposed, and proposed and tested the software to process the unclipped signal.

To test the behavior of the device in a simulated space environment a series of tests in a vacuum chamber is required: The Thermal Vacuum Chamber (TVAC) provides a test environment for experiments. This environment includes low and high temperature (space environment) combined with high vacuum. Furthermore, the TVAC allows component testing under space conditions, e.g. in the frame of the research project LISA, where the behavior of antenna components and mechanisms is being investigated. The TVAC is also used to qualify experiment rigs for the European sounding rocket REXUS, or the CubeSat MOVE.

Considering the internal volume (see figure 55 below) available of this chamber (Usable volume ca. ø 40 cm x 90 cm

) some tests to decrease the distance between the laser pointer and the PSD are require: in these tests it will be verified if the motor and the Hall sensor can provide a stable signal and verify if the new setup is able to work also with a laser pointer / PSD distance of approx. 50 cm.

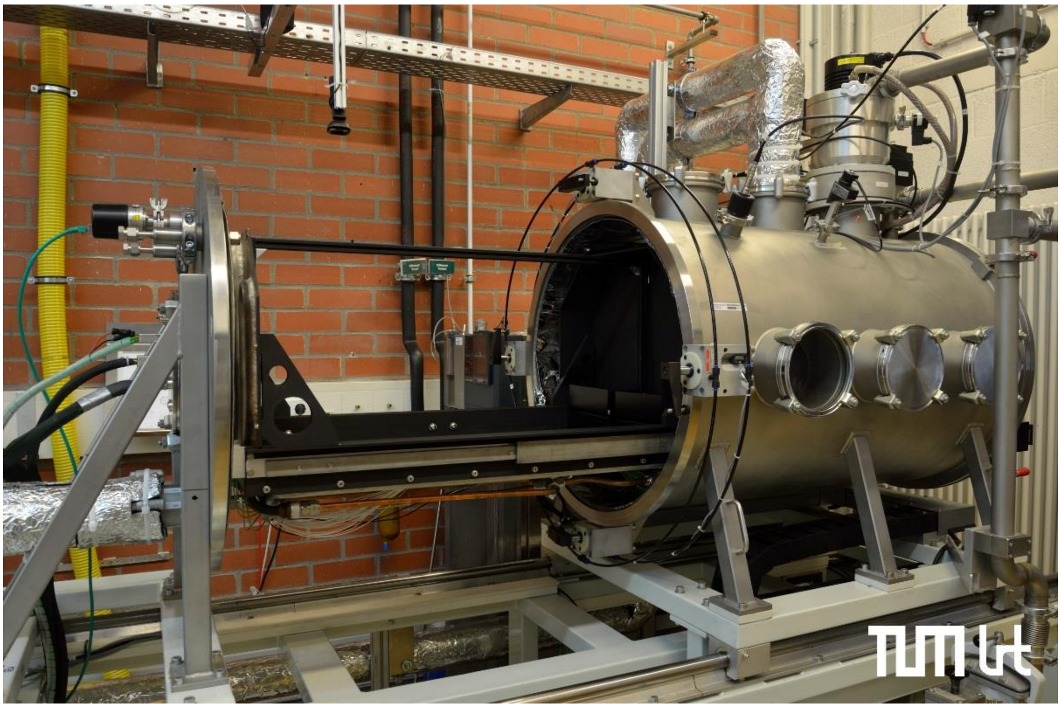

Figure 55: TVAC (Thermal Vacuum Chamber) of the LRT

Another test to perform is to use magnets of different residual magnetic field. In this work magnets of different shapes but identical residual magnetic field were used. Having a higher magnetic density, IT would be possible to have a higher maximum voltage which would mean having a steeper slope on both sides of the acquired signal, and consequently a more stable number of samples (less affected by the noise). This development could be useful in case it is necessary to increase the target precision.

The following phases of the tests will be to extend the tests to the elevation mechanism, considering the changing of the gear ratio of the mechanism and the space available in the case studied in this work, fastened at the top of the rotating azimuth shaft.

Furthermore, the procedure here developed and tested needs to be automatized, to make the machine autonomously perform each step to find the zero position (par 7.5), allowing the user to monitoring of each parameter each time is performed the sweep. Subsequently, it will be necessary to test if the queue of steps results reliable, to allow the integration of the device in the main system.

9.1 Elevation mechanism (preliminary considerations)

The main difference from the Azimuth mechanism and the Elevation mechanism stands in the different harmonic drive included in the motor: the gear ratio of this mechanical component is of 100:1, that in allow to the motor to perform:

200 steps per revolution, GR of 100: 1   360/100/200 = 0,018° per full step

To reach this accuracy an absolute encoder with 15bit of resolution (2^{15} = 32768, 2^{14} = 16384 considering 200x100 = 20000) is required to be able to monitor each step movement of the rotating shaft.

Considering a maximum sampling rate for the available microprocessors of t = 200 ms and assuming the motion of the magnet linear; at the geometrical distance available from the rotational axis r = 20 mm:

Linear distance travelled by the magnet in one rotation: C = 2 π r = 125,6 mm

Required spatial resolution: C/15bit = 125,6/ 32768 = 0,003856 mm

Allowed tangential velocity: V = s/t = 0,00385/ 0,2 = 0,01925 mm/s

Allowed angular velocity: w = v/r = 0,0009625 rad/sec, 0,0551°/sec

This is the maximum allowed angular velocity, considering the limitation of the sampling rate. The velocity is comparable to the azimuth velocity due to:

1. Inferior resolution required (not 16bit but 15 bit, for gear ratio of the mechanism)
2. Inferior radius of sweep (if the radius decreases, for the consideration made in the previous paragraph, the allowed max velocity decreases)

The assumptions made in this paragraph have to be tested and validated, with the same procedures see in chapter 6, the only difference being that the motion of the laser dot will be vertical instead of horizontal.

10 BIBLIOGRAPHY:

[1] Hoehn A., Harder J., Hager P., Design Characterization of an Electronic Steerable Ka-band Antenna Using Liquid Crystal Phase Shifters, in Proc. 30th Aerospace Mechanisms Symposium 2014

[2] Pfeiffer M., Purschke R., Harder J. Design, construction and testing of a 2 degree of freedom Ka-band antenna pointing mechanism, in Proc. 30th Aerospace Mechanisms Symposium 2009

[3] A. Francesconi, Aerospace systems I, notes, A.A. 2012/2013

[4] Ostler J., Evaluation and implementation of selected angular position sensors for 2-axis space mechanisms, 2015

[5] R. S. Popović, Hall effect devices, in Proc. 28th Aerospace Mechanisms Symposium 1994-2004

[6] Jankowski J., El-Ahmar S. and Oszwaldowski M., Hall sensor for extreme temperatures, Institute of Physics, Poznan University of Technology, in Proc. ESMATS 2009, Austria

[7] Gray code working principles: http://www.eetimes.com/document.asp?doc_id=1278809

[8] Absolute encoder: http://ecatalog.dynapar.com/ecatalog/absolute-encoders/en/AC36

[9] High resolution absolute orientation rotary magnetic encoder, US 8760153 B2, Anthony Parakka, US Patent (2009)

[10] Disk type of absolute-position magnetic encoder for rotary devices, US 5757180 A, US Patent, (2008)

[11] Rotation detecting device and bearing assembly equipped with such rotation detecting device, US 20100225309 A1, US Patent, (2011)

[12] Hall-sensor datasheet http://www.farnell.com/datasheets/1683360.pdf

[13] Thermal Environments: http://www.tak2000.com/data/planets/earth.htm

[14] PSD datasheet:https://www.hamamatsu.com/resources/pdf/ssd/s5990-01_etc_kpsd1010e.pdf)

[15] PSD working principles: https://www.hamamatsu.com/resources/pdf/ssd/psd_techinfo_e.pdf

[16] M. Pfeiffer, J. Harder, and U. Walter, “Development of a Compact Ka-Band Antenna Pointing Mechanism for Intersatellite Links on Small Satellites”, in Proc. ESMATS 2009, Austria.

[17] M. Shmulevitz and A. Halsband, “The Design, Development and Qualification of a lightweight Antenna Pointing Mechanism”, in Proc. 30th Aerospace Mechanisms Symposium, 1996.

[18] M. Herald and L. C. Wai, “Two-Axis Antenna Positioning Mechanism”, in Proc. 28th Aerospace Mechanisms Symposium 1994

[19] Czech M., Stoll E., Walter U., "Development of a low cost, medium accurate 2-axes pointing mechanism for small satellites", Proc. Deutscher Luft-und Raumfahrtkongress, Aachen, Germany, 2006

APPENDIX OF THE THESIS

11 APPENDIX A

11.1 A1 Motor control VI

11.1.1 Main vi

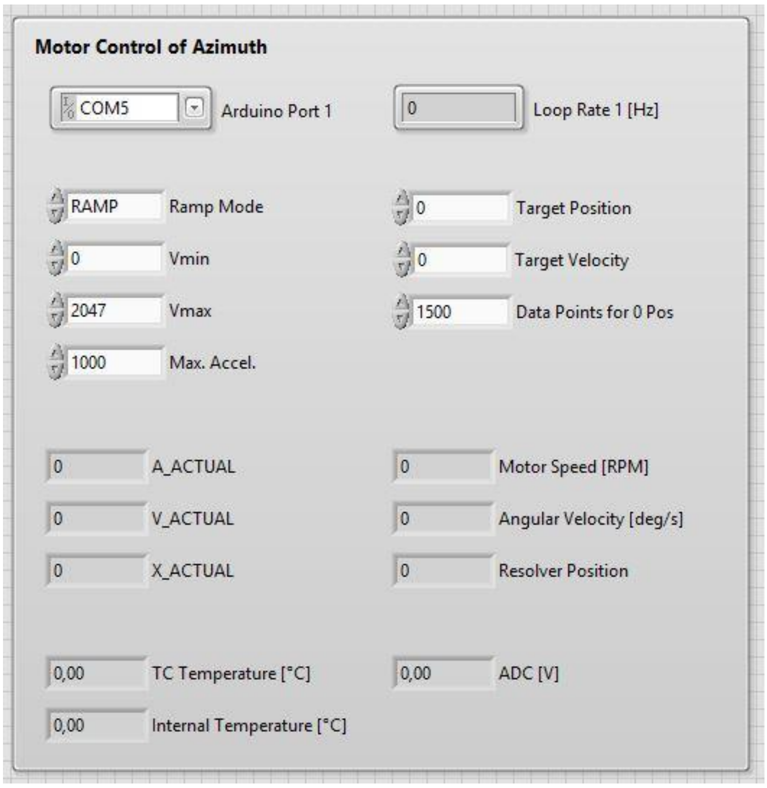

Motor Control of Azimuth

COM5 Arduino Port 1
0 Loop Rate 1 [Hz]

RAMP Ramp Mode
0 Vmin
2047 Vmax
1000 Max. Accel.

0 Target Position
0 Target Velocity
1500 Data Points for 0 Pos

0 A_ACTUAL
0 V_ACTUAL
0 X_ACTUAL

0 Motor Speed [RPM]
0 Angular Velocity [deg/s]
0 Resolver Position

0,00 TC Temperature [°C]
0,00 Internal Temperature [°C]
0,00 ADC [V]

Figure 56: Portion of the front panel of the main Vi

The Main.vi of the motor control allows the user to control the mechanism in different ways. For this applications, in the front panel the Ramp mode and the Velocity mode was included:

1. Ramp mode: the user sets the target position and the motor performs the sweep using the maximum velocity set in the Vmax numerical indicator. The default Vmax is 2047, the maximum allowed by the motor. For this mode, some numerical indicators that show the instantaneous position are shown, velocity and acceleration of the main cogwheel (are ana-

lytically calculated, without using sensor, only using gear ratio formula), allowing the user to set the maximum velocity allowed by the sample rate of the CPU (5Hz). It is important to take in consideration that the counting of the angular position of the shaft is not reliable: it is only a parameter used to give the command to the motor. The zero position of this counter changes each time a switching of the rotating speed occurs (this is this reason why there was the need for the device developed in this work!), for more details see paragraph 7.6.1.

2. Velocity mode: the user sets the rotational velocity of the motor, positive (clockwise) or negative (counterclockwise), and the motor keeps running until a new velocity is set by the user. This mode uses the same numerical indicators shown in the previous point.

In future works, the same technology will be extended to the elevation mechanism, and the front panel has already been extended at the end of this work. As far as the control panel of the vi is concerned, the block diagram is based on a main loop that runs at a loop rate of 200 ms. The data on this loop is exchanged through an SPI serial interface using the Lynx patch for the communication between LabVIEW and Arduino.

11.1.2 Sub-vi’s

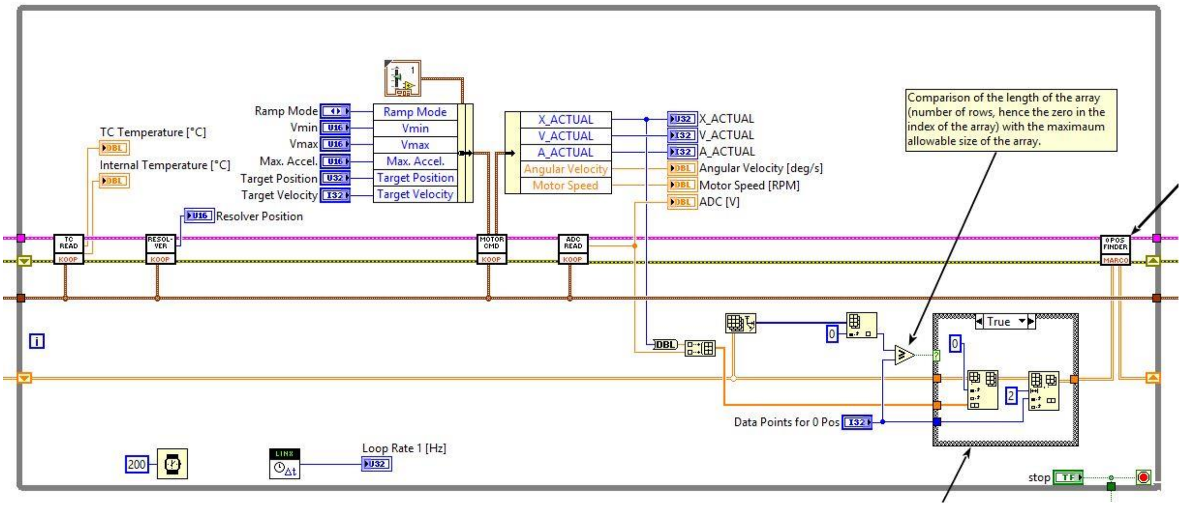

Comparison of the length of the array (number of rows, hence the zero in the index of the array) with the maximaum allowable size of the array.

Figure 57: Block diagram of the main vi for the motor control

The list of sub-vis of the main motor control vi includes:

1. a vi to configure and initialize the serial interface (SPI),
2. a vi to read the internal and room temperature (thermos-resistance attached to the motherboard)
3. a vi able to read the information from the resolver board (output included in the front panel of the main vi),
4. the sub-vi to command the motor, that has as inputs the mode, the velocity and the position that the motor has to adopt, and as output the real cinematic parameters the motor has during its operative life (X_actual, V_actual, A_actual, angular velocity in degrees per second and the speed of the motor)
5. a sub-vi able to read the output of the ADC, output that will be used in the zero position finder sub-vi as the analog input after being associated to an array of the positions of the shaft recorded for each moment. This sub-vis and all the loop structure, was copied and

pasted in the same vi in order to create the basic structure for the elevation mechanism, changing the proper parameters (i.e the gear ratio of the motor/harmonic drive).

11.2 Zero position VI

11.2.1 Main vi

This is the vi where the signal provided by the Hall sensor with the proximity on the magnet. In the front panel, it is possible to see several graphs in which all the shapes of the signal recorded are displayed and the shapes assumed by the signal after the processing through the fit methods selected in the preliminary phase. The list of the graphs includes: the shape of the signal without any kind of processing (running all the time, after the vi is lunched), the shape of the signal only when the voltage exceeds the threshold value set by the user, the shape of the signal after cubic spline fit, B-spline fit with chord length method, B-spline with equi-spaced method, B-spline with centripetal method and Gaussian fit. For each of the last methods a peak detector sub.vi was associated, able to find the x (in this case the respective and angular position) of the maximum of the curve. The utility of these fit methods was to have the shape of the main curve of the signal without being influenced by the noise of the sensors (it is possible to see the noise only by zooming on a 200% from the main graph display in the vi, included in the DVD attached in this work). All the graphs are also collected in a wider window than the main one at the center of the front panel to allow the user to compare them. All the used methods were included in the library of LabVIEW 2015, in the signal processing palette. In the front panel, the plot of the derivative of the signal is also included, with its corresponding shape after a B-spline fit; the usefulness of this additional tool has been already shown in the section threshold optimization (paragraph 6.4 of this thesis).

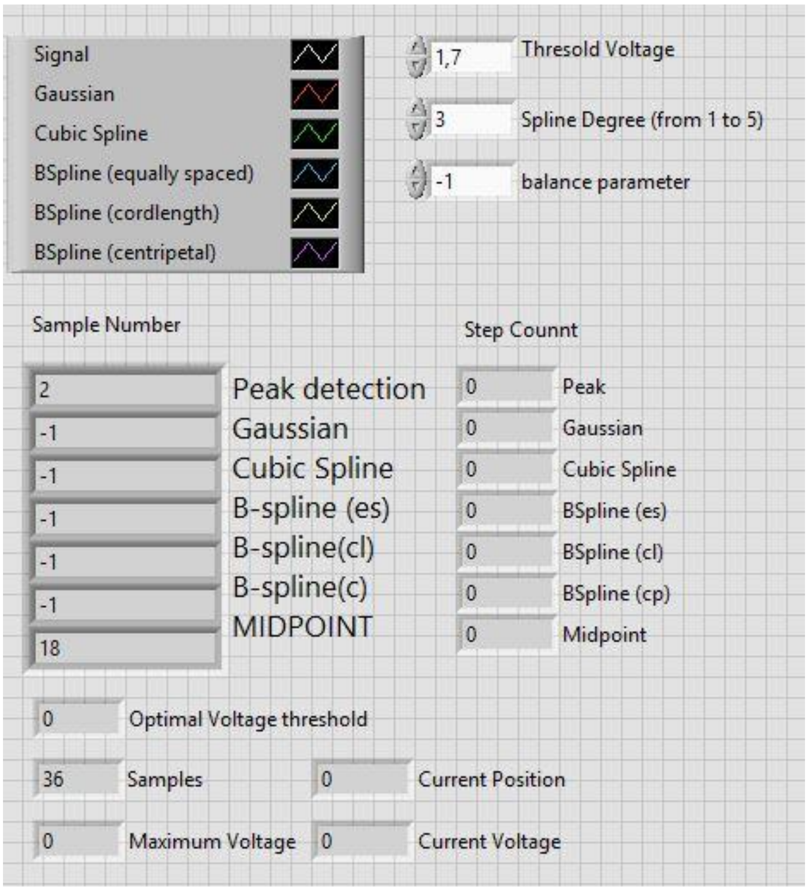

Signal
Gaussian
Cubic Spline
BSpline (equally spaced)
BSpline (cordlength)
BSpline (centripetal)

1,7 Thresold Voltage
3 Spline Degree (from 1 to 5)
-1 balance parameter

Sample Number		Step Counnt	
2	Peak detection	0	Peak
-1	Gaussian	0	Gaussian
-1	Cubic Spline	0	Cubic Spline
-1	B-spline (es)	0	BSpline (es)
-1	B-spline(cl)	0	BSpline (cl)
-1	B-spline(c)	0	BSpline (cp)
18	MIDPOINT	0	Midpoint

0 Optimal Voltage threshold
36 Samples
0 Current Position
0 Maximum Voltage
0 Current Voltage

Figure 58: Portion of the front panel of the Zero Position finder sub-vi

On the left side of the front panel some meaningful numerical indicators are also reported. Staring from the top: it is possible to set the threshold value for the sampling, the degree and the balance parameter of the spline fit method. Below there are two arrays that show the position of interest of each fit method used: the position of the peak of the signal, the position of the peak after the processing with the fit methods and the mid-point (obtained by counting the number of samples whose values exceeded the threshold value and dividing this amount by two); for each of these positions the count on the motor was associated, to have an idea of the repeatability on the position of the point of interest (in the final test phase we realized that this count was not reliable, see paragraph 7.6.1, for this reason the resolver included in the motor, more precise and more stable) was used. For these two arrays also some other interesting numerical indicator was included:

1. a counter of the number of samples that exceeded the threshold (to check if the shape of the signal was stable in a stable thermal environment),
2. the maximum voltage reached after performing the sampling, to see if the signal shape was influenced by the room temperature (if warmer the maximum voltage increases, if colder it decreases)
3. an indicator that shows the optimal threshold value to set in the second sweep (this was the maximum of the derivative of the first sweep, after having processed the clean signal using the B-spline method, to avoid the influence of noise)
4. An indicator of the instantaneous position of the motor in the step count.
5. An indicator of the output voltage from the ADC, to allow the user to know precisely when the threshold voltage, V_t, was reached.

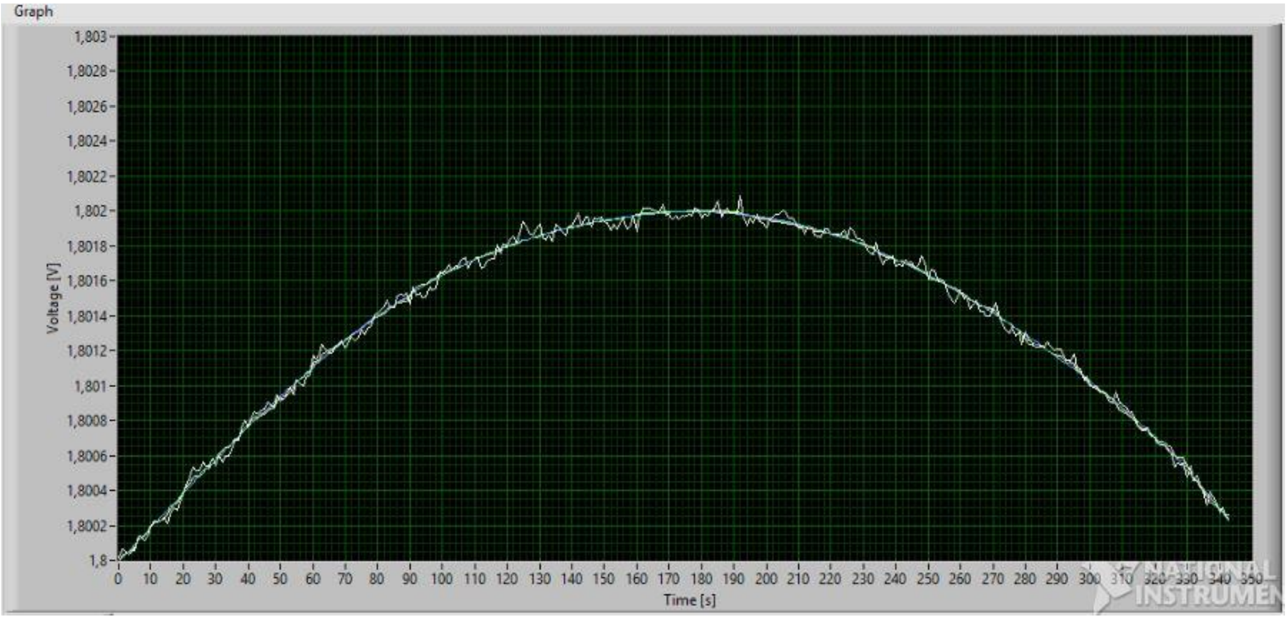

Figure 59: Waveform graph used to display the signal: top of the hump

11.2.2 B-spline sub-vi

This sub.vi is able to process the data acquired in real time and to yield the shape of the signal following the mathematical laws listed in paragraph 4.4.4. The sub.vi takes into account only the value that exceeds the threshold Voltage, V_t and sets the origin of the plot corresponding to the first sample that exceeds this threshold. During the sweep the plot is updated in real time, differently from the cubic spline that is able to yield the plot only when the dimension of the array of the X coordinates reaches the dimension of the array of the Y (with X the sample number and Y the corresponding voltage value detected) generating some issue for the data acquisition in real time. To collect the data two arrays are required and these are provided by the queue function of LabVIEW that is able to collect each voltage obtained in each cycle of the loop and store them. After that, each value is associated with the corresponding element of the array, obtained by calculating the dimension of the string that is created (position inside the signal) and the array obtained storing each position of the mechanism in the step count (position in the rotation of the main cogwheel). It is possible to set the B-spline method in different ways: in these tests, it was chosen to use the equally spaced method, the cord length method and the centripetal method. This decision was taken to have different methods to process the signal and to have different terms to compare. (It was possible to see the differences between these last modes, in terms of position of the maximum, only when the number of samples was more than 1000). The most reliable method, considering the stability of the position of the maximum in different sweeps, was the cord length method. The application of this tool is limited to the test phase, to give the user on the behavior of the curve of the signal “cleaned” from the noise; the applicability of this method in the system is forbidden due the limited capability of the microprocessor used on the spacecraft system.

11.2.3 Gaussian Fit sub-vi

As the B-spline method, to plot the results in the graph reported in the zero position main.vi it is required to have an array of a given size (Y) that matches an array of the same size (X). The sub-vi uses the equation and the main parameters are reported in paragraph 4.4.5. Considering the position of the maximum, the curve plotted behaves very similarly to the peak detection of the signal without any processing methods: it has been observed that, in the majority of the cases, the position of interest, as the zero position, occurs in the same sample: for this reason, considering how the noise affect this information, the Gaussian fit is not sufficiently reliable for the purpose. The convenience of this method is that IT is less influenced by some unpredicted perturbation of the signal and more stable. The drawback of this method is that its repeatability is comparable with the repeatability of a peak method that, due the required precision, is not a good candidate. In this application, no weight and no tolerance parameter was used. The default method available in the LabVIEW library (least square method) was used

11.2.4 Derivative tool sub-vi

The derivative tool is the fundamental sub-vi to optimize the threshold choice. Was used to calculate the most sensitive (steepest slope) part of the signal by taking the maximum of the curve provided. The vi requires an array and is able to estimate the steepness of the curve of interest point by point. For this reason, the obtained plot is influenced by the noise of the signal and requires a processing through a B-spline to find the maximum of the curve and to take in consideration the main trend of the curve. Looking at the graph displayed in the main vi, it is also possible to see how the noise has more influence on the plot in case of a slow sweep (3 in velocity in the vi of the motor control), providing peaks that can yield a wrong position of the maximum of the curve, requiring a further processing of the signal (in this application not affordable for the CPU limitation). For this reason, the fast sweep (velocity target 30), for the first sweep, is more efficient in terms of computational resources, providing a raw information on the position of the maximum, and its corresponding voltage (optimal threshold, V_{to}). In the picture below it is possible to see the derivative of the slow speed sweep signal before and after the processing through B-spline.

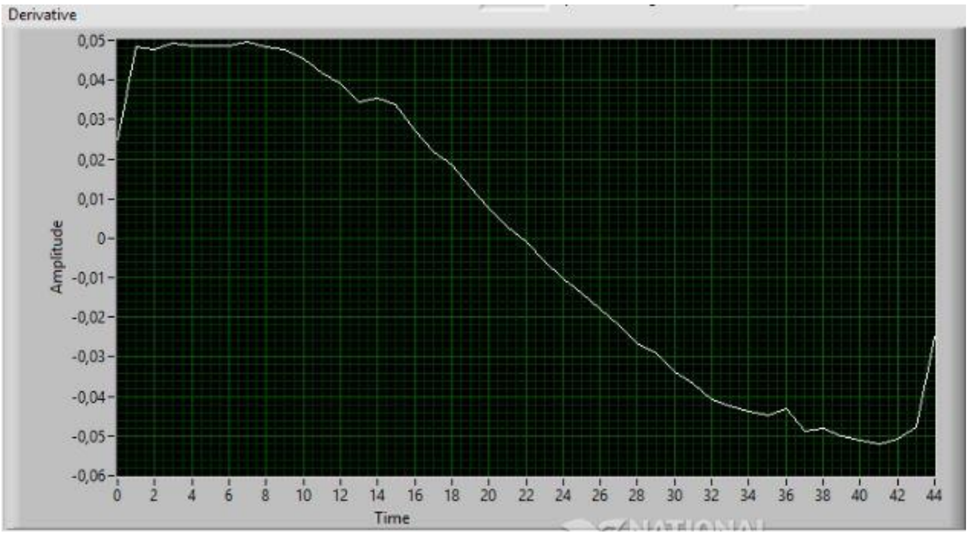

Figure 60: Waveform Graph showing the derivative of the main signal

Figure 61: Derivative graph processed with the B-spline method

11.3 Laser pointer/PSD VI

11.3.1 Arduino Laser Target

This VI was used in the final phase of the test. The VI was used to operate with the PSD and the laser pointer. In the picture below it is shown how the front panel looks like: it is possible to see the graph in which the position of the laser dot on the sensitive surface of the PSD was reproduced. The sensor was coupled with an ADC and the precision of the device was of 10bit of resolution. The output was in binary code and was converted through an SPI bus. The active area of the sensor was of 6x6mm and the display was configured to have the same dimensions (x = +- 3, Y+- 3 = 6x6, see graph displayed in figure 62). In the front panel below a numerical indicator to show the operational frequency is also included (most of the time 5Hz, the maximum allowed by the hardware used), two numerical indicators to show the position of the center of the laser dot in Cartesian coordinates (x, y) and the tool that allows the user to set the COM port to make the Arduino 256 Mega board communicate with the laptop.

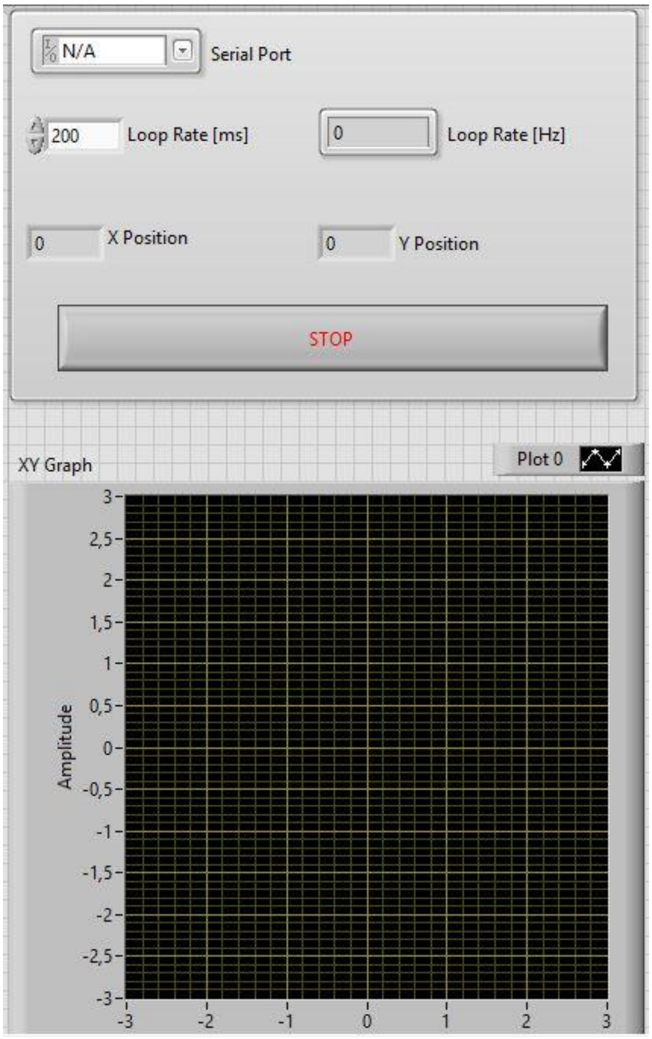

N/A Serial Port

200 Loop Rate [ms]

0 Loop Rate [Hz]

0 X Position

0 Y Position

Figure 62: Front Panel of the Laser Target vi

In the next picture the control panel of the previous picture is shown in which it is possible to see the software instruments used to display the output on the front panel. As for the VI of the motor control, the communication between Arduino and LabVIEW was possible through the Lynx interface, a tool downloadable from the VIPM (Vi Package Manager) available on the LabVIEW online "tool shop". This library includes the sub.vi to set the SPI bus (lynx spi settings) and the sub.vi to write or read in the bus (analog write, analog read, digital write, digital read). Included in the main loop of the vi there were the four input values from each side of the sensor (see paragraph 7.4.2, for the PSD working principle) expressed in binary code. They were collected in one array and read from the Lynx SPI digital read, and sent to the sub.vi able to convert this information in Cartesian coordinates; the equations required to do this are described in the next chapter.

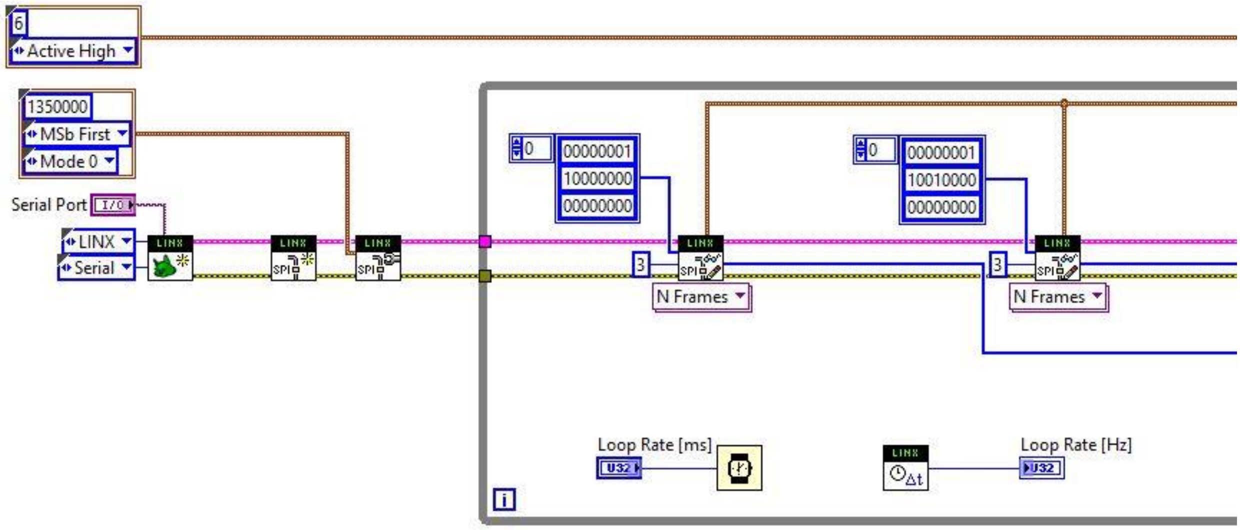

Figure 62: Block diagram of the Laser target vi (first half)

After exiting from the logical loop the Lynx sub.vi is closed and a report on the possible errors generated is created.

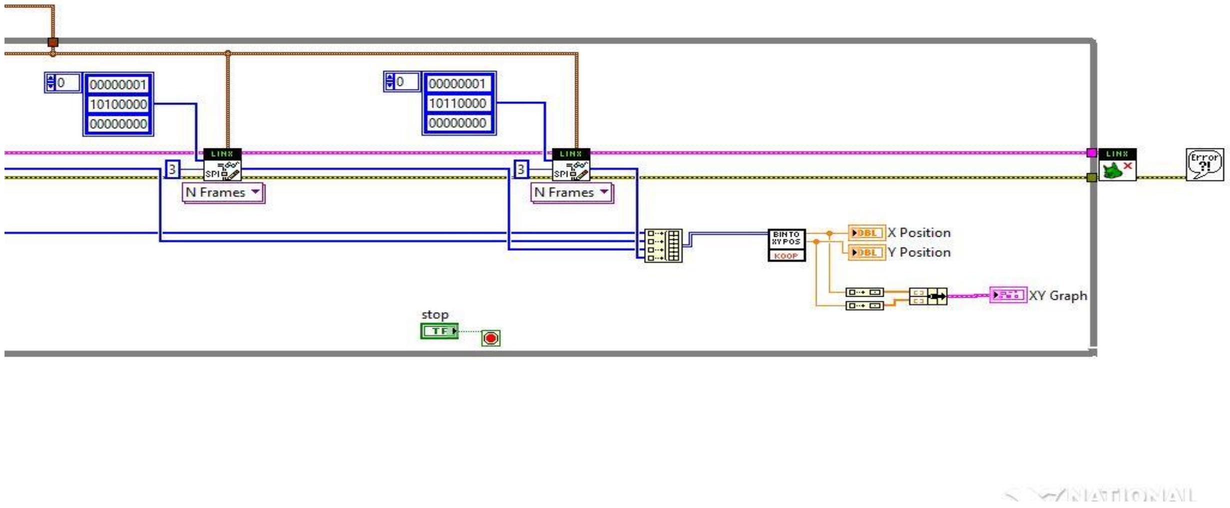

Figure 63: Block diagram of the Laser target vi (second half)

11.3.2 Convert Binary to Cartesian position (X, Y)

This sub-vi uses the input provided by the main vi, previously described, and converts the binary information in the Cartesian coordinates of the center of the laser dot in the waveform chart reported in the front panel of the main vi. To do this, an internal Matlab file was created in which the conversion formula needed to yield the right output have been included; the used formulas, available from the datasheet of the sensor, are the following:

$$\frac{(I_2 + I_3) - (I_1 + I_4)}{I_1 + I_2 + I_3 + I_4} = \frac{2x}{L}$$

$$\frac{(I_2 + I_4) - (I_1 + I_3)}{I_1 + I_2 + I_3 + I_4} = \frac{2y}{L}$$

Where:

1. I1, I2, I3, I4, are the currents on each side of the PSD sensor
2. L is the length of the active surface of the sensor
3. X and Y are the coordinates of position of the center of the laser dot

As for the previous files, the data are transmitted through SPI bus interface at a loop rate of 5 Hz.

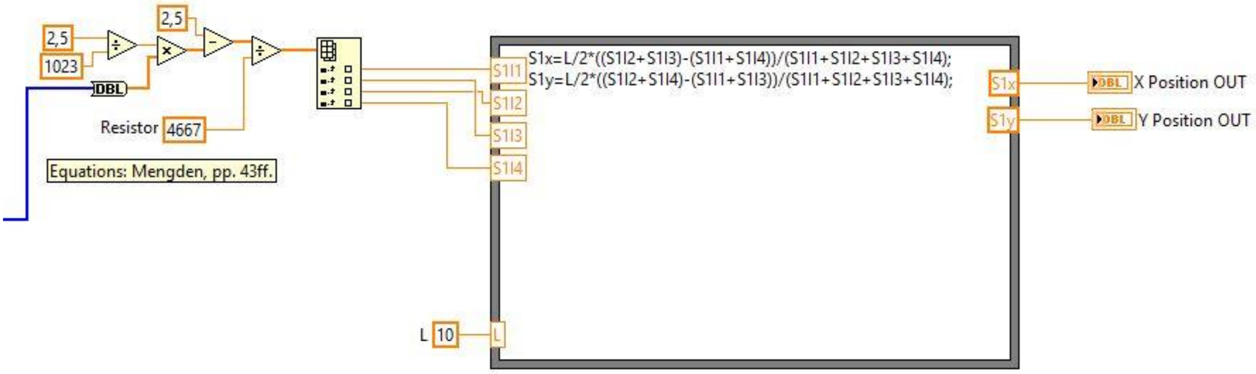

```
S1x=L/2*((S1I2+S1I3)-(S1I1+S1I4))/(S1I1+S1I2+S1I3+S1I4);
S1y=L/2*((S1I2+S1I4)-(S1I1+S1I3))/(S1I1+S1I2+S1I3+S1I4);
```

Figure 64: Block diagram of the Laser target sub-vi

12 APPENDIX B

12.1 Tables and results

In this section some of the main result used in this work are reported: the comments and the discussions have already been proposed in the main part of the thesis. To find the section where the table consulted is located in this document, it is possible to use the list of tables appearing in the introductive part of this thesis.

12.1.1 Mechanical/Electrical setup tests

The following data were used in the preliminary phase of this work, to set each component from a mechanical and electrical point of view

main gear speed[°/s] sampling rate[ms]	1	2	5	10
0.5	0.0005	0.001	0.002	0.005
1	0.001	0.002	0.005	0.01
5	0.005	0.01	0.025	0.05
10	0.01	0.02	0.05	0.1

Table 20: Angular resolution achievable by changing the main cogwheel speed and the sample rate

Radius [mm]	Linear resolution required [mm]
40	0.00376
50	0.00471
60	0.00565
70	0.00659

Table 21: Linear resolution required for each radius

Rotational speed [°/s] Radius [mm]	1	2	5	10
40	0.698	1.396	3.490	6.980
50	0.872	1.745	4.363	8.726

60	1.047	2.094	5.235	10.471
70	1.221	2.443	6.108	12.216

Table 22: Tangential velocity [mm/s] achievable changing the radius and the angular velocity

Main gear speed[°/s] sampling rate[ms]	**1**	**2**	**5**	**10**
0.5	0.00061	0.0012	0.0024	0.0061
1	0.0012	0.0024	0.0061	0.012
5	0.0061	0.012	0.03	0.061
10	0.03	0.024	0.061	0.122

Table 23: Angular resolution [°/s] achievable by changing the sampling rate and the rotational speed (in grey the resolution allowed for this application)

Radius [mm]	**Linear resolution required [mm]**
40	0.00376
50	0.00471
60	0.00565
70	0.00659

Table 24: Linear resolution required [mm] per each radius

Rotational speed [°/s] Radius [mm]	**1**	**2**	**5**	**10**
40	5 (0.00349mm)	1 (0.00139mm)	1(0.00349mm)	0.5 (0.00349mm)
50	5 (0.00436mm)	1 (0.00174mm)	1(0.00436mm)	0.5 (0.00436mm)
60	5 (0.00523mm)	1 (0.00209mm)	1(0.00523mm)	0.5 (0.00523mm)
70	5 (0.00615mm)	1 (0.00244mm)	1(0.00618mm)	0.5 (0.00618mm)

Table 25: Lowest sampling rate allowed to reach the resolution required

H[cm]	**d[cm]**	**Vmax[V]**	**Clipped signal**
/	∞	1,5	No
1,8	1,8	1,652	No
2,5	1,1	1,714	No
2,8	0,9	1,845	No
2,95	0,65	2,022	No
3	0,6	2,769	No
3,2	0,4	3,205	Yes
3,3	0,3	3,215	Yes

Table 26: Max Voltage achievable, depending on the distance sensor/magnet

12.1.2 Mid-point finder/peak detection reliability tests

Test n°	Peak	Mid-point	Samples	V_{max}[V]
1	651	644	1288	2,053
2	638	644	1288	2,060
3	662	654,5	1309	2,061
4	651	657,5	1315	2,083
5	668	663,5	1327	2,105
6	655	666	1332	2,113
Δ_{max}	30	22	44	0,060
Std.Dev.	10,34247	9,399025	18,79805	0,025333

Table 27: Comparison between the stability (in yellow the standard deviation) of the mid-point finder method and the peak-detector, threshold voltage 1,8 V

Test	Peak	Mid-point	Samples	V_{max}[V]
1	918	900,5	1801	2,205
2	879	906,5	1813	2,214
3	900	904	1808	2,218
4	885	903,5	1807	2,223
5	911	903,5	1807	2,227
6	892	910,5	1821	2,230
Δ_{max}	33	10	20	0,025
Std.Dev.	15,0831	3,402205	6,80441	0,009182

Table 28: Comparison between the stability (in yellow the standard deviation) of the mid-point finder method and the peak-detector, threshold voltage 1,7 V

Test	Samples	Peak	Gaussian	B-spline 1	B-spline 2	B-spline 3	Mid	V_{max}
1	1527	761	761	752	751	751	786,0	1,751
2	1545	724	723	729	727	727	772,5	1,749
3	1566	751	751	747	747	747	783,0	1,748
4	1540	716	715	720	718	718	770,0	1,748
5	1573	762	763	753	753	753	786,5	1,750
Delta max	33	49	48	33	35	35	16,5	000,3
Std dev	18,96576	21,44062	22,1991	14,85598	15,7226	15,7226	7,789416	0,001304

Table 29: Comparison on the stability of each method (non optimized threshold)

Test	Samples	Peak	Gaussian	B-spline 1	B-spline 2	B-spline 3	Mid	V_{max}
1	903	443	443	441	441	441	451,5	1,477
2	899	442	442	439	438	438	449,5	1,477
3	897	443	443	438	438	435	448,5	1,477
4	892	432	432	435	435	433	446,0	1,477

5	893	432	432	433	433	431	446,5	1,478
Delta max	11	9	9	8	8	10	5,5	0,001
Std dev	4,494441	5,8566	5,85662	3,193744	3,082207	3,974921	2,247221	0,000447

Table 30: Comparison on the stability of each method (nearly optimized threshold)

Test	**Samples**	**Peak**	**Gaussian**	**B-spline 1**	**B spline 2**	**B spline 3**	**Mid**	**V_{max}**
1	661	329	329	326	326	326	330,0	1,479
2	659	316	316	322	322	322	329,0	1,479
3	656	321	321	322	323	323	328,0	1,479
4	657	324	323	322	322	323	328,5	1,479
5	661	331	331	325	326	326	330,0	1,479
Delta max	5	15	15	4	4	4	2	0
Std dev	2,280351	6,058052	6,082763	1,949359	2,04939	1,870829	0,894427	0

Table 31: Comparison on the stability of each method (optimized threshold)

Test	**Samples**	**Peak**	**Gaussian**	**B-spline 1**	**B-spline 2**	**B-spline 3**	**Mid**	**Vmax**
1	505	5927(247)	5927(247)	5926(249)	5926(249)	5926(249)	5924(252,5)	2,087
2	509	5939(248)	5939(248)	5940(250)	5940(250)	5940(250)	5942(254,5)	2,087
3	506	5924(251)	5923(250)	5926(248)	5926(248)	5926(248)	5923(253,0)	2,087
4	509	5939(248)	5939(248)	5939(248)	5939(248)	5939(248)	5943(254,5)	2,087
5	507	5923(252)	5923(252)	5925(249)	5925(249)	5925(249)	5922(253,5)	2,087
6	510	5939(249)	5939(249)	5939(249)	5939(249)	5939(249)	5942(255,0)	2,087
7	507	5927(247)	5927(247)	5925(250)	5925(250)	5925(250)	5922(253,0)	2,087
8	511	5937(247)	5937(247)	5939(249)	5939(249)	5939(249)	5943(255,5)	2,088

Δmax1	5	4 (4)	4(4)	1(1)	1(1)	1(1)	2(2)	0,000
Δmax2	2	2(2)	2(2)	1(1)	1(1)	1(1)	1(1)	0,001
Std1	0,957427	2,629956	0,816497	0,816497	0,816497	0,816497	0,408248	0,000
Std2	0,957427	0,816497	0,957427	0,816497	0,500000	0,816497	0,645497	0,0005

Table 32: Comparison on the stability of each method (optimized threshold), with the ~~respective~~ corresponding step count

12.1.3 Validation tests

PSD/LASER POINTER DISTANCE (r) [m]	TARGET DIMENSION REQUIRED (l) [mm]
8	0,766
9	0,862
10	0,958
11	1,054

Table 33: Size of the target for each PSD/laser pointer distance

TEST N°	RESOLVER POSITION	PSD POSITION (X,Y)	NUMBER OF SAMPLES	MIDPOINT	MAX VOLTAGE
1	60844	(0,12, -0,12)	252	126	2,948
2	60842	(0,2, -0,2)	252	126	2,949
3	60846	(-0,12 , 0,12)	253	126,5	2,949
4	60842	(0,15, -0,15)	252	126	2,950
5	60844	(0,21 , -0,21)	252	126	2,950

Table 34: Result of the validation test: position of the shaft expressed in position of the resolver, position on the optical sensor, position in the signal plot

13 APPNDIX C

13.1 Circuits

In this section the main circuits used in this work are reported. The first is described in the section of the preliminary tests setup, paragraph 4.2. The second in paragraph 5.4, describing the electrical setup of the main part of the tests. The last in the section of the validation tests, with the lase pointer, in particular in paragraph 7.3.

13.1.1 Preliminary tests circuit

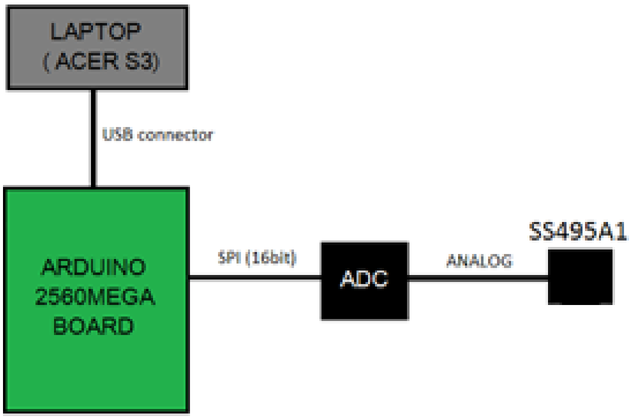

Figure 65: Preliminary test circuit

13.1.2 Fit methods reliability tests circuit

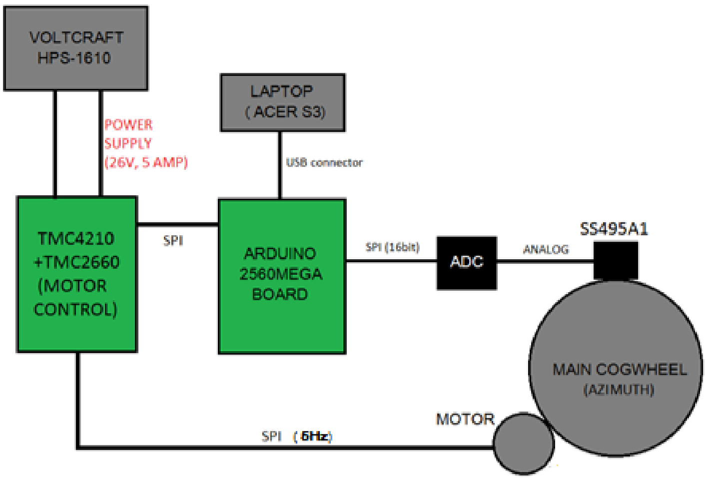

Figure 66: Fit method reliability tests circuit

13.1.3 Validation test circuit

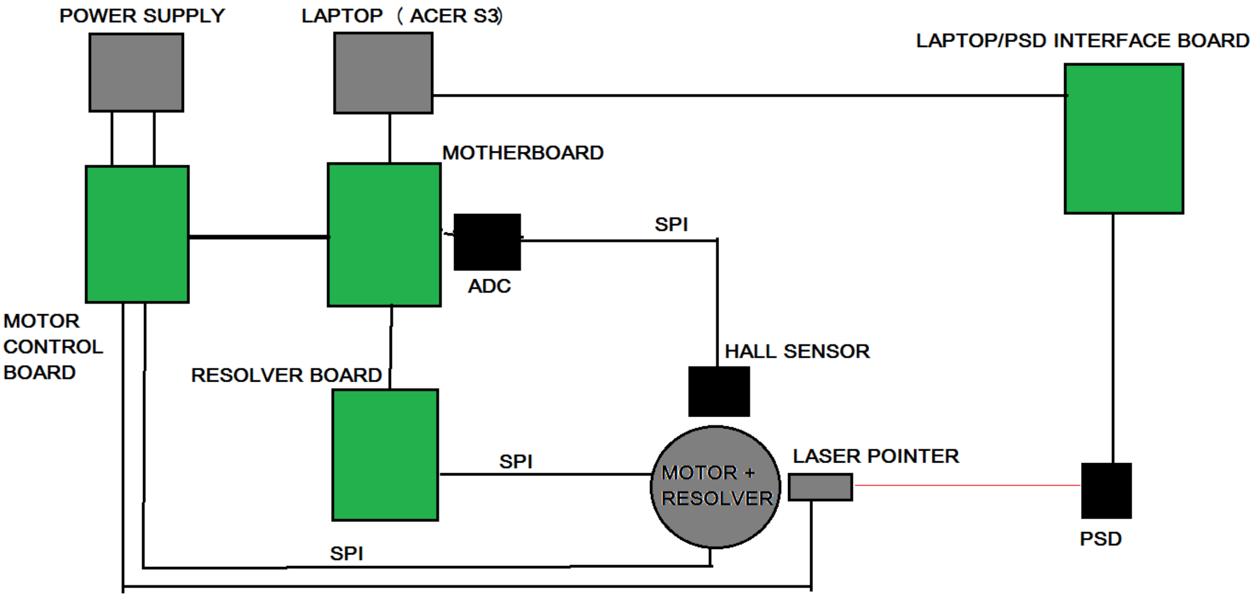

Figure 67: Validation tests circuit

14 APPENDIX D

14.1 Dvd content

In the DVD-R attached to this paper it is possible to find all the files used and created during this study. The files have been grouped in different folders:

1. The collection of all the data that were provided by the LRT at the beginning of the study, for example the bachelor thesis for the selection of the sensing technology (folder: Bachelor Arbeit)
2. A list of all the circuits and electrical setups used to perform the tests (folder: circuits)
3. A list of all the datasheets used for each electrical/mechanical component
4. A digital version of this thesis
5. A collection of all the presentations given during the thesis preparation (file.ppt)
6. A collection of all the reports delivered month by month during the thesis preparation
7. A collection of all the data collected during the test, in each configuration/setup used in this work
8. A folder of all the electrical and mechanical sketches of the tests setups
9. All the vi's used to interface each component of the setups